

---

Electronic Theses and Dissertations, 2004-2019

---

2015

## Mass Spectral Studies to Investigate Butylbenzene Fragmentation Pathway and Pyrolysis Products.

Balasubramaniam Lingam  
*University of Central Florida*

 Part of the [Chemistry Commons](#)

Find similar works at: <https://stars.library.ucf.edu/etd>

University of Central Florida Libraries <http://library.ucf.edu>

This Doctoral Dissertation (Open Access) is brought to you for free and open access by STARS. It has been accepted for inclusion in Electronic Theses and Dissertations, 2004-2019 by an authorized administrator of STARS. For more information, please contact [STARS@ucf.edu](mailto:STARS@ucf.edu).

---

### STARS Citation

Lingam, Balasubramaniam, "Mass Spectral Studies to Investigate Butylbenzene Fragmentation Pathway and Pyrolysis Products." (2015). *Electronic Theses and Dissertations, 2004-2019*. 1278.  
<https://stars.library.ucf.edu/etd/1278>

MASS SPECTRAL STUDIES TO INVESTIGATE BUTYLBENZENE FRAGMENTATION  
PATHWAY AND PYROLYSIS PRODUCTS

by

BALASUBRAMANIAM LINGAM  
B.S. University of Mumbai, 1998  
M.S. University of Mumbai, 2001

A dissertation submitted in partial fulfillment of the requirements  
for the degree of Doctor of Philosophy  
in the Department of Chemistry  
in the College of Sciences  
at the University of Central Florida  
Orlando, Florida

Spring Term  
2015

Major Professor: Michael E. Sigman

© 2015 Balasubramaniam Lingam

## ABSTRACT

In this dissertation research, two fundamental studies involving gas chromatography mass spectrometry of n-butylbenzene and pyrolysis products are presented. In the first study, fragmentation pathways of n-butylbenzene in quadrupole ion trap have been investigated. At low energy, product ion corresponding to  $m/z$  92 and  $m/z$  91 are formed via competitive parallel dissociation. Studies have also shown that at higher energy  $m/z$  92 has sufficient internal energy to undergo further fragmentation yielding  $m/z$  91 via consecutive dissociation. Thus in order to discern the fragmentation pathways of n-butylbenzene, the technique of two-dimensional correlation spectroscopy (2DCOS) was applied to the mass spectral data. Application of 2DCOS resulted in two 2D correlation spectra namely synchronous and asynchronous. A third spectra known as coherence spectra was obtained from the ration of asynchronous to synchronous correlation intensities. For the elucidation of n-butylbenzene fragmentation pathways, all the three spectra were utilized in this study. The second study in this dissertation involves investigation of pyrolysis products to aid in fire debris analysis. One of the major concerns in fire debris analysis is that pyrolysis products can mask the patterns of compounds of interest and make the chromatographic results interpretation extremely difficult. One of the approaches for investigating the formation of pyrolysis products is to subject the commonly found building materials to controlled heating in laboratory. In this study, new heating methodologies for controlled heating of substrates involving furnace, paint-cans and flat steel pans have been developed. The substrates used for investigating pyrolysis products were polystyrene, polyvinylchloride, polybutadiene, yellow-pine, nylon carpet and padding. Experiments were also performed to investigate the influence of hydrocarbons on the formation of pyrolysis.

*To my Parents:*

Thangamuthu Lingapandian & Logathai Lingam

*To my Siblings:*

Ganeshram Lingam & Thangakirubhakaran Lingam

*To my Guru:*

Sridevi Krishnamurthy

## ACKNOWLEDGMENTS

Completion of this doctoral dissertation would not have been possible without the support and encouragement of several people and I would like to take this opportunity to express my sincere gratitude to all of them. Foremost, I would like to express my deepest gratitude to my research advisor Dr. Michael Sigman, for his constant guidance, patience and support throughout my graduate studies. I would also like to thank Dr. Andres Campiglia, Dr. Christian Clausen, Dr. Howard Miles and Dr. Alfons Schulte for agreeing to be a part of my dissertation committee and providing their inputs throughout. I would especially like to thank Douglas Clark and Mary Williams for sharing their knowledge and experiences during instrumentation training and providing research assistance whenever needed. I also want to thank my lab mates past and present at the National Center for Forensic Science Jessica Frisch-Daeillo, Caitlin Kneapler, Erin Waddell, Katie White, Kelly McHugh Dana-Marie Dennis and Allie Flores for their invaluable support and encouragement. I am also indebted to lot of other people who have stood by me at all times and it is to them I also owe my deepest gratitude. My chawl friends: Yogesh Shetty, Nilesh Satam, Jayshree Shinde and Pravin Poojari. My school mates: Umesh Shinde and Sanjeev Mehra. My Junior college friend, Sadique Mohammed Shafat. My B.S. mates: Mandar Sawant, Raju Banushe, Dominic Fernandes, Santosh Sukumaran Irada, Sujata Elsangi, Muthurajan Palani, Arif Khan and Rajesh Bhadale. My M.S. mates: Girish Barot, Gauri Nayak, Santosh Pandey, Arvind Pandey, Rahul Edwankar, Chitra Edwankar, Pravith Warrior, Pramod, Hemant Sharma and Randhir Yadav. My work place friends at Ruia College and Therapeutic Drug Monitoring Laboratory: Krishna Agarwal, Ganesh Patil, Vishal Patil, Prasad Dasalkar and Rahul Berde. My friends and seniors at IPCA Laboratories: Deepti Ayyar, Shweta Shah, Neha Jariwala,

Shankar Patil, Pradeep and Rajashri. My friends from FL: Amar Patel, Sushant Bokil, Ranjit Deshpande, Himanshu Saxena, Chetak Patel, Saral Shah, Atul Asati, Gautam Medhi, Pankaj Kadwani, Prabhu Doss Mani, Simranjeet Singh, Jyoti Katoch, Karthika Nair-Salvi, Aditya Kolli, Jayantho Das, Krishnaveni, Meghal Parikh, Prachi Dalal, Raj Gautam, Sandesh Sankarappa, and Siddharth Banerjee. My sisters: Seema Pandey, Pancy Patel, Neha Panara, Suchi Dwivedi, Rupam Sharma and Junmi Saikia. My dearest students: Abishek Sawant, Riyaz Taj, Akhilesh Aynipully, Shaikh Nasrin Begum and Prashanthi Seelam. My guardians: Srinu Mama, Palak Patel, Sonal Patel, Santosh Amin (Late), Chandan Saikia and Surabhi Saikia. My Teachers: Dr Sheikh, Dr. Vidyagauri Lele, Dr. Vijay Dabholkar, and Dr. Kiran Mangaonkar. Finally, I would like to thank my parents for their constant prayers, unconditional love and encouragement during this exciting journey.

## TABLE OF CONTENTS

LIST OF FIGURES .....	x
LIST OF TABLES .....	xiv
PROJECT 1: APPLICATION OF TWO DIMENSIONAL CORRELATION SPECTROSCOPY TO STUDY MASS SPECTRAL DATA OF SIMPLE MOLECULES.....	1
CHAPTER 1: INTRODUCTION.....	2
1.1. Project Overview .....	2
1.2. Principles of Generalized Two-Dimensional Correlation Spectroscopy .....	5
1.2.1. General Scheme .....	5
1.2.2. Properties of Generalized Two-Dimensional Correlation Spectra .....	7
CHAPTER 2: BACKGROUND.....	13
2.1. Quadrupole Ion Trap Mass Spectrometry.....	13
2.1.1. Instrumentation .....	13
2.1.2. Ion Motion in Quadrupole Field .....	16
2.1.3. Resonant Excitation and Ion Ejection.....	21
2.2. Collision-Induced Dissociation.....	21
2.2.1. Tandem Mass Spectrometry .....	22
2.2.2. Elucidation of Dissociation Pathways.....	25
2.2.3 Previous Studies of Dissociation Pathways by 2DCOS .....	27
CHAPTER 3: EXPERIMENT.....	47
3.1. Gas Chromatography Tandem Mass Spectrometry of n-butylbenzene .....	48
3.2 Simple Kinetic Model.....	49
3.3: Data Analysis for 2DCOS Application.....	51
CHAPTER 4: RESULTS AND DISCUSSION.....	53
4.1: 2DCOS Analysis of n-butylbenzene.....	53
4.1.1. Varying CID Energy at Constant Excitation Time .....	55
4.1.2. Varying Excitation Time at Constant CID Energy .....	63
4.2: 2DCOS Analysis of Kinetic Model .....	68
CHAPTER 5: CONCLUSIONS .....	74
5.1. Significance .....	74
5.2. Future Work.....	75
PROJECT 2: INVESTIGATIVE STUDY OF FORMATION OF PYROLYSIS PRODUCTS FROM CONTROLLED BURNS TO AID IN FIRE DEBRIS ANALYSIS.....	76
CHAPTER 6: INTRODUCTION.....	77
6.1. Overview of Fire Debris Analysis .....	77
6.2. Overview of Interfering Products .....	77
6.3. Overview of Pyrolysis .....	78
6.3.1. Random Scission.....	79



6.3.2. Side-group Scission .....	80
6.3.3. Depolymerisation .....	81
6.4. Purpose of Research.....	82
CHAPTER 7: FIRE DEBRIS ANALYSIS.....	85
7.1. Collection of Fire Debris. ....	85
7.2. Extraction of ILR .....	86
7.2.1. Solvent Extraction.....	86
7.2.2. Dynamic Headspace Concentration .....	87
7.2.3. Passive Headspace Concentration.....	87
7.2.4. Headspace Concentration Using Solid Phase Micro Extraction (SPME).....	89
7.3. Detection of ILR .....	90
7.3.1. Gas Chromatography-Mass Spectrometry (GC-MS).....	90
7.3.2. Interpretation of Results.....	93
CHAPTER 8: CONTROLLED BURNS .....	96
CHAPTER 9: MATERIALS AND METHODS .....	101
9.1: Controlled Heating in Furnace: .....	101
9.1.1. Investigation of New Products Formed from Co-Pyrolysis.....	105
9.2: Controlled Heating in Paint Cans .....	108
9.2.1: Normal Destructive Distillation Method (NDDM) .....	108
9.2.2: Destructive Distillation No Condensate Method (DDNCM) .....	110
9.2.3: Residue and Condensate Analysis .....	111
9.3: Controlled Heating in Flat Steel Pans.....	115
9.3.1: Top-Heat Pan .....	116
9.3.2: Bottom-Heat Pan.....	118
9.4: Time Study of Pyrolysis Products. ....	120
9.5: Time Study and Quantitative Analysis .....	122
CHAPTER 10: RESULTS AND DISCUSSIONS .....	125
10.1: Controlled Burns in Furnace.....	125
10.1.1: Pyrolysis of PS at 1, 5, and 8 Minutes .....	126
10.1.2: Pyrolysis of PVC at 1, 5, and 8 Minutes.....	129
10.1.3: Pyrolysis of PB at 1, 5, and 8 Minutes.....	132
10.1.4: Co-Pyrolysis of PS and PVC .....	133
10.1.5: Co-Pyrolysis of PS and PB .....	140
10.1.6: Summary of 1B and 2B Experiments from (PS+PVC) and (PS+PB) .....	146
10.2: Controlled Burns in Paint Cans .....	147
10.2.1: Pyrolysis of PS in Paint Can .....	148
10.2.2: Pyrolysis of PVC .....	150
10.2.3: Co-Pyrolysis of PS and PVC .....	151
10.2.4: Comparison of PS and PVC 1B Experiments from Furnace and Paint Can.....	154
10.2.5: Pyrolysis of Yellow Pine (YP).....	154
10.3: Controlled Heating in Steel Pans .....	157
10.3.1: Pyrolysis of Yellow Pine .....	158

10.3.2: Pyrolysis of Nylon Carpet and Padding.....	160
10.4: Time Study and Quantitative Analysis .....	162
10.4.1: Yellow Pine with Hydrocarbons by NDDM.....	162
10.4.2: Yellow Pine with Hydrocarbons by Top-Heat Method .....	164
10.4.3: Yellow Pine with Hydrocarbons by Bottom-Heat Method .....	165
10.4.4: Time Study of Nylon Carpet and Padding with Hydrocarbons .....	166
10.4.5: Nylon Carpet and Padding with Hydrocarbons by Top-Heat Method .....	168
10.4.6: Nylon Carpet and Padding with Hydrocarbons by Bottom-Heat Method.....	169
CHAPTER 11: CONCLUSION .....	171
11.1. Significance .....	171
11.2. Future Work.....	172
APPENDIX: COPYRIGHT PERMISSIONS.....	173
REFERENCES .....	185

## LIST OF FIGURES

Figure 1: Schematic diagram of cross section of quadrupole ion trap.....	14
Figure 2: Shapes of potential surface: (a) ion position accelerating away from the trap center at the r.f. phase; (b) ion position accelerating towards the center .....	15
Figure 3: Stability diagram representing $q_z$ axis intersecting the $\beta z = 1$ boundary at $q_z = 0.908$ .....	20
Figure 4: Internal energy distribution and formation of product ions .....	24
Figure 5: (a) and (b) represent the schematic of MEK and $d_3$ -MEK dissociation pathways.....	31
Figure 6: Schematic representation of TES dissociation pathway.....	32
Figure 7: The coherence spectral intensities and variation in rate constants .....	32
Figure 8: Pictorial representation of model 2 (Figure 7), parallel with $k_{ab} = 1$ and $k_{ac} = 1$ : (a) plot of concentration vs time; (b) synchronous spectrum; (c) asynchronous spectrum; (d) coherence spectrum.....	34
Figure 9: Pictorial representation of model 5 (Figure 7), consecutive with $k_{ab} = 1$ and $k_{bc} = 1$ : (a) plot of concentration vs time; (b) synchronous spectrum; (c) asynchronous spectrum; (d) coherence spectrum.....	36
Figure 10: Pictorial representation of model 7 (Figure 7), mixed with $k_{ab} = 1$ , $k_{ac} = 1$ and $k_{bc} = 1$ : (a) plot of concentration vs time; (b) synchronous spectrum; (c) asynchronous spectrum; (d) coherence spectrum .....	38
Figure 11: Pictorial representation of model 8 (Figure 7), mixed resembling consecutive with $k_{ab} = 1$ , $k_{ac} = 0.1$ and $k_{bc} = 1$ : (a) plot of concentration vs time; (b) synchronous spectrum; (c) asynchronous spectrum; (d) coherence spectrum. ....	39
Figure 12: Pictorial representation of model 9 (Figure 7), mixed resembling parallel with $k_{ab} = 1$ , $k_{ac} = 1$ and $k_{bc} = 0.1$ : (a) plot of concentration vs time; (b) synchronous spectrum; (c) asynchronous spectrum; (d) coherence spectrum .....	40
Figure 13: Pictorial representation of MEK: (a) breakdown curve as a function of excitation time; (b) breakdown curve of collision induced dissociation energy; (c) coherence spectrum as a function of excitation time; (d) coherence spectrum as a function of collision induced dissociation energy. ....	43

Figure 14: Pictorial representation of d <sub>3</sub> -MEK: (a) breakdown curve as a function of excitation time; (b) breakdown curve of collision induced dissociation energy; (c) coherence spectrum as a function of excitation time; (d) coherence spectrum as a function of collision induced dissociation energy. ....	44
Figure 15: Pictorial representation of TES: (a) breakdown curve as a function of excitation time; (b) coherence spectrum.as a function of excitation time .....	46
Figure 16: (a) Dissociation scheme for a simple kinetic model representing n-butylbenzene; (b) dissociation products of precursor ion <i>m/z</i> 134.....	50
Figure 17: EI mass spectra of n-butylbenzene collected by varying CID energy (0.0-1.8)V at 11 ms excitation time .....	54
Figure 18: 2DCOS analysis of varying CID energy and constant excitation time (11 ms): (a) breakdown curve of normalized intensity vs CID energy; (b) synchronous spectrum; (c) asynchronous spectrum; (d) coherence spectrum. ....	57
Figure 19: 2DCOS analysis of varying excitation time and constant CID energy (0.6 V): (a) breakdown curve of normalized intensity vs excitation time (ms); (b) synchronous spectra; (c) asynchronous spectra; (d) coherence spectra. ....	64
Figure 20: 2DCOS analysis of kinetic model: (a) breakdown curve of normalized intensity vs time (ms); (b) synchronous spectra; (c) asynchronous spectra; (d) coherence spectra.....	69
Figure 21: Random scission demonstrated using polyethylene.....	80
Figure 22: PVC representing side-group scission mechanism .....	81
Figure 23: Polymethacrylate undergoing depolymerisation to yield monomer.....	82
Figure 24: Passive headspace adsorption (a) paper clip holding activated charcoal strip; (b) heating device for adsorption of volatiles onto charcoal strip .....	88
Figure 25: Pictorial representation of gas chromatography mass spectrometry (GC-MS).....	91
Figure 26: Schematic representation of experimental setup for generating pyrolysis reference samples using a tube furnace .....	101
Figure 27: Elution of vapors (pyrolysates) with pentane for GC-MS analysis.....	103
Figure 28: Residue analysis .....	104
Figure 29: Pyrex vial with vapors condensed at the front end.....	105
Figure 30: Pictorial representation of one-boat and two-boat experiments .....	106

Figure 31: Analysis of residues from 2B experiment .....	107
Figure 32: Normal destructive distillation method .....	109
Figure 33: Destructive Distillation No Condensate Method (DDNCM) .....	110
Figure 34: Schematic representation of Condensate and Residue Analysis .....	112
Figure 35: Pictorial representation of paint-cans containing residues generated by NDDM and DDNCM.....	113
Figure 36: Pictorial representation of paint-cans containing condensates and residues investigated separately .....	114
Figure 37: Experimental setup for controlled burns by Top-Heat method utilizing steel pan ...	116
Figure 38: Aluminum boat carrying nylon carpet and padding for Top-Heat method.....	117
Figure 39: (a) Experimental setup for controlled burns by Bottom-Heat method utilizing steel pan; (b) Nylon carpet and padding on aluminum boat for Bottom-Heat method...	119
Figure 40: Pictorial representation of time study experiments for yellow pine.....	121
Figure 41: Pictorial representation of time study experiments for nylon carpet and padding ....	122
Figure 42: List of standards used for quantification .....	123
Figure 43: Chromatographic results of PS (a) Vapors, (b) Condensate, (c) Residue. ....	126
Figure 44: Chromatographic results of PVC (a) Vapors, (b) Condensate, (c) Residue.....	129
Figure 45: Chromatographic results of PB (a) Vapors, (b) Condensate, (c) Residue.....	132
Figure 46: Chromatographic results from PS and PVC (1B) experiment (a) Vapors, (b) Condensate, (c) Residue.....	134
Figure 47: Chromatographic results from PS and PVC (2B) experiment (a) Vapors, (b) Condensates. ....	137
Figure 48: Chromatographic results from PS and PVC (2B) experiment (a) PS residue from PS and PVC 2B experiment (b) PVC residue from PS and PVC 2B experiment..	139
Figure 49: Chromatographic results from PS and PB (1B) experiment (a) Vapors, (b) Condensate, (c) Residue.....	141

Figure 50: Chromatographic results from PS and PB (2B) experiment (a) Vapors, (b) Condensate .....	144
Figure 51: Chromatographic results from PS and PB (2B) experiment (c) PS residue from PS and PB 2B experiment (d) PB residue from PS and PB 2B experiment .....	145
Figure 52: Chromatographic results of PS from (a) NDDM (b) DDNCM, (c) Condensate (d) Residue .....	148
Figure 53: Chromatographic results of PVC from (a) NDDM (b) DDNCM, (c) Condensate (d) Residue .....	150
Figure 54: Chromatographic results of PS and PVC 1B from (a) NDDM (b) DDNCM, (c) Condensate (d) Residue .....	152
Figure 55: Chromatographic results of yellow-pine from (a) NDDM (b) DDNCM, (c) Condensate (d) Residue .....	155
Figure 56: Chromatographic results of YP by (a) Top-Heat Method (b) Bottom-Heat method.....	158
Figure 57: Chromatographic results of combination of nylon carpet and padding by (a) Top-Heat Method (b) Bottom-Heat method.....	160
Figure 58: Chromatograms and quantification results from time study experiment of yellow-pine and HC mixture by NDDM .....	162
Figure 59: Chromatograms and quantification results from time study experiment of yellow-pine and HC mixture by Top-Heat method .....	164
Figure 60: Chromatograms and quantification results from time study experiment of yellow-pine and HC mix by Bottom-Heat method .....	165
Figure 61: Chromatograms and quantification results from time study experiment of nylon carpet, padding and HC mix by NDDM .....	166
Figure 62: Chromatograms and quantification results from time study experiment of nylon carpet, padding and HC mix by Top-Heat method .....	168
Figure 63: Chromatograms and quantification results from time study experiment of nylon carpet, padding and HC mix by Bottom-Heat method .....	169

## LIST OF TABLES

Table 1: Sequential Order Analysis of Cross-Peaks .....	10
Table 2: Sequential Order Rule Based on Coherence Spectra.....	11
Table 3: Schematic of Dissociation Schemes for Simple Kinetic Models .....	30
Table 4: Rate Constants for the Simple Kinetic Model Representing Mixed Dissociation Scheme .....	50
Table 5: Noda's Sequential Order Rules to Determine Product Ion Formation as a Function of Varying CID Energy at Constant Excitation Time .....	60
Table 6: Noda's Sequential Order Rules to Determine Product Ion Formation as a Function of Varying Excitation Time at Constant CID Energy .....	66
Table 7: Noda's Sequential Order Rules to Determine Product-Ion Formation as a Function of Applied Perturbation for Modelled Data.....	72
Table 8: Compounds and Their Retention Times from Pyrolysis of PS in Furnace.....	126
Table 9: Compounds and Their Retention Times from Pyrolysis of PVC in Furnace .....	130
Table 10: Compounds and Their Retention Times from Pyrolysis of PB in Furnace .....	132
Table 11: Compounds and Their Retention Times from Pyrolysis of PS and PVC 1B Experiment in Furnace .....	135
Table 12: Compounds and Their Retention Times from Pyrolysis of PS and PVC 2B Experiment in Furnace .....	138
Table 13: Compounds and Their Retention Times from Pyrolysis of PS and PB 1B Experiment in Furnace .....	142
Table 14: Identified Compounds and Their Retention Times from Controlled Heating of PS Using Paint Cans. ....	149
Table 15: Identified Compounds and Their Retention Times from Controlled Heating of PVC Using Paint Cans .....	151
Table 16: Identified Compounds and Their Retention Times from Controlled Heating of PS and PVC 1B Experiment Using Paint Cans .....	153

Table 17: Identified Compounds and Their Retention Times from Controlled Heating of YP in Paint Cans. ....	156
Table 18: Identified Compounds and Their Retention Times from Controlled Heating of YP by Top-Heat and Bottom-Heat Methods .....	158
Table 19: Identified Compound and Retention Times Match from Controlled Heating of Combination of Nylon Carpet and Padding from Top-Heat and Bottom-Heat methods. ....	160
Table 20: Identified Compounds and Their Retention Times from Yellow-Pine and HC Mix .....	163
Table 21: Identified Compound and Their Retention Times from Nylon Carpet, Padding, and HC Mix.....	167



**PROJECT 1: APPLICATION OF TWO DIMENSIONAL CORRELATION  
SPECTROSCOPY TO STUDY MASS SPECTRAL DATA OF SIMPLE  
MOLECULES**

# CHAPTER 1: INTRODUCTION

## 1.1. Project Overview

To investigate the average internal energy deposited into an ion upon resonant excitation in an ion trap, n-butylbenzene is extensively used for mass spectral study. Upon activation in tandem experiments, the molecular ion of n-butylbenzene ( $m/z134$ ) undergoes competitive dissociation via two processes. At low activation energy ( $\sim 1.1$  eV), the molecular ion undergoes McLafferty rearrangement to yield  $C_7H_8^{+}$  ( $m/z92$ ), while at higher activation energy ( $\sim 1.7$  eV), the molecular ion undergoes direct cleavage of  $C_3H_7^{\bullet}$ , resulting in the formation of  $C_7H_7^{+}$  ( $m/z91$ ). The structures of the product ions  $m/z92$  and  $m/z91$  resulting from the dissociation of n-butylbenzene have been identified by various mass spectrometry techniques<sup>1</sup>. Because of its well-characterized energetics upon activation and its simple fragmentation mechanisms, n-butylbenzene is often referred to as the “thermometer molecule”<sup>2</sup>.

Charge exchange mass spectrometry was performed in an earlier study to gauge the average internal energy of the n-butylbenzene molecular ion<sup>3</sup>. In one study, photodissociation of n-butylbenzene was performed in an ion cyclotron resonance ion trap in conjunction with Fourier-transform and double-resonance techniques to determine the ratio of the product ions  $m/z92$  and  $m/z91$  at several wavelengths. The value for the branching ratio was obtained from the analysis of effect of thermal excitation of ions as a function of ion internal energy<sup>4</sup>. Baer et al. studied photoelectron photoion coincidence (PEPICO) along with time of flight (TOF) mass spectrometry to investigate the dissociation dynamics of n-butylbenzene<sup>5</sup>. Levson et al.

performed collisional activation and charge stripping excitation of n-butylbenzene in a magnetic sector mass spectrometer and described the rearrangement process that yielded  $m/z92$ <sup>6</sup>. Computational methods using statistical modeling techniques have also been obtained under a simplified fragmentation scheme<sup>6b, 7</sup>.

Most studies carried out to investigate the dissociation of n-butylbenzene were based on the fact that the formation of the product ions  $m/z92$  and  $m/z91$  was a competitive process and the ratio of  $m/z91/92$  abundance was a function of average internal energy deposited into the parent ion ( $m/z134$ ). However, in 1996, March et al. performed double resonance experiments using a waveform generator and demonstrated that upon resonant excitation of the n-butylbenzene molecular ion,  $m/z92$  possesses sufficient kinetic energy, internal energy, or both to undergo further fragmentation to produce  $m/z91$  via loss of a hydrogen atom. Therefore, for a molecule like n-butylbenzene, three dissociation pathways can be considered. The first dissociation pathway is where the formation of primary product ions  $m/z92$  and  $m/z91$  from the precursor ion  $m/z134$  is a parallel process (parallel dissociation). The second dissociation pathway is where the formation of  $m/z91$  is a result of consequent fragmentation of  $m/z92$  (consecutive dissociation); in this case  $m/z91$  would be a secondary product ion. The third dissociation pathway is a combination of parallel and consecutive dissociation, termed mixed dissociation<sup>1, 8</sup> where one of the primary product ions can have sufficient internal energy to undergo further fragmentation.

In addition to double resonance experiments to investigate dissociation pathways in mass spectrometry, methods such as stored waveform inverse fourier transform (SWIFT)<sup>9</sup> and

statistical test of equivalent pathways (STEP)<sup>10</sup> have been reported in literature. Both these methods are based on the interpretation of breakdown curves generated using ion intensities. According to the SWIFT method, primary product ions and secondary product ions are related if the intensity of the primary product ions decreases and the intensity of the secondary product ions increases by the same magnitude. While this method is good for determining consecutive dissociation pathways, the interpretation may be difficult when the number of dissociation products is large with varying intensities. The STEP method uses Dixon's q-test to assign primary and secondary products ions. The drawback of this method is that it cannot identify products that result from mixed dissociation where some product ions may have resulted from primary and secondary dissociation pathway, respectively<sup>8</sup>.

While the above methods were effective in elucidating dissociation pathways in mass spectrometry studies, they require specialized modification of instruments to obtain spectral intensities. Another technique that has been reported to study dissociation pathways is based on the application of generalized two dimensional correlation spectroscopy (2DCOS) to kinetic modeled data of parallel<sup>11</sup> and consecutive reaction<sup>12</sup> schemes. This method is a perturbation-based technique that yields synchronous and asynchronous spectra, which are then used to obtain coherence spectra by taking the ratio of asynchronous to synchronous correlation intensities to characterize the modelled reaction schemes.

In this dissertation research, the application of generalized 2DCOS has been demonstrated to elucidate the fragmentation mechanism of n-butylbenzene. The applied perturbations were

collision induced dissociation (CID) energy and excitation time also referred to as excitation energy and excitation time respectively. The mass spectral intensities for the precursor and product ions were obtained by keeping one perturbation constant and varying the other and vice-versa. From the synchronous and asynchronous correlation intensities, coherence spectra were obtained to characterize the dissociation mechanisms. To corroborate the dissociation mechanism of n-butylbenzene, the technique of generalized 2DCOS was also applied to study modeled data and other simple molecules such as methylethylketone (MEK), deuterated MEK (d3MEK), and tetraethylsilane (TES)<sup>8</sup>. The primary objective of this research was to demonstrate the ability of the 2DCOS technique to elucidate the dissociation mechanisms in MS<sup>2</sup> experiments without any instrument modification.

## 1.2. Principles of Generalized Two-Dimensional Correlation Spectroscopy

### 1.2.1. General Scheme

In 2DCOS when an additional external perturbation is applied to stimulate the system during spectroscopic measurement, the measured spectrum undergoes a distinct change in its overall response and is referred to as a dynamic spectrum. The perturbations applied can be thermal, magnetic, electrical, chemical, mechanical, or even acoustic, as each perturbation has a unique effect on the system of interest<sup>13</sup>. For a perturbation-induced variation of a spectral intensity  $y(m, t)$  observed at a fixed interval of external variable  $t$  between  $T_{min}$  and  $T_{max}$ , the dynamic spectrum  $\tilde{y}(m, t)$  is defined by equation 1.1 as

$$\tilde{y}(m, t) = y(m, t) - \bar{y}(m) \quad \text{for} \quad T_{min} \leq t \leq T_{max} \quad (1.1)$$

$$0 \quad \text{otherwise}$$

Here  $\bar{y}(m)$  represent the reference spectrum of the system which can be simply set to *zero* or in most cases, the reference spectrum may be the average of  $y(m_i)$  given by equation 1.2.

$$\bar{y}(m) = \frac{1}{T_{max} - T_{min}} \int_{T_{min}}^{T_{max}} y(m, t) dt \quad (1.2)$$

The underlying principle of the 2DCOS technique is a quantitative comparison of spectral intensity variations along the perturbation variable  $t$  between  $T_{min}$  and  $T_{max}$ . Cross-correlation analysis of such a set of dynamic spectra yields 2D correlation spectra defined by Equation 1.3:

$$X(m_1, m_1) = \langle \tilde{y}(m_1, t) \cdot \tilde{y}(m_2, t') \rangle \quad (1.3)$$

Here  $\langle \rangle$  denotes the cross-correlation function along the perturbation variable  $t$ , and  $X(m_1, m_1)$  represents the intensity of the 2D correlation, which is the measure of similarity or dissimilarity of spectral intensity variations measured at two different spectral variables,  $m_1$  and  $m_2$ . Equation 1.3 can be further simplified by mathematically treating it as a complex number function comprising a real and imaginary part represented by Equation 1.4.

$$X(m_1, m_2) = \Phi(m_1, m_2) + i\Psi(m_1, m_2) \quad (1.4)$$

The overall similarities or in-phase trends between the two separate intensity variations measured at the spectral variables  $m_1$  and  $m_2$  are represented by  $\Phi(m_1, m_2)$  and referred to as synchronous 2D correlation intensity. Similarly, the overall dissimilarities or out-of-phase trends are represented by  $\Psi(m_1, m_2)$ , referred to as asynchronous 2D correlation intensity<sup>14</sup>.

### 1.2.2. Properties of Generalized Two-Dimensional Correlation Spectra

The two components of the 2D correlation intensity, synchronous and asynchronous, can be further simplified to yield a more useful spectrum known as the generalized 2D correlation spectrum. For a given set of dynamic spectra expressed in matrix notation collected along the variable  $t$  at every equally spaced increment, the synchronous 2D correlation intensity can be obtained by pre-multiplying the dynamic spectrum matrix by its transpose and dividing by  $k-1$  (see equation 1.5), where  $k$  denotes the number of applied perturbations.

$$\Phi(m_1, m_2) = \frac{1}{k-1} \tilde{y}(m_1)^T \tilde{y}(m_2) \quad (1.5)$$

Mathematically, the peaks observed at diagonals are auto-correlated and are therefore referred to as auto-peaks. The magnitude of the auto-peak intensity is always positive and represents the overall extent to which the spectral intensity varies for a specific variable  $m$ . In other words, auto-peaks will be observed for any region in the spectrum undergoing significant intensity

change. The off-diagonal peaks observed in the spectrum are referred to as cross-peaks, and they represent the coincidental changes observed at different spectral variables  $m_1$  and  $m_2$ . The coincidental changes observed in the 2D synchronous spectrum can be interpreted based on the sign of the cross-peak intensity. If the sign of the synchronous crosspeaks is positive, the intensities of the spectral variables at  $m_1, m_2$  are either increasing or decreasing together; conversely, if the sign of the synchronous cross-peaks is negative, the spectral intensities observed at the spectral variables  $m_1$  or  $m_2$  are changing in opposite directions<sup>15</sup>.

While asynchronous 2D correlation intensity can be computed in many ways, most of them are complicated however, the simplest and the most computationally efficient method to obtain a 2D asynchronous spectrum is given by equation 1.6

$$\Psi(m_1, m_2) = \frac{1}{k-1} \tilde{y}(m_1)^T N_{jk} \tilde{y}(m_2) \quad (1.6)$$

where  $N_j = 0 \quad (j = k)$

$$\frac{1}{\pi(k-j)} \quad (j \neq k)$$

It can be observed from equation 1.6, that the expression for obtaining asynchronous 2D correlation intensity is similar to the synchronous 2D correlation expression except for the term  $N_{jk}$ , representing a Hilbert-Noda transformation matrix where  $j$  and  $k$  represent the row and column, respectively.



The asynchronous 2D correlation spectrum is antisymmetric with respect to the diagonal and is characterized by the absence of auto-peaks. Since it represents the out-of-phase trends observed at two different spectral variables  $m_1$  or  $m_2$ , its advantage lies in its ability to differentiate between overlapped signals arising from different origins. The signs of the asynchronous cross-peak intensities can take either positive or negative values. Positive asynchronous cross-peak intensity implies that the change at  $m_1$  occurs predominantly before  $m_2$  in the sequential order of  $t$ ; negative asynchronous cross-peak intensity implies that  $m_1$  occurs after  $m_2$ . The above rules of interpretation are reversed if  $\Phi(m_1, m_2) < 0$ . If the intensity of the cross-peak observed at  $m_1$  and  $m_2$  is zero, the spectral intensity change observed at the respective spectral variables occurs at the same perturbation. Similarly if the intensity of the cross-peak observed at the same spectral variables  $m_1$  and  $m_2$  in the synchronous spectra is zero, then no relationship can be drawn for the spectral intensity change based on perturbation<sup>15-16</sup>. The rules for determining the order in which a spectral event occurs based on the signs of synchronous and asynchronous peak intensity are referred to as sequential order analysis and are summarized in Table 1. It should be noted that the signs of 2D correlation spectral intensities may change depending upon the order of matrix multiplication<sup>8, 16</sup>.

Table 1: Sequential Order Analysis of Cross-Peaks

$\Phi(m_1, m_2)$	$\Psi(m_1, m_2)$	Sequential order of spectral events
+	+	$m_1$ before $m_2$
-	-	$m_1$ before $m_2$
+	-	$m_2$ before $m_1$
-	+	$m_2$ before $m_1$

The relationship between synchronous and asynchronous 2D correlation intensities can also be analyzed through global correlation phase angle, which is defined as the arctangent of the ratio of asynchronous to synchronous correlation intensities as given by Equation 1.7.

$$\Theta(m_1, m_2) = \arctan \frac{\Psi(m_1, m_2)}{\Phi(m_1, m_2)} \quad (1.7)$$

Global phase angle is similar to the concept of phase difference between two responses observed at two different spectral variables. The process of obtaining synchronous and asynchronous 2D correlation intensities is complicated, and one of the requirements is normalization of amplitude; however, the advantage of using the global phase angle is that the effects of amplitudes cancel out during the division of asynchronous to synchronous 2D correlation intensities. This concept can also be extended to study non-periodic signals having complicated waveforms. In generalized 2DCOS, the term coherence spectrum is used, which is similar to the concept of

global phase angle. The coherence spectrum is denoted by  $R$  and is defined as the ratio of asynchronous to synchronous 2D spectra given by equation 1.8.

$$R = \frac{\Psi(m_1, m_2)}{\Phi(m_1, m_2)} \quad (1.8)$$

The signs of the peaks observed in the coherence spectrum can be positive or negative. Based on their signs the sequential order rules may be applied for interpretation of a spectral event as summarized in Table 2

Table 2: Sequential Order Rule Based on Coherence Spectra

$\Theta(m_1, m_2)$	Sequential order of spectral events
+	$m_1$ before $m_2$
-	$m_2$ before $m_1$
0	No peak observed

It should be noted that although the signs of the 2D correlation intensities determine the sequential order of spectral events, the signs may change depending upon the order of matrix multiplication to obtain synchronous, asynchronous, and coherence 2D correlation intensities. In this dissertation research, the spectral variables under study are ions corresponding to precursor and products produced from mass spectrometry experiments of compounds. The 2D correlation

spectra obtained from the application of the 2DCOS technique was used to analyze the relationship between precursor and product ions, referred to as precursor-product ions peak, and between product ions, referred to as product-product peaks. A detailed study is discussed in the next chapter.

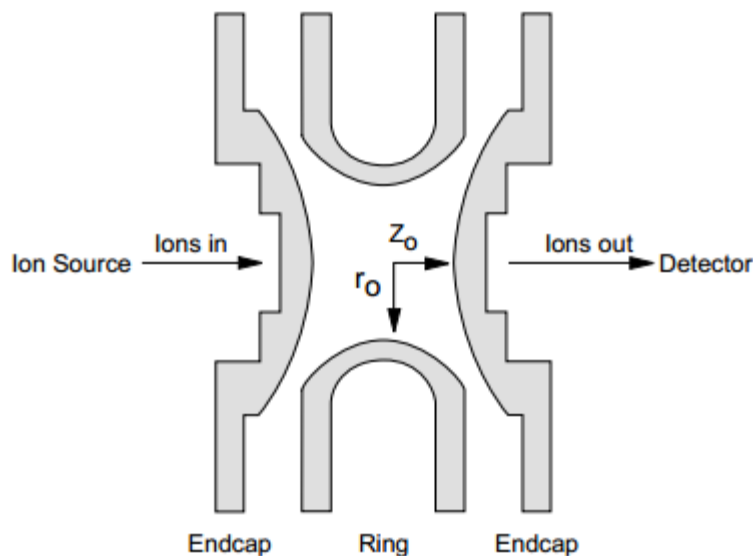
## CHAPTER 2: BACKGROUND

### 2.1. Quadrupole Ion Trap Mass Spectrometry

Mass spectrometers equipped with quadrupole ion traps (QIT) are commonly used instruments due to their high sensitivity, compactness, easy operation, and low cost<sup>17</sup>. QIT is basically a three-dimensional analogue of a linear quadrupole mass filter allowing several mass selectivity operations in succession<sup>18</sup>. As a result, multiple stages of tandem mass spectrometry experiments can be performed in a relatively simple way. QIT was invented in 1960 by Paul and Steinwedel, and their pioneering work was honored with a Nobel Prize in Physics in 1989<sup>19</sup>. The relatively simple operations in QIT hyphenated with gas and liquid chromatography has led to the adoption of these instruments in both academia and industries.

#### *2.1.1. Instrumentation*

QIT comprises two end-cap electrodes and one ring electrode, all having hyperboloid geometry. The end-cap electrodes are virtually identical, resembling small inverted saucers, while the ring electrode resembles a serviette positioned symmetrically between the two end-cap electrodes. The hyperboloid geometry of the electrodes was designed to establish an ideal quadrupole field when the ring electrode is subjected to r.f. potential while the two end-caps electrodes are grounded. Figure 1 shows a schematic of the cross-sectional view of QIT, where  $r_0$  represents the radius of the ring electrode and  $2z_0$  represents the distance between the end-cap electrodes along the axis of the ion trap<sup>20</sup>.



(Note: Figure adapted with permission from “Ion Trap Mass Spectrometry” by R.Graham Cooks; see Appendix)

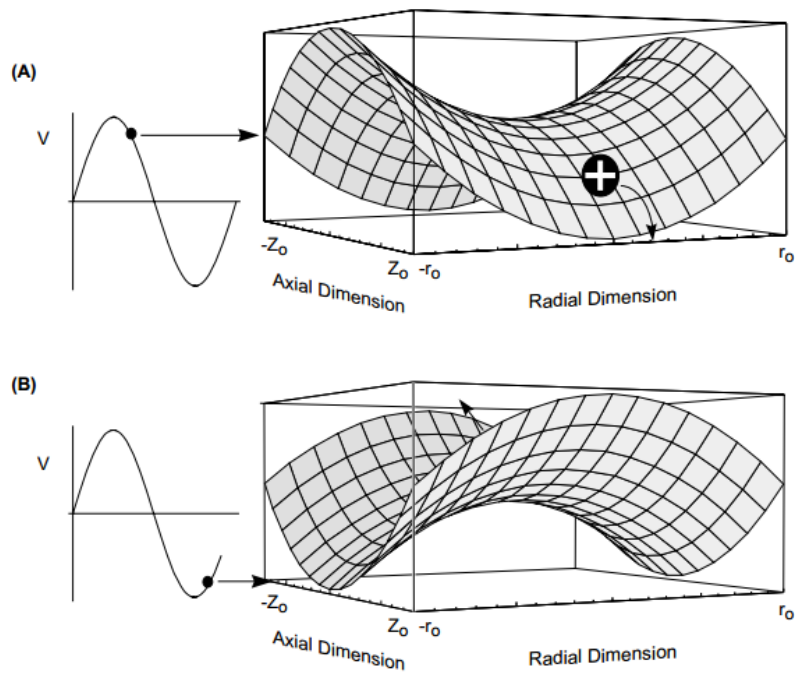
Figure 1: Schematic diagram of cross section of quadrupole ion trap

For an ideal quadrupole field, the relationship between the end-cap electrodes distance and the radius of the ring electrode should obey the following condition, represented by Equation 2.1. However, in order for the ions to enter and exit the trap, the two end-cap electrodes require apertures, which may induce distortions in the field geometry. Therefore, to overcome these field distortions, commercially available instruments have modified the ion trap by altering the electrode dimensions, referred to as a stretch ion trap<sup>20</sup>.

$$r_0^2 = 2z_0^2 \quad (2.1)$$

In a quadrupole field, a saddle-shaped potential surface is generated on application of r.f. potential to the ring electrode. Further, the shape of the potential surface is reversed with the

signs of the r.f. potential. In other words, the shape of the potential surface will change with the sinusoidal oscillations of r.f. potential at a given frequency. This change in the shape of the potential surface, which in turn depends upon the sign of r.f. potential, affects the axial and radial motions of the ions in the trap, causing them to focus along one motion while defocussing along the other and vice-versa<sup>18</sup>. Thus, in order for the ions to be trapped they should be confined on the potential surface as though they were trapped in a pseudo-potential well by balancing the focusing and defocusing forces under appropriate conditions.



(Note: Figure adapted with permission from “Ion Trap Mass Spectrometry” by R.Graham Cooks; see Appendix)

Figure 2: Shapes of potential surface: (a) ion position accelerating away from the trap center at the r.f. phase; (b) ion position accelerating towards the center

In QIT the ions formed externally are focused to the center of the ion trap. Ions with low mass to charge ( $m/z$ ) ratio dwell close to the center of the trap, which are further surrounded by ions with the next higher  $m/z$  ratio, and so on. Each of these ions with different  $m/z$  ratios will oscillate at a different frequency. The extraction of ions of low  $m/z$  ratio from the center of the trap in the presence of surrounding ions of high  $m/z$  ratio is not easy, as the ions of low  $m/z$  ratio may experience perturbation due to space charging, resulting in ion signals with poor mass resolution. The resolution is improved by increasing the amplitude of the r.f. frequency applied to the ring electrodes while maintaining the frequency at the end-cap electrodes at a fixed value<sup>20</sup>. As a result the ions with low  $m/z$  ratio near the trap center come into resonance with the fixed frequency at the end-cap electrodes. The effects of resonance is a significant reduction of space charging effect and an increase in the kinetic energy of the ions in the axial direction as they reach the detector in clusters, yielding a higher resolution. This way all the ions are ejected from the trap in order of increasing  $m/z$  ratio by bringing them into resonance successively and impinging upon the detector to create a mass spectrum.

### *2.1.2. Ion Motion in Quadrupole Field*

In a quadrupole field the motion of ions is different from that of field-free regions, magnetic or electric sectors. The dynamics in a quadrupole field are such that the ion experiences a strong restoring force upon its deviation from the center of the trap. To describe the ion motion in a quadrupole field in terms of regions of stability and instability, mathematical solution was obtained by applying second-order linear differentials to Mathieu's original equation, given by equation 2.2.



$$\frac{d^2u}{d\xi^2} + (a_u - 2q_u \cos 2\xi)u = 0 \quad (2.2)$$

Here the three coordinate axes  $x$ ,  $y$ , and  $z$  are represented by  $u$  and  $\xi$  is a dimensionless parameter equal to  $\Omega t/2$ , where  $\Omega$  represents radial frequency of the r.f. potential applied to the ring electrode; and  $t$  denotes time.  $a_u$  and  $q_u$  are additional dimensionless parameters referred to as stability or trapping parameters that describe the stability of ions along the axial and radial directions<sup>20</sup>. For an ion having mass  $m$  and charge  $e$  at a given point in the quadrupole field, the force experienced can be obtained by using the fundamental expression for force, which is the product of mass and acceleration as given by equation 2.3.

$$F = ma = m \frac{d^2x}{dt^2} = -e \frac{\partial \phi}{\partial x} \quad (2.3)$$

Here  $a$  represents the acceleration and  $\phi$  denotes the quadrupole potential at any point in the coordinate axes within the field. The expression for quadrupole potential is given by equation 2.4 below.

$$\phi = \frac{\phi_0}{r_0^2} (\lambda x^2 + \sigma y^2 + \gamma z^2) \quad (2.4)$$

Here the potential applied to the ring electrode is represented by  $\phi_0$  which can be either r.f. potential alone represented by  $V \cos \Omega t$  or in combination with direct current (D.C) potential  $U$ ,

represented by  $U + V \cos \Omega t$  respectively. It can be observed from equation 1.12 that the potential increase quadratically along the x, y, and z coordinates. Also, Laplace condition for any point in an electric field requires the second differential of potential at that point to be equal to zero<sup>21</sup>. When the above conditions are met and differentials are applied to the force experienced by an ion at any point within the coordinate axes, an expression for trapping parameters can be obtained as given by equation 2.5. Here  $a_z$  and  $q_z$  represents the trapping potentials for an ion along the radial and axial directions respectively.

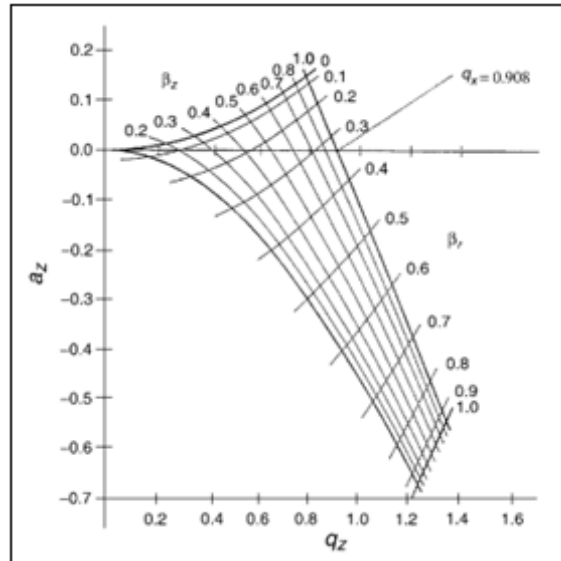
$$a_z = \frac{-8eU}{mr_0^2\Omega^2} \qquad q_z = \frac{4eV}{mr_0^2\Omega^2} \qquad (2.5)$$

Since the ion motion is focused along the axial direction, ion traps mostly use  $q_z$  as the trapping parameter in which trapping can be effected by changing the amplitude  $V$  of the r.f.potential, and D.C. potential is not required. However, it should be noted that in commercial ion traps, since the electrode assembly has a stretched geometry, the trapping parameters are calculated by taking into account the new dimensions where the geometry is stretched by approximately 57 percent<sup>8</sup>. The expressions for trapping parameters in a stretched geometry are represented by equation 2.6 and 2.7 respectively.

$$a_r = \frac{8eU}{m(r_0^2 + 2z_0^2)\Omega^2} \quad q_r = \frac{-4eV}{m(r_0^2 + 2z_0^2)\Omega^2} \quad (2.6)$$

$$a_z = \frac{-16eU}{m(r_0^2 + 2z_0^2)\Omega^2} \quad q_z = \frac{8eV}{m(r_0^2 + 2z_0^2)\Omega^2} \quad (2.7)$$

From equations 1.14 and 1.15, we see that  $a_z = -2a_r$  and  $q_z = -2q_r$ , implying that the stability or trapping parameters along the radial  $r$  and axial  $z$  directions differ by a factor of two. The storage of ions in an ion trap depends on the stability of the ion trajectory in  $r$  and  $z$  directions simultaneously. The stability region in which the trajectory of ion is stable is given by a mathematical solution to Mathieu's equation. Stability regions can be obtained from the stability diagram represented by Figure 3, which is basically a plot of  $a_z$  versus  $q_z$  consisting of characteristic curves also referred to as boundaries<sup>21</sup>.



(Note: Adapted with permission from “Quadrupole ion trap mass spectrometry, a view at the turn of the century” by Raymond E. March, International Journal of Mass Spectrometry, volume 200, issues 1-3, December 2000, Pages 285-312; see Appendix)

Figure 3: Stability diagram representing  $q_z$  axis intersecting the  $\beta_z = 1$  boundary at  $q_z = 0.908$

These boundaries comprise characteristics values corresponding to a new trapping parameter  $\beta_z$  given by Equation 2.8.

$$\beta_z = \sqrt{\frac{q_z^2}{2}} \quad (2.8)$$

The stability diagram is also used to determine the low mass cut off (LMCO) value that is the lowest  $m/z$  ratio that can be stored in the ion-trap. The  $q_z$  value of 0.908 corresponding to the point of intersection at  $\beta_z = 1$  stability boundary on the  $q_z$  axis is used as the working point to calculate the LMCO value.

### 2.1.3. Resonant Excitation and Ion Ejection

The ions confined in QIT can be excited by two secular frequencies, axial and radial. Resonant excitation at axial secular frequency however is frequently used. Excitation of ions can be effected by applying small oscillating potentials in millivolts across the end-cap electrodes, resulting in the movement of ions away from the center of the trap where they experience a greater trapping field. Before the ions are resonantly excited, they are cooled as they collide with helium atoms, resulting in a decrease in kinetic energy. Resonant excitation of ions can also be effected to increase ion kinetic energies for depositing internal energy in ions through collision with helium atoms. Resonant excitation is also used to eject ions by ramping the amplitude of the r.f. potential applied to the ring electrode<sup>22</sup>. This mode of ion ejection is referred to as mass-selective axial instability or simply axial modulation. Ions confined within the ion-trap are associated with a  $q_z$  value. The  $q_z$  values of ions with low  $m/z$  ratio are extended towards the  $\beta_z = 1$  stability boundary, while those having high  $m/z$  ratio have  $q_z$  values near the origin. As mentioned before, at  $\beta_z = 1$  stability boundary, the  $q_z$  axis intersects at a  $q_z$  value of 0.908. As the ions approach this value, the trajectories of trapped ions become unstable axially and are ejected<sup>22</sup>. A mass spectrum is thus obtained when resonantly ejected ions pass through the holes of end-cap electrodes and impinge upon an electron multiplier, resulting in ion signals in the increasing order of  $m/z$  ratio.

### 2.2. Collision-Induced Dissociation

In QIT, the technique of collision-induced dissociation (CID) is frequently used for determining ion structures by applying resonant excitation voltage to selected ionic species. This causes the

ions to move away from the center of the trap to a region of higher potential with an increase in kinetic energy. Consequently, the ions collide with helium atoms, and some of the kinetic energy is converted to ion internal energy. CID is performed with the objective of dissociating the isolated ions to produce fragment ions and trap them. The isolated ions are usually referred to as precursor ions and the fragment ions as product ions. Internal energy deposition in ions during CID is also influenced by the amount of time during which they are subjected to collisions with helium atoms, referred to as excitation time or activation time. Another factor that influences the ion internal energy is collisional cooling, which can be effected by removal of excitation voltage<sup>21</sup>. As a result, ion kinetic energies are quenched more readily than ion internal energies; thus, ions become kinetically relaxed and are focused near the center of the trap. This process allows further deposition of internal energy, which in turn may induce further fragmentation. Although CID remains the most common ion activation technique for inducing fragmentation in tandem mass spectrometry experiments, several other techniques have been used by researchers for ion activation<sup>23</sup>. In this dissertation research, an ion activation technique based on CID was used to induce fragmentation in test molecules; all other activation methods are beyond the scope of this research.

### *2.2.1. Tandem Mass Spectrometry*

The ability to perform a series of mass-selective operations is known as tandem mass spectrometry (MS/MS) or (MS<sup>2</sup>). The objective of the first operation is to isolate ions corresponding to a particular  $m/z$  ratio. In the second operation, the isolated ions are subjected to CID in the presence of a buffer gas, usually helium atoms, to produce fragment ions. Isolated

ions are designated as parent ions or precursor ions; fragment ions are designated as product ions. QIT operates in pulsed mode, and, therefore, successive mass-selective accumulation of ionic species is possible over time, unlike in instruments involving triple quadrupole, where mass-selective operations are carried out in space. The number of collisions during CID between the mass-selected ions and helium atoms is in the few hundreds; as a result, the energy transfer occurring in a single collision is sufficient to access the dissociation pathway corresponding to the lowest activation energy. Similarly the dissociation pathways corresponding to high activation energy can be accessed by alternating periods of excitation and collisional cooling. The above process of isolating ions and subjecting them to CID can be repeated with mass-selected product ions to induce further fragmentation, and so on. Prior to ion activation, the molecule under study is ionized by an electron beam having energy of 70 electron-volts (eV). Consequently some part of the energy slightly greater than the ionization threshold of the molecule is transferred to the molecule to yield a radical ion. This method of ionization is termed electron ionization, and the corresponding mass spectra generated are known as EI spectra. Structural elucidation of unknown molecules can be carried out by careful examination of EI spectra as the majority of classes of compounds have characteristic fragmentation patterns. The abundance and type of products that results from the fragmentation of precursor ion is a function of the total internal energy of the ionized molecule, which in turn may vary depending upon the type of ionization, bath-gas<sup>24</sup>, size of the molecule, and any other techniques that may be adapted to affect the internal energy, such as CID as discussed previously. Since fragmentation is governed by total internal energy, it is imperative to consider the distribution of internal energy of the population of molecular ions designated by  $P(E)$ .

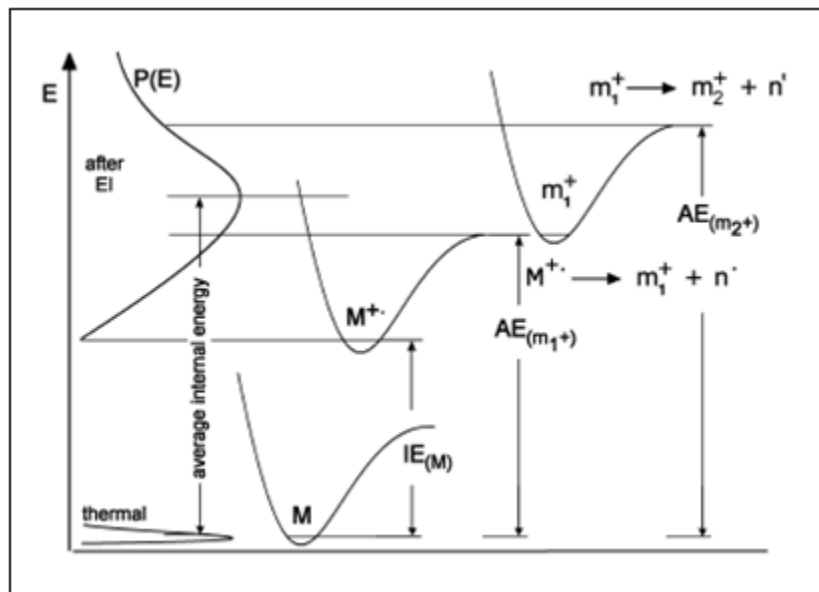


(Figure adapted from *Mass Spectrometry* by J. H. Gross, 2<sup>nd</sup> Edition )

Figure 4: Internal energy distribution and formation of product ions

As per the Frank-Condon diagram represented by Figure 4, upon electron ionization of 70 eV the majority of the molecular ions occupy the vibrationally excited level, which for most of them is higher than the dissociation energy level. Fragmentation of molecular ions represented by  $M^{+\bullet}$  may yield primary product ions represented by  $m_1^+$  or  $m_1^{+\bullet}$  by loss of a radical ion or neutral molecule during fragmentation.

The formation of ions is not governed by one specific internal energy applicable to all ions; instead the energy is distributed in a broad range<sup>25</sup>. This distribution of energy represented by  $P(E)$  applies to a large set of ions as each of these ions is associated with a defined internal energy ranging from a little above ionization energy to approximately 10 eV. The energy of the



excited ions present near the tail of  $P(E)$  fragments to yield primary product ions having energy high enough to undergo further fragmentation to yield secondary products represented by  $m_2^+$ .

### 2.2.2. *Elucidation of Dissociation Pathways*

Most of the analysis carried out for structural elucidation of molecular ions is based on the study of possible dissociation pathways that are responsible for the observed mass spectrum. Although CID remains the most commonly used method for  $MS^n$  experiments to determine dissociation pathways of the fragmentation products, the results observed for  $n=2$  may change with the results observed for higher stages of  $n$ . In  $MS^2$  experiments, primary product ions generally lose their internal energy upon collision with bath gas and are least activated. This effect arises because the primary product ions are no longer in resonance with the voltage applied at the ring electrodes. As seen in Figure 4, the formation of secondary product ions is possible only if the primary product ion has excess internal energy to undergo further fragmentation, yielding secondary product ions.

In this section some of the techniques that have been used for the investigation of dissociation pathways are discussed. Energy resolved mass spectrometry, which is based on the analysis of breakdown curves, is one such method<sup>26</sup>. A breakdown curve is essentially a plot of normalized abundances of the precursor and product ions as a function of internal energy change<sup>8</sup>. Internal energy of the precursor ions can be affected by varying the amplitude of the CID voltage or the amount of time during which the CID energy was applied. Induction periods are usually observed at the onset of the breakdown curves, because internal energy of the precursor ion at

the onset is below the appearance energy of the lowest energy dissociation channel. According to the interpretation of the breakdown curve, the ions are related if corresponding relative abundance changes with the same magnitude. Primary product ions would decrease in intensity, whereas secondary product ions would decrease in intensity with the same magnitude; however, the limitation of this technique is that interpretation becomes more complex for a large number of products with varying intensities<sup>8</sup>.

Another technique commonly used for elucidation of dissociation pathways is known as double resonance. This technique basically involves isolation of precursor ions followed by activation through CID. The product ions so formed are accompanied by simultaneous ejection of a particular product ion from the trap as they form. The primary objective of using the double resonance technique is to investigate the source of product ions, or in other words whether the product ion of interest is a result of fragmentation of a precursor ion (primary product ion) or fragmentation from a primary product ion (secondary product ion). Double resonance technique along with tandem mass spectrometry and  $MS^n$  experiments has been used to demonstrate that the dissociation pathways accessed in  $MS^3$  using two-step collisional activation may be different from that accessed in  $MS^2$  experiments, which involve collisional activation in one step. While some of the methods used for elucidation of dissociation pathways are effective, they require instrument modification to perform these experiments.

### *2.2.3 Previous Studies of Dissociation Pathways by 2DCOS*

In this dissertation research, dissociation pathways of chemical entities have been studied by application of 2DCOS. Previous work carried out to study the dissociation pathways by 2DCOS has been discussed in this section. Chin and Lin used the technique of 2DCOS to study kinetic models of reactions in which products can be formed directly from the reactant through a competitive process (parallel dissociation) or product formation takes place in consecutive steps involving intermediates (consecutive dissociation)<sup>11-12</sup>. The kinetic models were based on the infra-red (IR) spectrum analyzed as a function of rate constants and absorption coefficients. The applied perturbation was time for the 2DCOS analysis, performed by varying rate constant, absorption intensity, and signal-to-noise (S/N) ratio. For parallel reaction, the kinetic scheme involved one reactant having three absorption bands with corresponding absorption coefficients and three products each having one absorption band and corresponding absorption coefficient. The reference spectrum was chosen to be zero so that the magnitudes of the synchronous peaks were all positive. The synchronous spectra showed both auto-peaks and cross-peaks corresponding to reactant-reactant, reactant-product, and product-product pairs. However, in asynchronous spectra only cross-peaks corresponding to reactant-product pairs were observed. For the parallel reaction scheme, variation in the rate constant, absorption coefficient, and S/N ratio affected the synchronous and asynchronous correlation intensities; however, for the coherence spectrum, the variation had no effect and showed cylindrical-shaped correlated peaks with equal intensities. For the consecutive reaction, the kinetic scheme involved reactant, intermediate, and product, each with one absorption band and corresponding absorption coefficient. For the 2DCOS analysis, the correlations between reactant-intermediate,

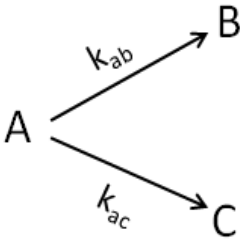
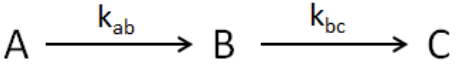
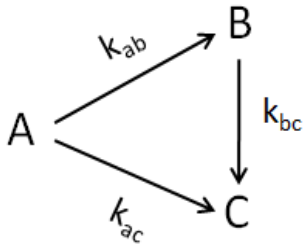
intermediate-product, and reactant-product pairs were studied by varying rate constants, absorption coefficients, S/N ratio, and reference spectrum. Similar to parallel reaction scheme, when the reference spectrum was zero, the magnitude of the intensities corresponding to all the synchronously correlated peaks were positive, which may otherwise change for a reference spectrum other than zero. For instance, when dynamic average was used as reference spectrum, the signs of synchronously correlated peaks characterizing the intermediate species changed. Another significant effect of an appropriately selected reference spectrum was the reduction in the number of asynchronously correlated peaks. For instance, under steady state condition when dynamic average was selected as the reference spectrum, the intensity of the reactant-intermediate correlated peak decreased and the intensity of the intermediate-product correlated peak attained the intensity of the reactant-product correlated peak. This unique feature was used to identify reactions following the consecutive scheme. Also the coherence spectrum for the consecutive scheme showed a similarity to the parallel reaction scheme in terms of having cylindrical-shaped peaks, except that the peaks had plateau-type features with unequal intensities<sup>8, 12</sup>.

Sigman et al. studied the fragmentation of *m*-nitrotoluene and nitrobenzene by electron ionization in QIT. The author was the first to demonstrate the application of the 2DCOS technique for investigating dissociation pathways of gaseous molecular ions in tandem mass spectrometry experiments, also referred to as two-dimensional correlation mass spectrometry (2D-CMS). The perturbation applied was CID energy, which was effected by increasing the excitation voltage for a fixed amount of time. The analysis of 2D correlation intensities observed

at spectral variables  $m_1$  and  $m_2$  showed competitive loss of NO at low CID and loss of NO<sub>2</sub> at high CID to yield ions [M-NO]<sup>+</sup> and [M-NO<sub>2</sub>]<sup>+</sup>, respectively. The analysis also demonstrated the formation of a [M-NO-CO]<sup>+</sup> ion occurring at CID energy higher than [M-NO]<sup>+</sup> ion but lower than that of the [M-NO<sub>2</sub>]<sup>+</sup> ion<sup>16</sup>. The results from the 2D-CMS experiment were in agreement with the results obtained from photoelectron photoion coincidence (PEPICO) and infrared multiple photon dissociation (IRMPD) studies.

In a similar study Frisch<sup>8</sup> applied the 2DCOS technique to investigate the dissociation pathways of sodium and ammonium adducts of oligoperoxides. The applied perturbation to collect mass spectral data was varying excitation time while keeping excitation voltage constant to induce CID. For the study, kinetic models simulating parallel, consecutive, and mixed dissociation schemes were used. The kinetic models were divided into two categories: simple kinetic models and large kinetic models. Simple kinetic models were based on three components representing one precursor ion and two product ions; large kinetic models were based on more than three components representing one precursor ion and the remaining representing product ions. For simple kinetic models, the precursor ion was referred to as A and was arbitrarily assigned an  $m/z$  ratio of 90, while the product ions were referred to as B and C with assigned  $m/z$  ratio of 75 and 60. Table 3 shows the schematic of possible dissociation pathways for simple kinetic models with three components represented by A, B, and C respectively. The spectral intensities corresponding to the precursor and product ions in the kinetic models represented their concentrations respectively.

Table 3: Schematic of Dissociation Schemes for Simple Kinetic Models

Parallel	Consecutive	Mixed
		

Prior to 2DCOS analysis the modeled data were normalized such that the sum of intensities across a particular perturbation equals one. The applied perturbation for all the kinetic models was time. For 2DCOS analysis, the dynamic spectrum of modeled data was obtained using zero reference spectrums such that the dynamic spectra were identical to the original matrix. To further investigate the effects of rate constant on the 2D correlation spectra, the rate constants were varied for all the kinetic dissociation schemes. Additionally, the effect of noise and sampling frequencies on the 2D correlation spectra was also investigated.

The results obtained from the 2DCOS analysis of simple kinetic models were compared with the 2DCOS results obtained from tandem mass spectrometry of simple molecules such as methyl ethyl ketone (MEK), deuterated MEK ( $d_3$ -MEK), and tetra ethyl silane (TES). Previous studies on MEK have shown that its molecular ion with  $m/z$  ratio of 72 undergoes parallel dissociation via  $\alpha$ -cleavage to yield product ions with  $m/z$  ratios of 57 and 43, respectively<sup>8</sup>. To confirm the dissociation of MEK occurs via  $\alpha$ -cleavage to yield  $m/z$  57 and  $m/z$  43,  $d_3$ -MEK was synthesized

in the laboratory. A similar tandem mass spectrometry analysis of d<sub>3</sub>-MEK resulted in product ions with *m/z* ratios of 57 and 46, respectively. Figure 5(a) and (b) represents the schematic of dissociation pathways of MEK d<sub>3</sub>-MEK.

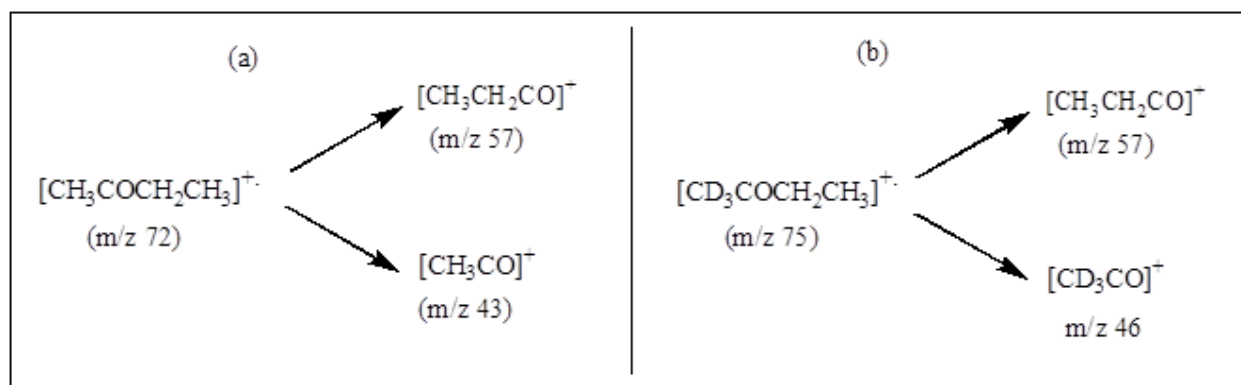


Figure 5: (a) and (b) represent the schematic of MEK and d<sub>3</sub>-MEK dissociation pathways

The analysis of d<sub>3</sub>-MEK confirmed that the formation of *m/z* 43 in MEK was a result of direct  $\alpha$ -cleavage of the precursor ion (*m/z* 72) and not the result of fragmentation of *m/z* 57, further confirming that the dissociation pathway of MEK to yield *m/z* 57 and *m/z* 43 is purely parallel.

Dissociation characteristics of TES have been previously reported. Figure 6 represents the schematic of the dissociation pathway of TES. Frisch et al. performed tandem mass spectrometry of TES, and the result was analyzed to study the consecutive dissociation pathway by 2DCOS.

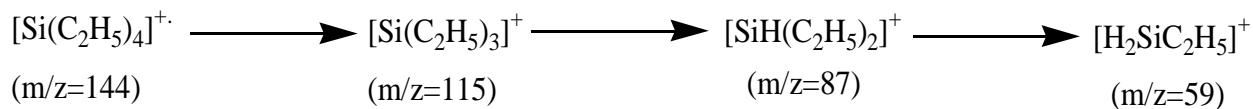


Figure 6: Schematic representation of TES dissociation pathway

It should be noted that for all the kinetic models, Frisch varied the rate constant to study their effects on the coherence spectral intensities. The rate constant was varied from 0 to 2 for parallel and consecutive dissociation schemes and from 0.1 to 1 for mixed dissociation schemes. Figure 7 represents the effect of variation in rate constants on coherence spectral intensities

Model	Dissociation Mechanism	Rate Constants			Coherence Spectral Peak Intensities <sup>a</sup> ( $m_1/m_2$ )		
		$k_{ab}$	$k_{ac}$	$k_{bc}$	A/C	A/B	B/C
1	Parallel	1	2	0	1.32	1.32	0.00
2	Parallel	1	1	0	0.96	0.96	0.00
3	Parallel	2	1	0	1.32	1.32	0.00
4	Consecutive	1	0	2	0.81	0.41	0.38
5	Consecutive	1	0	1	0.85	0.50	0.29
6	Consecutive	2	0	1	1.50	0.77	0.37
7	Mixed	1	1	1	1.07	0.77	0.21
8	Mixed (resembles consecutive)	1	0.1	1	0.84	0.52	0.26
9	Mixed (resembles parallel)	1	1	0.1	0.98	0.94	0.03

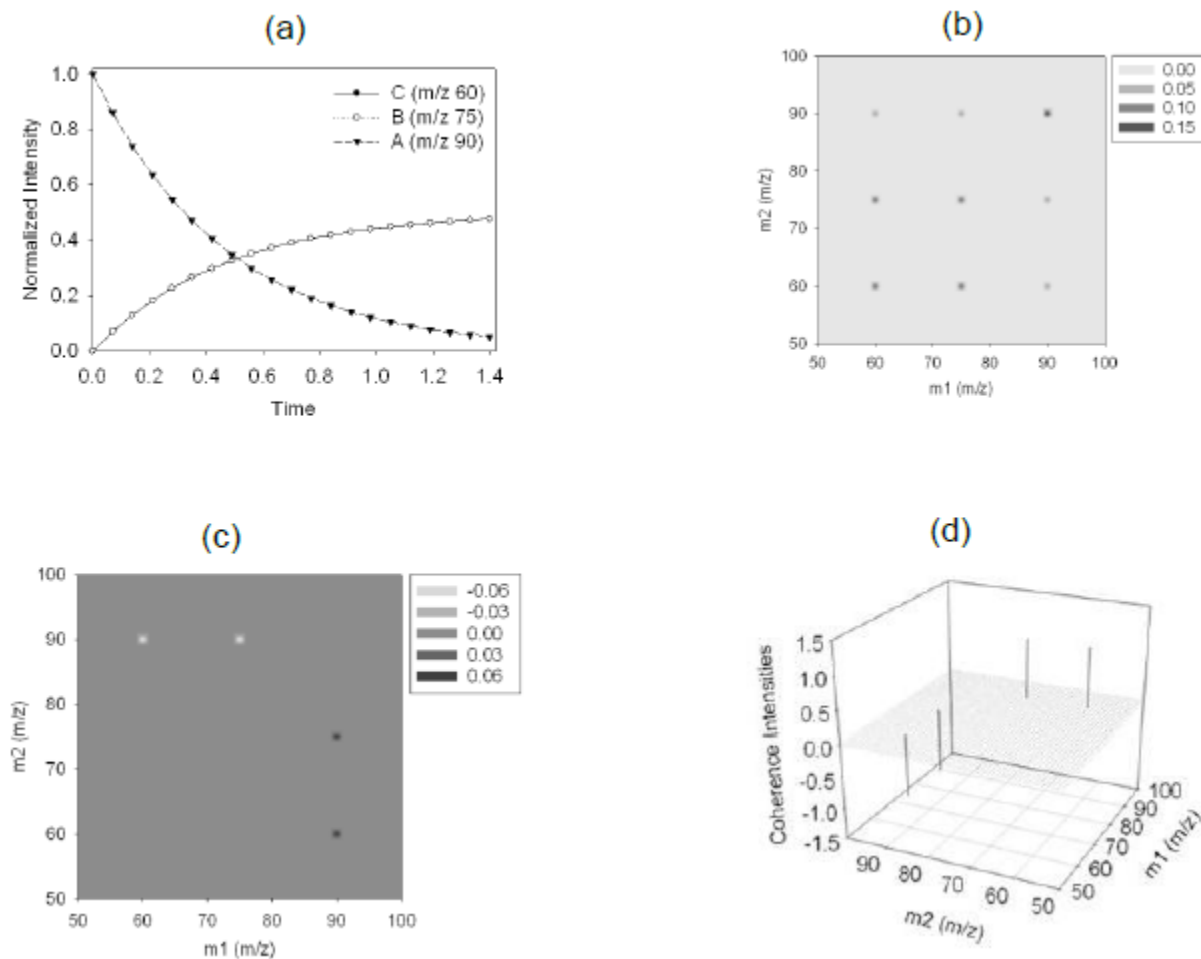
<sup>a</sup>The peak intensities were calculated using data from the entire perturbation window.

(Adapted from the Dissertation “Tandem Mass Spectrometric Analysis of Ammonium and Sodium Oligoperoxide Adducts with the Application of Two-Dimensional Correlation Spectroscopy and Computational Chemistry” with permission from Frisch Jessica Lynne; see Appendix)

Figure 7: The coherence spectral intensities and variation in rate constants



As seen from Figure 7, three models for each dissociation schemes representing parallel, consecutive, and mixed dissociation schemes were studied. The spectral intensities corresponding to the precursor and product ion concentrations were plotted as a function of time to obtain breakdown curves. Synchronous and asynchronous correlated spectra were obtained from 2DCOS analysis, while the ratio of asynchronous to synchronous 2D correlation intensities was used to obtain a coherence spectrum for each model. The result obtained from 2DCOS analysis was pictorially presented in the form of breakdown curves, synchronous, asynchronous and coherence spectra and interpreted respectively.

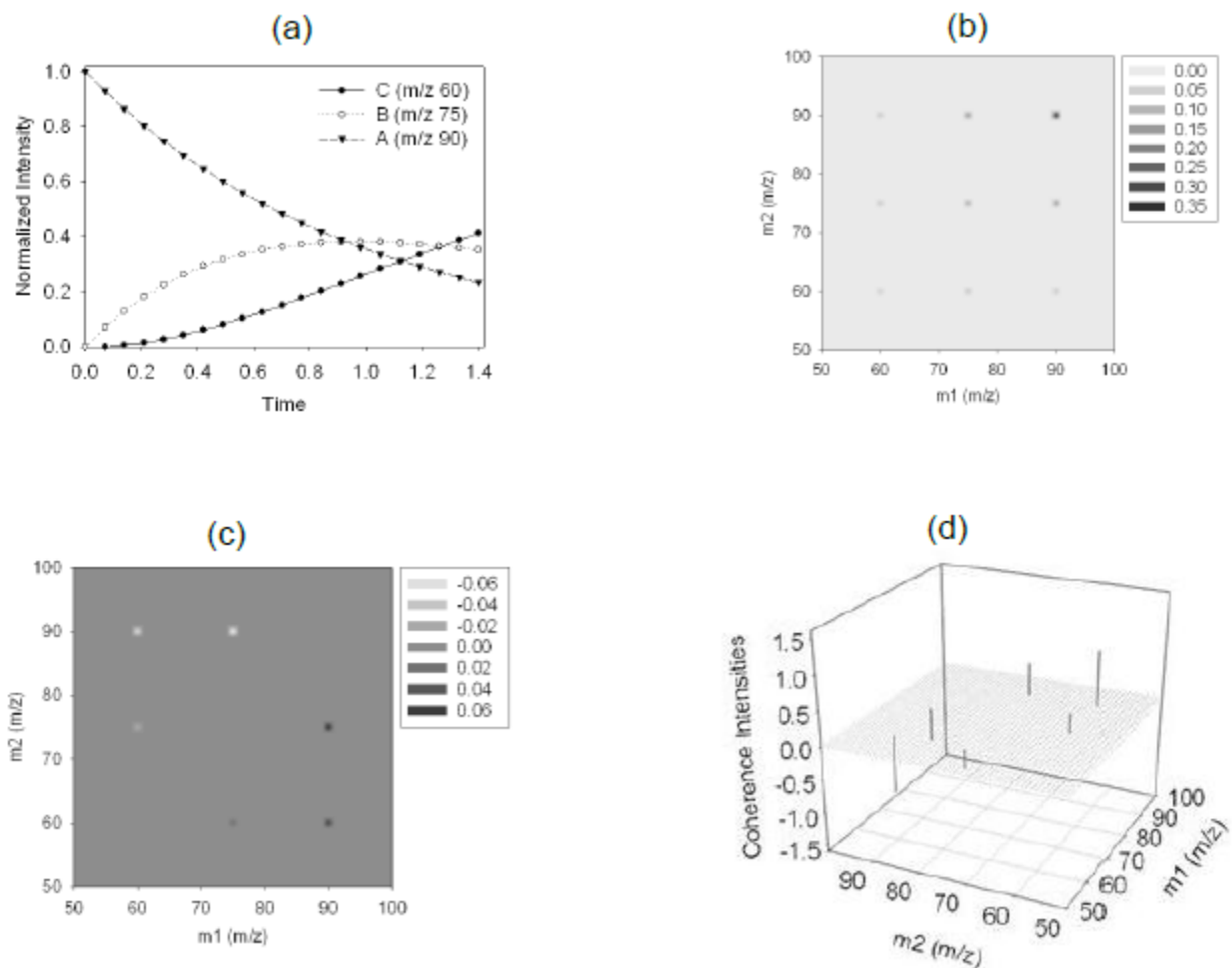


(Adapted from the Dissertation “Tandem Mass Spectrometric Analysis of Ammonium and Sodium Oligoperoxide Adducts with the Application of Two-Dimensional Correlation Spectroscopy and Computational Chemistry” with permission from Frisch Jessica Lynne; see Appendix)

Figure 8: Pictorial representation of model 2 (Figure 7), parallel with  $k_{ab}=1$  and  $k_{ac}=1$ : (a) plot of concentration vs time; (b) synchronous spectrum; (c) asynchronous spectrum; (d) coherence spectrum

Figure 8 shows a pictorial representation of breakdown curves 2D correlation spectra and coherence spectra for parallel dissociation scheme with rate constants arbitrarily set to 1. The signs of the synchronous 2D correlation intensities were all positive because of the zero

reference spectrum. In the asynchronous spectra, the correlated cross-peaks represented precursor-product ions defined by A/B and A/C, where A was the precursor and B and C were product ions, respectively. It should be recalled that asynchronous correlation intensities show only the dissimilarities or out-of-phase trends. Therefore, only the peaks corresponding to precursor-product ions were observed in the asynchronous spectra representing an increase in product ion intensities as the precursor ion intensities decrease. The peaks corresponding to the product-product ions (B/C) correlation were absent in the asynchronous 2D spectra, as they exhibit only in-phase trends because product-product ions will always increase for a parallel dissociation scheme. The coherence spectra showed two peaks corresponding to precursor-product ions with equal intensities, while the peak corresponding to product-product ions was not observed. When the rate constants were changed as shown in model 1 and 3, the coherence spectral intensities corresponding to precursor-product ions were equal except for their magnitude as compared to model 2.

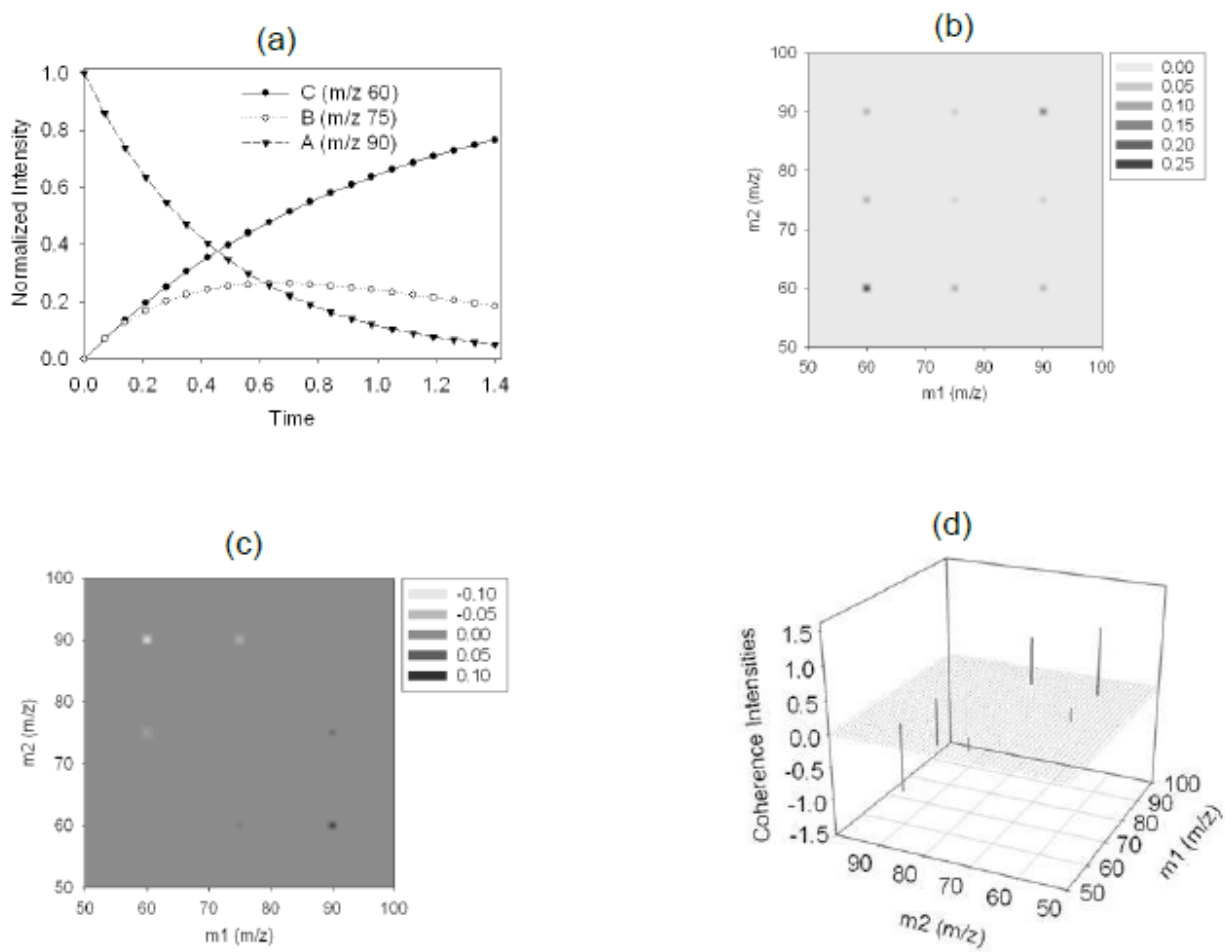


(Adapted from the dissertation “Tandem Mass Spectrometric Analysis of Ammonium and Sodium Oligoperoxide Adducts with the Application of Two-Dimensional Correlation Spectroscopy and Computational Chemistry” with permission from Frisch Jessica Lynne; see Appendix)

Figure 9: Pictorial representation of model 5 (Figure 7), consecutive with  $k_{ab} = 1$  and  $k_{bc} = 1$ : (a) plot of concentration vs time; (b) synchronous spectrum; (c) asynchronous spectrum; (d) coherence spectrum.

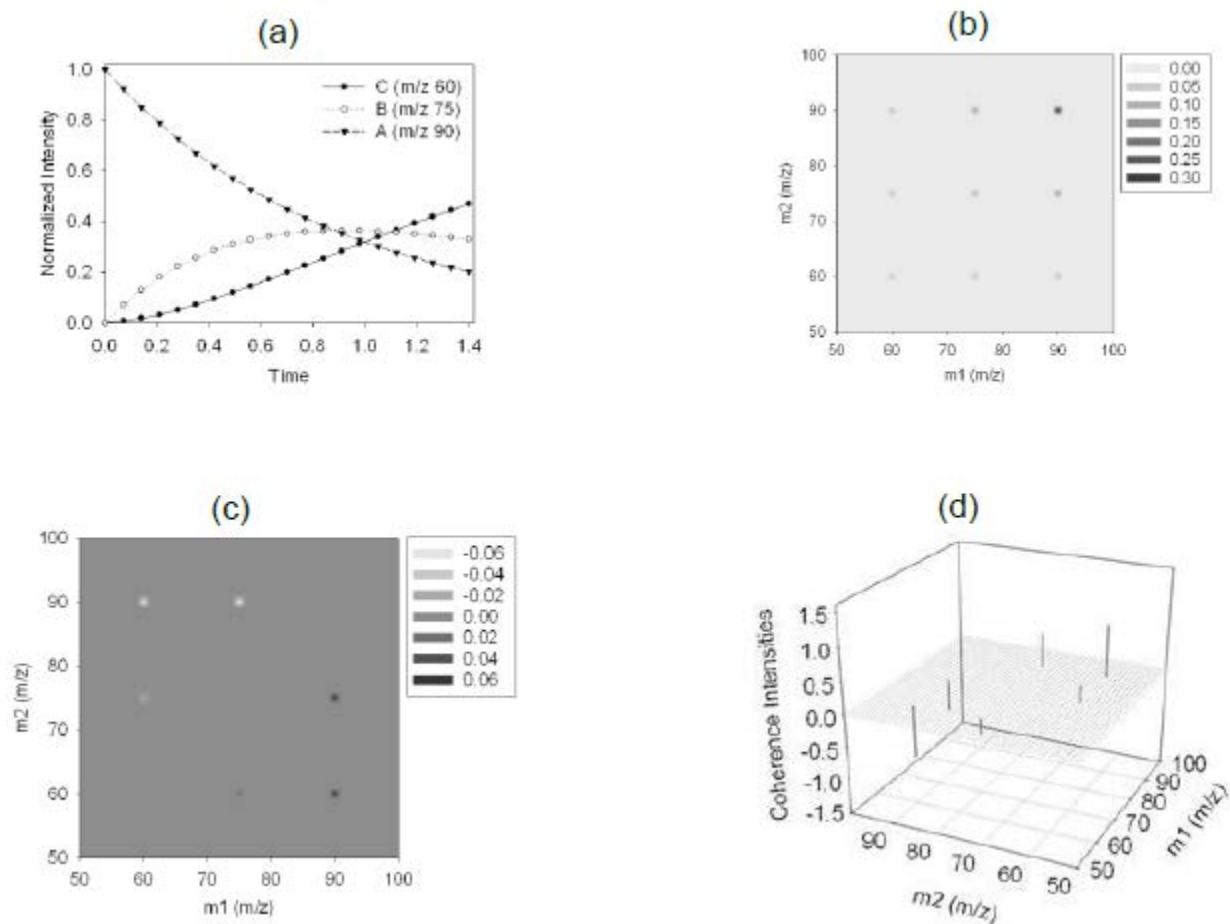
The result for the simple kinetic model representing a consecutive dissociation scheme is pictorially presented in Figure 9, where the rate constant was arbitrarily taken as one. The consecutive dissociation scheme is characterized by the presence of precursor ion (A),

intermediate product ion (B), and product ion (C). The intermediate product ion can also be referred to as the primary-product ion which undergoes further dissociation, yielding a product ion also referred to as a secondary-product ion. The synchronous spectra for the consecutive dissociation scheme showed an additional peak (B/C) corresponding to intermediate-product-product ion which was not observed in synchronous spectra for the parallel dissociation scheme. Another characteristic of the consecutive dissociation scheme is that since the product ion formation results from dissociation of the intermediate product ion, the intermediate ion showed characteristics of increase and decrease in intensity over the applied perturbation while the product ion showed only an increase in the intensity over the applied perturbation. Coherence spectra were characterized by the presence of three peaks with unequal intensities, unlike in the parallel scheme where the intensities were equal. When the effect of rate constants on the coherence spectral intensities was investigated by changing the value of the rate constants as shown in model 4 and 6 (Figure 7), a similar trend as for model 5 was observed, with three peaks of unequal intensities with overall intensities dependent upon the value of the rate constant.



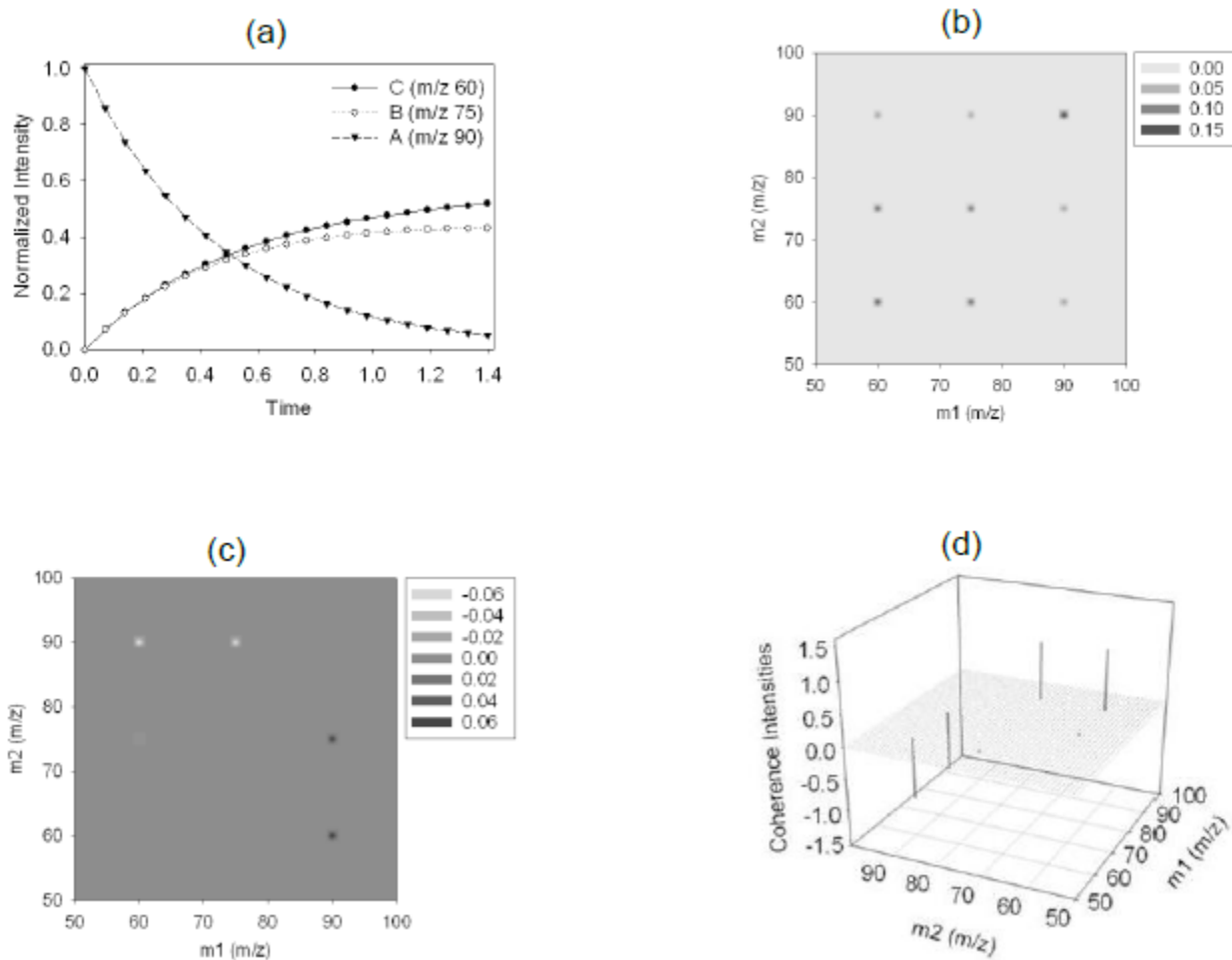
(Adapted from the dissertation “Tandem Mass Spectrometric Analysis of Ammonium and Sodium Oligoperoxide Adducts with the Application of Two-Dimensional Correlation Spectroscopy and Computational Chemistry” with permission from Frisch Jessica Lynne; see Appendix)

Figure 10: Pictorial representation of model 7 (Figure 7), mixed with  $k_{ab}=1$ ,  $k_{ac}=1$  and  $k_{bc}=1$ :  
 (a) plot of concentration vs time; (b) synchronous spectrum; (c) asynchronous spectrum; (d) coherence spectrum



(Adapted from the dissertation “Tandem Mass Spectrometric Analysis of Ammonium and Sodium Oligoperoxide Adducts with the Application of Two-Dimensional Correlation Spectroscopy and Computational Chemistry” with permission from Frisch Jessica Lynne; see Appendix)

Figure 11: Pictorial representation of model 8 (Figure 7), mixed resembling consecutive with  $k_{ab} = 1$ ,  $k_{ac} = 0.1$  and  $k_{bc} = 1$ : (a) plot of concentration vs time; (b) synchronous spectrum; (c) asynchronous spectrum; (d) coherence spectrum.



(Adapted from the dissertation “Tandem Mass Spectrometric Analysis of Ammonium and Sodium Oligoperoxide Adducts with the Application of Two-Dimensional Correlation Spectroscopy and Computational Chemistry” with permission from Frisch Jessica Lynne; see Appendix)

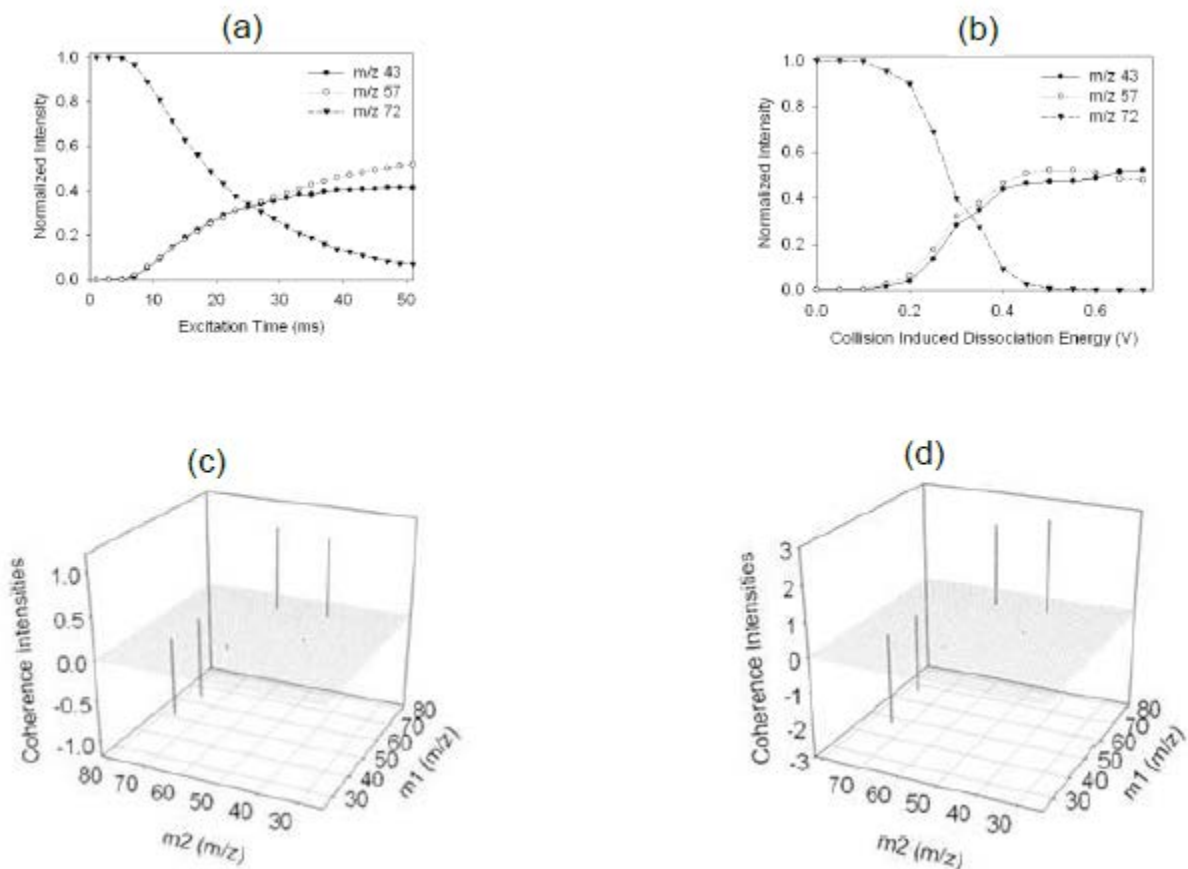
Figure 12: Pictorial representation of model 9 (Figure 7), mixed resembling parallel with  $k_{ab} = 1$ ,  $k_{ac} = 1$  and  $k_{bc} = 0.1$ : (a) plot of concentration vs time; (b) synchronous spectrum; (c) asynchronous spectrum; (d) coherence spectrum

For mixed dissociation schemes, three models were investigated by varying the rate constants such that in one of the models all the rate constants were arbitrarily taken as one (model 7), while



the other two models were made to resemble the consecutive and parallel kinetic models represented by models 8 and 9, respectively. For the most part synchronous and asynchronous spectra for all the three mixed dissociation models were similar to consecutive dissociation schemes. In mixed dissociation model that resembled the parallel model (model 9), weak peak corresponding to an intermediate product-product ion (B/C, 75/60), was observed in the asynchronous spectra. Also the coherence plot for the mixed like-parallel model resembled the coherence plot of the pure parallel model in terms of the precursor correlated peaks (A/B, 90/75 and A/C, 90/60), which were almost equal in intensity. The only notable difference was that the precursor-intermediate product ion peak (A/B) was slightly less intense than the precursor-product ion peak (A/C). The author also analyzed the coherence plots over the entire perturbation range, referred to as an expanding window coherence plot, and observed that at lower perturbation the mixed like-parallel dissociation model had precursor-product ion (A/C) and precursor-intermediate product ion (A/B) peaks of almost equal intensity and a weak intermediate product-product ion peak. However at higher perturbations, the mixed like-parallel dissociation model resembled the consecutive model. Due to this behavior it was concluded that Hilbert-Noda sequential order rules may not necessarily apply in determining the order of events<sup>8</sup>. This may be attributed to the non-monotonic nature of the intermediate product ion where it shows both an increase and a decrease in intensity over the perturbation range. For a mixed like-consecutive dissociation model (model 8), the coherence spectral intensities were nearly same as for the pure consecutive dissociation model (model 4). In general, coherence spectra for mixed dissociation yielded results that were more characteristic of consecutive dissociation models.

2DCOS was also applied to mass spectral data of simple molecules like MEK, d<sub>3</sub>-MEK, and TES to study their dissociation pathways. The mass spectral data for the simple molecules were obtained by varying the excitation times as the applied perturbation. MEK is known to undergo parallel dissociation via two alpha-cleavages. The precursor ion of MEK having  $m/z$  ratio 72 dissociates to yield product ions having  $m/z$  ratios 57 and 43, respectively.

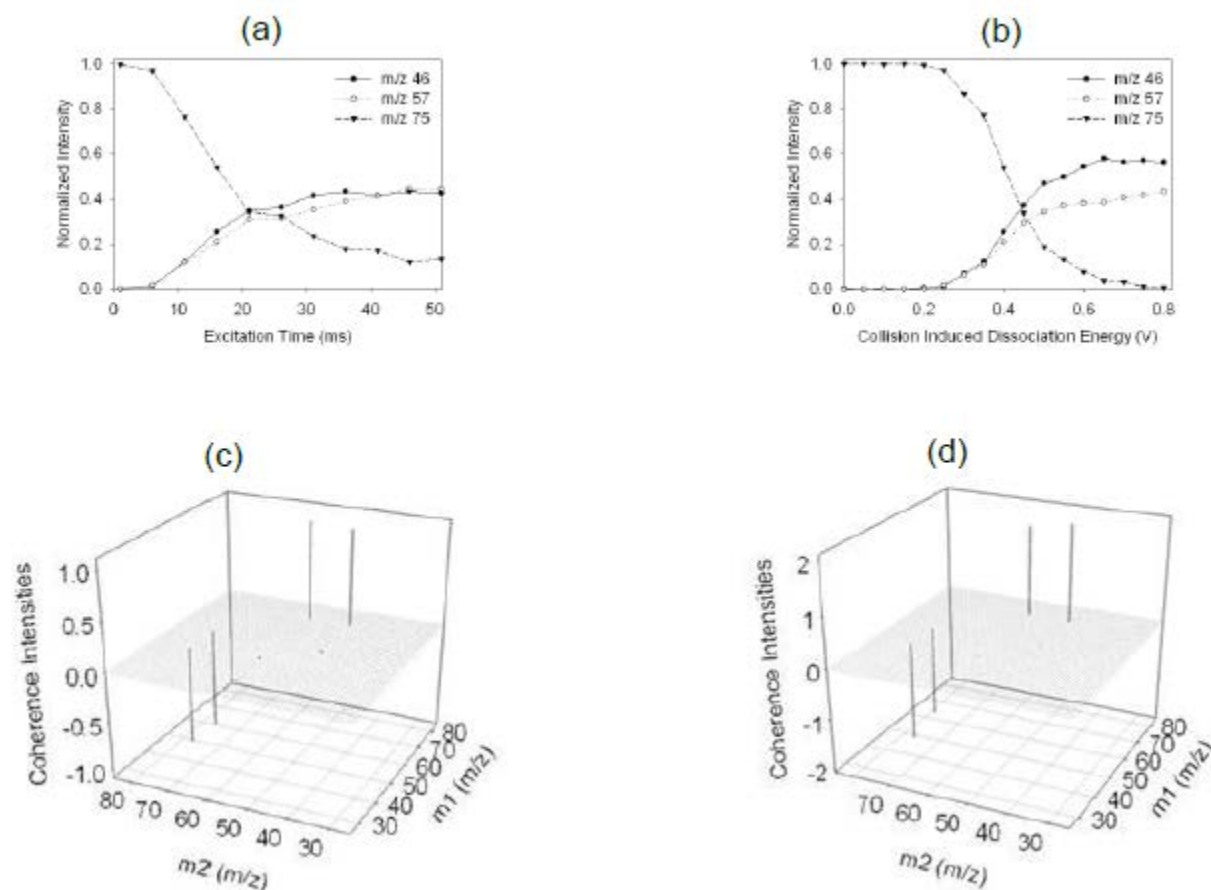


(Adapted from the dissertation “Tandem Mass Spectrometric Analysis of Ammonium and Sodium Oligoperoxide Adducts with the Application of Two-Dimensional Correlation Spectroscopy and Computational Chemistry” with permission from Frisch Jessica Lynne; see Appendix)

Figure 13: Pictorial representation of MEK: (a) breakdown curve as a function of excitation time; (b) breakdown curve of collision induced dissociation energy; (c) coherence spectrum as a function of excitation time; (d) coherence spectrum as a function of collision induced dissociation energy.

The results from the 2DCOS analysis of MEK (Figure 13) show coherence spectra for MEK resembling those of the parallel dissociation model. The precursor-product ion peaks 72/57 and 72/43 were almost of equal intensity, as expected based on the results from the simple kinetic models for parallel dissociation models. A weak 57/43 also appeared, which is not characteristic

of parallel dissociation. This deviation from the modelled data was attributed to instrumental noise, as each data point results from separate scan events.

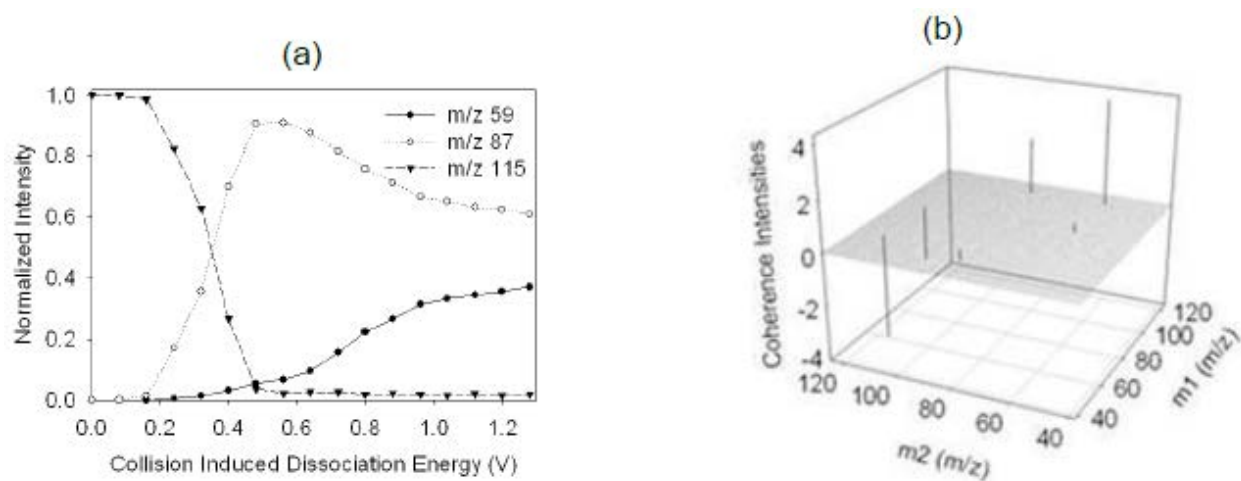


(Adapted from the dissertation “Tandem Mass Spectrometric Analysis of Ammonium and Sodium Oligoperoxide Adducts with the Application of Two-Dimensional Correlation Spectroscopy and Computational Chemistry” with permission from Frisch Jessica Lynne; see Appendix)

Figure 14: Pictorial representation of  $d_3$ -MEK: (a) breakdown curve as a function of excitation time; (b) breakdown curve of collision induced dissociation energy; (c) coherence spectrum as a function of excitation time; (d) coherence spectrum as a function of collision induced dissociation energy.

To further confirm that the product ion corresponding to  $m/z$  ratio 43 results from alpha cleavage and not as a result of further dissociation of  $m/z$  ratio 57,  $d_3$ -MEK was synthesized and analyzed in a similar way (Figure 14). The hypothesis here was that if the product ion corresponding to  $m/z$  ratio 43 also results from consecutive dissociation of  $m/z$  ratio 57, the product ions corresponding to  $m/z$  ratios 57, 46, and 43 should be observed. However, the product ion with  $m/z$  ratio 43 was not observed in  $d_3$ -MEK analysis, which confirmed that product ions with  $m/z$  ratio 57 and 43 result from competitive parallel dissociation and that weak peaks corresponding to 57/43 observed in the coherence spectra of MEK may be due to instrumental noise.

TES was analyzed to study consecutive dissociation pathways and be compared with the 2DCOS results of the consecutive dissociation model.



(Adapted from the dissertation “Tandem Mass Spectrometric Analysis of Ammonium and Sodium Oligoperoxide Adducts with the Application of Two-Dimensional Correlation Spectroscopy and Computational Chemistry” with permission from Frisch Jessica Lynne; see Appendix)

Figure 15: Pictorial representation of TES: (a) breakdown curve as a function of excitation time; (b) coherence spectrum.as a function of excitation time

No molecular ion of TES having  $m/z$  ratio 144 was observed; therefore, the primary product ion corresponding to  $m/z$  ratio 115 was chosen as the precursor for tandem mass spectrometry experiments.  $MS^2$  analysis of  $m/z$  ratio 115 dissociated to yield product ions having  $m/z$  ratio 87 and 59, respectively. Further  $MS^2$  analysis of product ion  $m/z$  ratio 87 revealed that it undergoes dissociation to yield  $m/z$  ratio 59. The coherence spectra obtained from the 2DCOS analysis of TES was in agreement with the consecutive dissociation model. Three peaks with varying intensities were observed, with the weak intermediate product-product ion peak corresponding to  $m/z$  ratio 87/59.

## CHAPTER 3: EXPERIMENT

The previous chapter discusses the work by Frisch, where the author applied the 2DCOS technique to study dissociation pathways of simple molecules undergoing parallel and consecutive dissociations in tandem mass spectrometry experiments. In this dissertation research, the thermometer molecule n-butylbenzene, well known for its dissociation energetics, will be investigated. As discussed in Chapter 1, at lower energy the precursor ion of n-butylbenzene with  $m/z$  ratio 134 undergoes competitive dissociation, yielding product ions with  $m/z$  ratios 92 and 91, respectively, while at higher energy, the product ion corresponding to  $m/z$  ratio 92 has sufficient internal energy to undergo further dissociation, yielding product ion 91. Thus, upon activation n-butylbenzene shows characteristics of both parallel and consecutive dissociation as a function of internal energy deposited into the precursor ion  $m/z$  134.

In the experimental section presented here, investigation of the dissociation pathways of n-butylbenzene as a function of applied perturbation is described. The applied perturbations were CID energy and excitation time. The perturbations applied to obtain mass spectral data were primarily based on the work by Sigman et al.<sup>16</sup> and Frisch<sup>8</sup> respectively. The mass spectral data were acquired by varying CID energy while holding excitation time constant and vice-versa. Headspace analysis of n-butylbenzene was performed using gas chromatography mass spectrometry. A simple kinetic model simulating the dissociation pathway of n-butylbenzene was also made in MS-Excel (Microsoft Corporation, Redmond WA). 2DCOS was applied to the experimental and kinetic modelled data to yield synchronous, asynchronous, and coherence spectra. The dissociation pathways of n-butyl benzene were investigated based on the

interpretation of the above-mentioned spectra obtained for both the experimental and kinetic modelled data.

### 3.1. Gas Chromatography Tandem Mass Spectrometry of n-butylbenzene

Headspace analysis of n-butylbenzene was performed in a ThermoFinnigan Trace GC 2000 coupled to a PolarisQ quadrupole ion trap mass spectrometer equipped with HP-5MS column (Agilent Technologies Inc). The GC column was approximately 30 meters in length with an internal diameter of 0.25 mm. The coating inside the column was (5% -phenyl)-methylpolysiloxane, which was 0.25 micron in thickness. For the analysis, 15 microliters of headspace was injected into a split/splitless injection port maintained at a temperature of 150° C. The oven was maintained at an initial temperature of 50° C held constant for 1 minute and then ramped by 10° C/min to attain a final temperature of 250° C. The carrier gas was helium maintained at a constant flow rate of 0.9 mL/min.

The molecules of n-butylbenzene eluting from the GC column were ionized by the electron ionization method. The energy associated with the electron beam for ionization was maintained at 70 eV, and the ionization source temperature was maintained at 200 °C. Helium was used as a dampening gas at a constant flow of 0.3 mL/ min. For tandem mass spectrometry analysis, two sets of mass spectral data were collected by isolating the precursor ion  $m/z$  ratio 134 at an isolation width of 1 Dalton, which is a default value. The first set of mass spectral data comprised ten scan events obtained by varying the CID energy from 0.0V to 1.8V at increments of 0.2V while keeping the excitation time constant. For each scan event corresponding to a



particular CID energy, 3 micro scans were performed at a max ion time of 25 ms. The second set of mass spectral data was obtained by holding CID energy constant as the excitation time was varied from 1 to 81 ms at increments of 5 ms. The mass spectral data in a PolarisQ ion trap mass spectrometer can be obtained at three different trapping potential values represented by  $q_z$ . However, for this research a constant  $q_z$  value of 0.45 was used for obtaining both mass spectral data sets.

### 3.2 Simple Kinetic Model

For the sake of comparing the mass spectral data obtained from the tandem mass spectrometry experiment, a simple kinetic model simulating the dissociation pathway of butylbenzene based on first order kinetics was made in MS-Excel. The precursor and product ions were assigned using letters from A to E, where A was the precursor ion while the remaining were product ions. The schematic of the dissociation kinetics for simple kinetic model is represented in Figure 16.

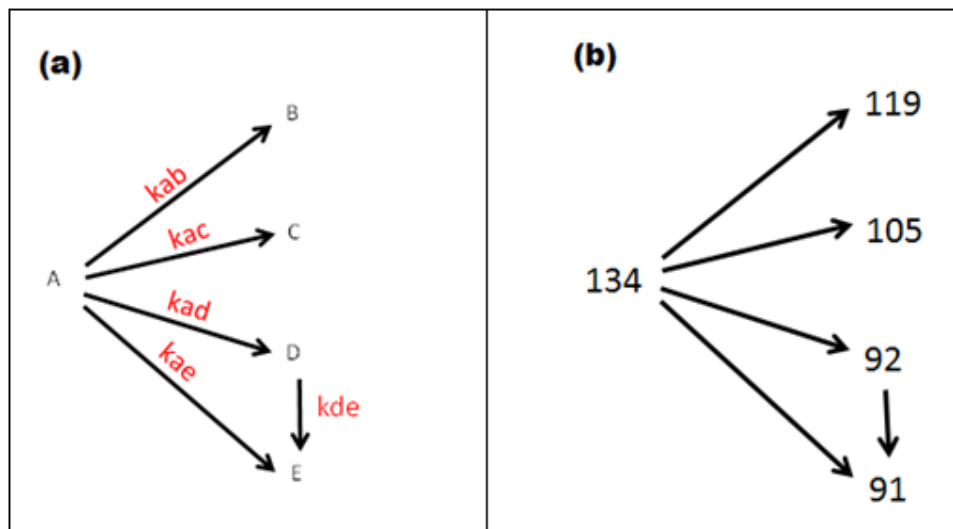


Figure 16: (a) Dissociation scheme for a simple kinetic model representing n-butylbenzene; (b) dissociation products of precursor ion  $m/z$  134.

The values of rate constants represented by  $k_{ab}$ ,  $k_{ac}$ ,  $k_{ad}$ ,  $k_{ae}$ , and  $k_{de}$  were arbitrarily chosen such that they resembled the dissociation pathway of n-butylbenzene. Table 4 shows the arbitrary values of rate constants used for making the simple kinetic model. The applied perturbation for the kinetic model was arbitrary time ranging from 0 to 2 ms at increments of 0.07 ms. The concentration of the precursor ion A at time zero was arbitrarily assigned as 1, while for product ions B, C, D, and E the concentrations were assigned as 0.

Table 4: Rate Constants for the Simple Kinetic Model Representing Mixed Dissociation Scheme

Model	Dissociation Scheme	$k_{ab}$	$k_{ac}$	$k_{ad}$	$k_{ae}$	$k_{de}$
1	Mixed	0.3	0.3	2.0	0.3	0.3

The kinetic equations used to generate the concentration of the precursor and product ions as a function of applied perturbations in the model are represented by the equations 3.1 to 3.5 respectively.

$$-\frac{d[A]}{dt} = k_{ab}[A] + k_{ac}[A] + k_{ad}[A] + k_{ae}[A] \quad (3.1)$$

$$\frac{d[B]}{dt} = k_{ab}[A] \quad (3.2)$$

$$\frac{d[C]}{dt} = k_{ac}[A] \quad (3.3)$$

$$\frac{d[D]}{dt} = k_{ad}[A] - k_{de}[D] \quad (3.4)$$

$$\frac{d[E]}{dt} = k_{ae}[A] + k_{de}[D] \quad (3.5)$$

### 3.3: Data Analysis for 2DCOS Application

Prior to application of 2DCOS, both the experimental and kinetic modelled data were arranged such that the intensities corresponding to all the spectral variables obtained for a particular perturbation were arranged in columns. This arrangement of spectral intensities measured at every perturbation was repeated to yield a raw data matrix. In the second step, the spectral intensities were normalized such that the sum of spectral intensities across a particular perturbation was equal to one. This normalization was accomplished by taking the ratio of intensity corresponding to one spectral variable across a perturbation to the sum of intensities

corresponding to all the spectral variables across the same perturbation to yield another data matrix containing normalized intensities.

For the 2DCOS analysis, the data matrix consisting of normalized intensities was used. The dynamic spectra for the analysis were calculated based on a zero reference spectrum. The synchronous and asynchronous correlated spectral intensities were calculated employing Mathematica and Matlab software. For the interpretation of results, contour plots of synchronous and asynchronous 2D correlated spectra were constructed using SigmaPlot11.0 software. It should be noted that the interpretation of synchronous and asynchronous 2D correlated spectra was based on average reference spectra, and the interpretation of coherence spectra will be based on zero reference spectra.

## CHAPTER 4: RESULTS AND DISCUSSION

### 4.1: 2DCOS Analysis of n-butylbenzene

The results from the tandem mass spectrometry ( $MS^2$ ) experiment of n-butylbenzene are presented in this section. Recall that two sets of mass spectral intensities were obtained involving CID energy and excitation time as the applied perturbations. The first set of mass spectral intensities was obtained by varying CID energy while holding excitation time constant over the entire perturbation range; the second set of mass spectral intensities was obtained by varying excitation time by holding CID energy constant over the entire perturbation range. The primary objective was to investigate the fragmentation pathways of the precursor ion  $m/z$  134 as a function of applied perturbation by the application of 2DCOS. Application of 2DCOS resulted in two 2D correlation spectra: synchronous and asynchronous. Another spectrum, a coherence spectrum, was also obtained by taking the ratio of asynchronous to synchronous correlated spectral intensities.

This chapter will also discuss the results obtained from the 2DCOS analysis of kinetic modelled data. The spectral intensities corresponding to 2D synchronous and asynchronous correlated spectra are presented in the form of 2D contour plots. In this research, interpretation of results will be based on the analysis of synchronous, asynchronous, and coherence spectra. It should be noted that all the results obtained from the 2DCOS analysis are based on a zero reference spectrum. Prior to applying 2DCOS to analyze the experimental data and kinetic modelled data, the mass spectral intensities corresponding to these data sets were normalized. The normalized

intensities were then used to obtain breakdown curves to pictorially represent the fragmentation pathways of n-butylbenzene for both experimental and kinetic modelled data.

Figure 17 shows the EI mass spectra of butylbenzene headspace collected by varying CID energy ranging from 0.0V to 1.8V at 0.2V increments while holding excitation time constant at 11 ms.

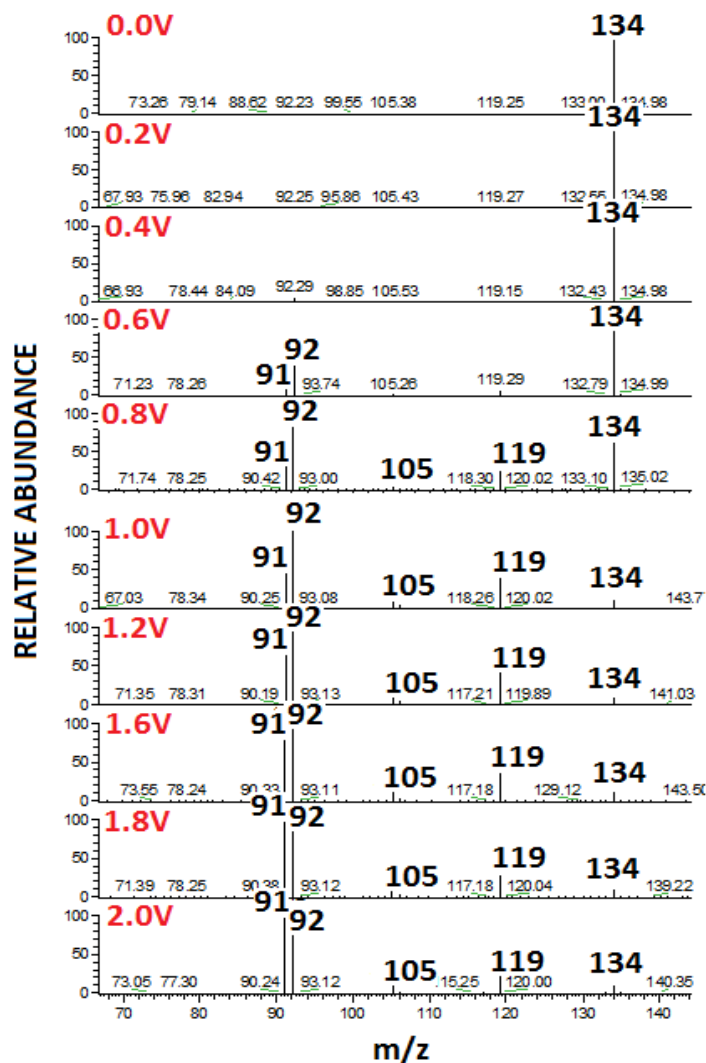


Figure 17: EI mass spectra of n-butylbenzene collected by varying CID energy (0.0-1.8)V at 11 ms excitation time

From the above EI mass spectra it can be observed that fragmentation increases with increase in CID energy. The increase in fragmentation with CID energy is attributed to the amount of internal energy deposited into the precursor ion, which is proportional to the CID energy.<sup>27</sup> At 0.6V CID energy, fragmentation of precursor ion 134 is observed, as is evident by the presence of relatively less intense product ions corresponding to  $m/z$  ratios 91, 92, 105, and 119, respectively. As the CID energy is increased further, the intensity of the precursor ion  $m/z$  134 decreases with the increase in the intensity of the product ions. Another significant observation was the increase in the branching ratio of product ions  $m/z$  91/92 at higher CID energy. This observation has been attributed to information derived from reports that at higher energy product ion  $m/z$  92 may have sufficient internal energy to undergo further dissociation to yield product ion  $m/z$  91.<sup>1 28</sup> The succeeding sections in this chapter will discuss the energetics associated with the fragmentation pathways based on the interpretation of results obtained from the 2DCOS analysis.

#### *4.1.1. Varying CID Energy at Constant Excitation Time*

In this section the results from the 2DCOS analysis of mass spectral intensities obtained by varying CID energy at constant excitation time will be discussed to study the correlation between the precursor-product ion pairs and between product-product ion pairs. It should be noted that the perturbation changes observed at spectral variables  $m1$  and  $m2$  in this research were  $m/z$  ratios. For the interpretation of results, the correlation between the precursor ion and product ion involved was represented as a precursor/product ion pair. For example the correlation between the precursor ion  $m/z$  134 and product ion  $m/z$  91 observed at spectral variables  $m1$  and  $m2$  was

represented as 134/91. The correlation between the above two ions can also be represented as 91/134, depending upon the order of matrix multiplication that was performed to obtain the 2D correlated spectra. Similar representations as shown above have been used to show the correlation between the different product ions resulting from the dissociation of the precursor ion.



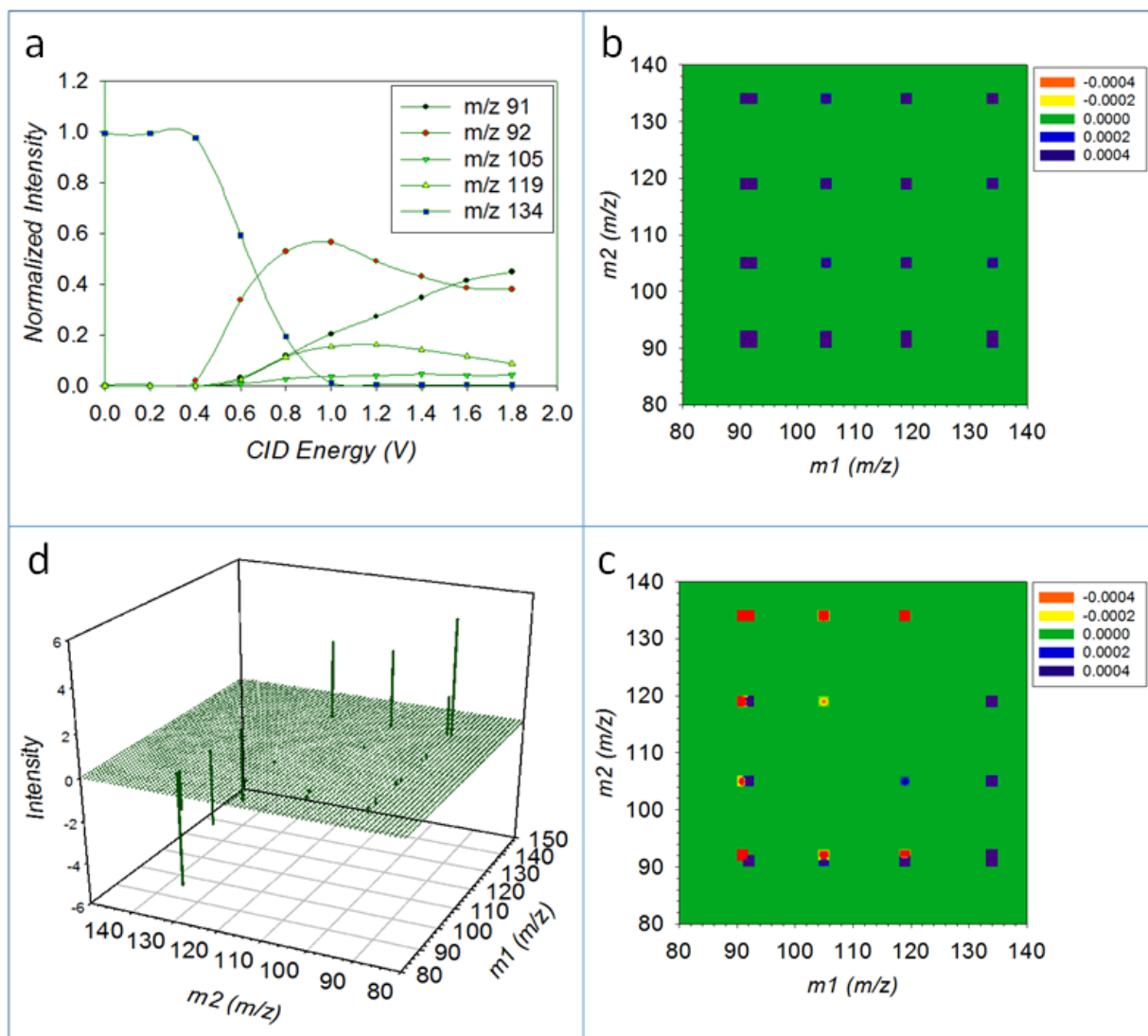


Figure 18: 2DCOS analysis of varying CID energy and constant excitation time (11 ms): (a) breakdown curve of normalized intensity vs CID energy; (b) synchronous spectrum; (c) asynchronous spectrum; (d) coherence spectrum.

The effect of varying CID energy on the precursor ion while holding excitation time constant is represented in the form of a breakdown curve in Figure 18 (a). It can be observed from the breakdown curve that the product ions  $m/z$  ratio 91, 92, 105, and 119 under investigation are formed with different rates as the precursor ion 134 decays. Also observed at the onset of the

breakdown curve is an induction period up to CID energy of 0.4V. During the induction period, the internal energy of the precursor ion is less than the appearance energy associated with the lowest energy fragmentation pathway; as a result, the precursor ion does not undergo fragmentation to yield product ions.<sup>25</sup> Similarly at higher CID energy, resonance ejection may surpass resonance excitation, which affects the linearity of the curve as a result of a decrease in the trapping efficiency.<sup>22</sup>

The synchronous spectrum representing the in-phase changes measured at spectral variables  $m_1$  and  $m_2$  shows characteristic auto-peaks along the diagonal. It should be noted that the intensities of the auto-peaks are always positive as they represent the maximum spectral intensity variation measured at a specific spectral variable over the entire perturbation range. Similarly cross-peaks observed at the off-diagonal positions represent spectral intensity variations or out-of-phase changes measured at two different spectral variables over the applied perturbation range.<sup>29</sup>

Recall that the sign of cross peaks can be either positive or negative, unlike auto-peaks, which always take positive values. In the synchronous spectrum shown in Figure 18 (b), the precursor ion  $m/z$  134 and all the product ions corresponding to  $m/z$  91, 92, 105, and 119, respectively, exhibit auto-peaks along the diagonal. At the off diagonal positions, the peaks corresponding to the precursor-product ion pairs represented by 134/91, 134/92, 134/105, and 134/119 and the product-product ion pairs represented by 119/91, 119/92, 119/105, 105/91, 105/92, and 92/91 exhibit cross-peaks, respectively. It can be observed that the signs of the cross-peaks are all positive, resulting from the utilization of zero reference spectra. Similar results were also

observed by Chin, Lin,<sup>12</sup> and Frisch,<sup>8</sup> where they used zero reference spectra to perform 2DCOS analysis.

As for the asynchronous spectrum, recall that it is anti-symmetric with respect to the diagonal and is characterized by the presence of only cross-peaks. It should also be noted that asynchronously correlated cross-peaks are developed only when the spectral intensity variations observed at  $m_1$  and  $m_2$  are out of phase with each other, which in turn depends upon the sign of the cross-peak. A positive cross-peak sign implies that the spectral intensity change at  $m_1$  occurs predominantly before  $m_2$ , while a negative sign implies that the spectral intensity change at  $m_2$  occurs before  $m_1$ . The above interpretation is of course reversed if the sign of the same cross-peak in the synchronous spectrum is negative. In this research, the sequential order rules by Noda as summarized in Table 1 will be used to determine the energetics associated with the formation of product ions resulting from the dissociation of precursor ion  $m/z$  134. The sequence of product ion formation with the decay of precursor ion over the applied CID energy at constant excitation time is summarized in Table 5 below.

Table 5: Noda's Sequential Order Rules to Determine Product Ion Formation as a Function of Varying CID Energy at Constant Excitation Time

<b>Cross-Peaks observed at spectral variables (m1/m2)</b>	<b>Synchronous spectrum <math>\Phi</math> (m1, m2)</b>	<b>Asynchronous spectrum <math>\Psi</math> (m1, m2)</b>	<b>Sequential order of product ion formation over applied perturbation (CID) range</b>
134/91	+	+	m/z134 occurs at lower CID than m/z91
134/92	+	+	m/z134 occurs at lower CID than m/z92
134/105	+	+	m/z134 occurs at lower CID than m/z105
134/119	+	+	m/z134 occurs at lower CID than m/z119
119/91	+	+	m/z119 occurs at lower CID than m/z91
119/92	+	-	m/z92 occurs at lower CID than m/z119
119/105	+	+	m/z119 occurs at lower CID than m/z105
105/91	+	+	m/z105 occurs at lower CID than m/z91
105/92	+	-	m/z92 occurs at lower CID than m/z105
92/91	+	+	m/z92 occurs at lower CID than m/z91

As shown in Table 5, the signs of the cross-peaks observed in asynchronous and synchronous spectra were used to evaluate the formation of product ions when subjected to varying amounts of CID energy. Application of Noda's sequential order rules shows that the product ion corresponding to  $m/z$  ratio 92 is formed at the lowest CID energy, followed by  $m/z$  119, 105, and

91, respectively. Thus, the formation of product ion  $m/z$  92 at lower energy and the formation of  $m/z$  91 at higher energy is in agreement with previous studies performed to study the energetics of n-butylbenzene.<sup>1 30 31 32</sup>

In order to investigate the further dissociation of  $m/z$  92 to yield  $m/z$  91 at higher energy, a coherence spectrum was utilized. It should be noted that in the research presented here, the product ion corresponding to  $m/z$  ratio 92 is also referred to as intermediate. Recall from Frisch's work<sup>8</sup> (see Figure 7), for a purely parallel dissociation scheme, only the peaks corresponding to the precursor-product ions pairs (A/B and A/C) with equal intensity were observed in the coherence spectrum. In addition, the A/B and A/C peak intensities were independent of the value of rate constants. For a purely consecutive dissociation scheme, however, an additional peak corresponding to an intermediate-product ion pair (B/C) was observed. Also observed for the pure consecutive dissociation scheme was that all peaks corresponding to precursor-product ion pairs (A/B, A/C) and the intermediate-product ion pair (B/C) had unequal intensity, with B/C being the least intense peak compared to the other peaks. For a mixed dissociation scheme, the coherence spectra resembled the coherence spectra of the consecutive dissociation scheme in terms of the number of peaks. Also, the intensities of the peaks varied with the value of the rate constants, such that the coherence spectra of the mixed dissociation scheme resembled either mixed like-consecutive or mixed like-parallel dissociation schemes, represented by models 9 and 8 in Figure 7, respectively.

The coherence spectrum for n-butylbenzene as seen in Figure 18 (d) resembles the coherence spectra of the mixed dissociation scheme that looks like parallel. Four peaks corresponding to precursor-product ion pairs represented by 134/91, 134/92, 134/105, and 134/119 were observed in the coherence spectrum. The peaks corresponding to 134/105 and 134/119 were identical; that is, they had equal intensities as was observed for the parallel dissociation scheme; however, the intensity of the peaks corresponding to 134/91 and 134/92 were not of the same intensity as 134/105 and 134/119. The peak at 134/92 corresponding to a precursor-intermediate ion pair was relatively smaller than other peaks observed in the coherence spectra. Another notable difference was that the peak at 134/91 corresponding to a precursor-product ion was the tallest. Also observed was a weak peak corresponding to intermediate-product ion pair 92/91. The intensity of this peak, however, was so small that it may not be indicative that product ion  $m/z$  92 is an intermediate, and at higher CID energy it undergoes further fragmentation yielding product ion  $m/z$  91. Comparing the peak intensities of the precursor-product ion pairs at 134/92 and 134/91 with the peak intensities of 134/119 and 134/91 ion pairs suggests that product ions  $m/z$  92 and  $m/z$  91 are not formed via purely parallel dissociation, or they would have had intensities equal to product ions  $m/z$  119 and  $m/z$  105, respectively. The presence of other weak peaks corresponding to product-product ion pairs may be attributed to instrumental noise. Similar results were observed by Frisch<sup>8</sup> when random noise was incorporated in the data matrix to investigate the effect of noise on coherence spectral intensities.

#### 4.1.2. Varying Excitation Time at Constant CID Energy

The results presented in this section are from 2DCOS analysis of mass spectral intensities obtained by varying excitation time at constant CID energy for n-butylbenzene. For the 2DCOS analysis, mass spectral intensities obtained at CID energy of 0.6V were selected. As seen in Figure 17, at this CID energy the precursor ion  $m/z$  134 is almost intact, and very few product ions are formed. Thus, in order to study the effect of varying excitation time on the formation of product ions, the excitation time was varied, ranging from 1 to 81 ms at 5 ms increments.

The effect of varying excitation time on product formation is presented in the form of the breakdown curve shown in Figure 19 (a). It can be observed that for varying excitation time at constant CID energy, no induction period was observed. This absence of induction period may be attributed to the fact that at the onset of excitation time, the appearance energy associated with lowest energy dissociation pathways is slightly more than the internal energy of the precursor ion. This observation is also evident from the mass spectrum of n-butylbenzene at 0.6V CID energy (see Figure 17), where the precursor ion  $m/z$  134 is the most abundant species, and relatively very few products are observed.

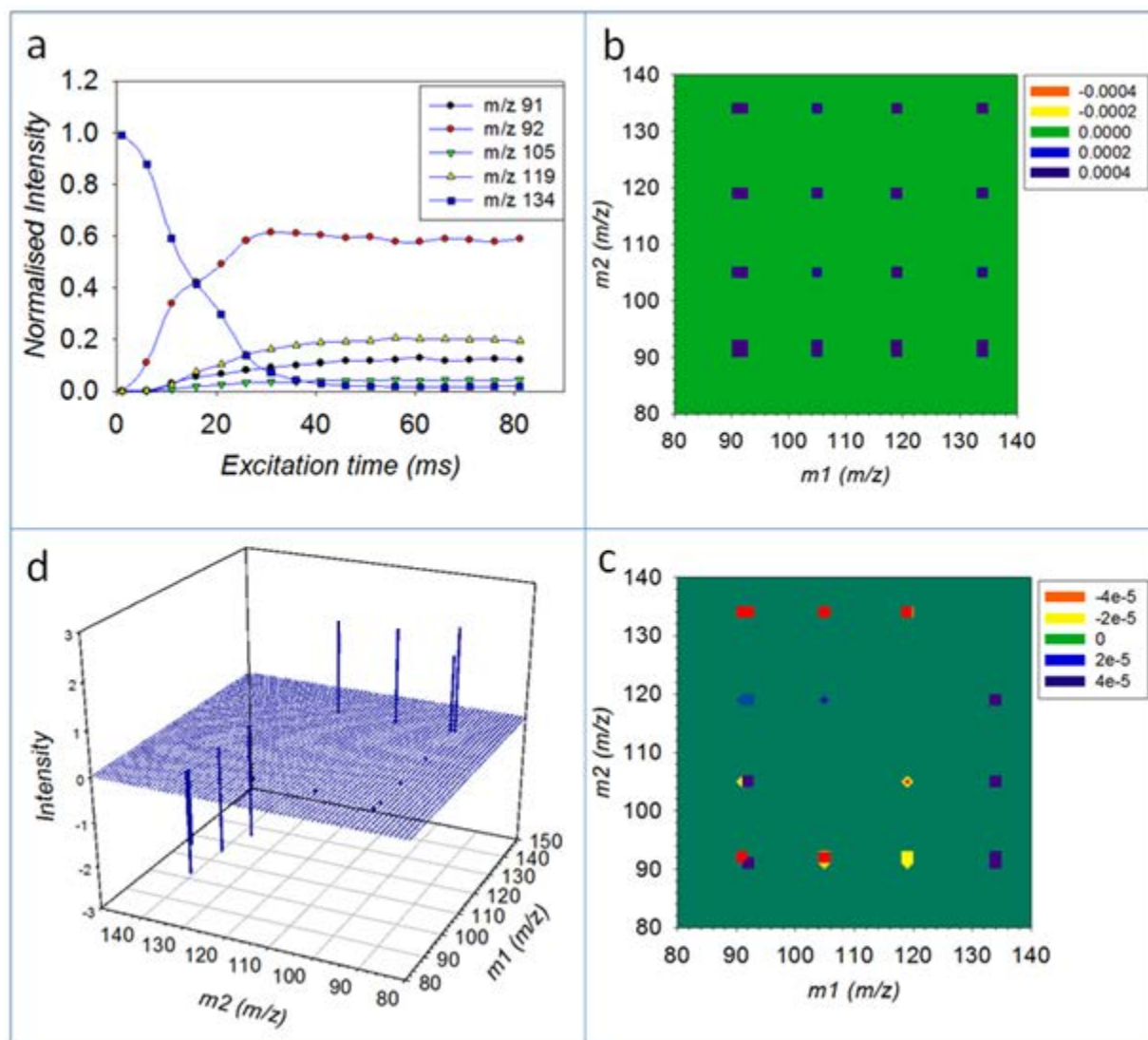


Figure 19: 2DCOS analysis of varying excitation time and constant CID energy (0.6 V): (a) breakdown curve of normalized intensity vs excitation time (ms); (b) synchronous spectra; (c) asynchronous spectra; (d) coherence spectra.

The synchronous spectrum for varying excitation time at constant CID energy as shown in Figure 18 (b) is similar to that obtained by varying CID energy at constant excitation time. Along the diagonal positions, the synchronous spectrum exhibits characteristic auto-peaks while at the



off-diagonal positions, cross-peaks corresponding to the precursor-product ion pairs 134/119, 134/105, 134/92, and 134/91 are observed. Also observed are peaks corresponding to product-product ion pairs (119/91, 119/92, 119/105, 105/91, 105/92) and intermediate-product ion pair 92/91. The signs of all the auto-peaks and cross-peaks take positive values, which can be attributed to the use of zero reference spectra.

The asynchronous spectrum for varying excitation time at constant CID energy is represented by Figure 18 (c). As expected, it is characterized by the absence of auto-peaks along the diagonal. Cross-peaks corresponding to product-product ion pairs and an intermediate-product ion pair can be observed at the off-diagonal positions. Based on the signs of the cross-peaks observed in the synchronous and asynchronous spectrum, Noda's sequential order rules were applied to determine the rates associated with the formation of product ions. The results obtained from the sequential order analysis are presented in Table 6.

Table 6: Noda's Sequential Order Rules to Determine Product Ion Formation as a Function of Varying Excitation Time at Constant CID Energy

<b>Cross-Peaks observed at spectral variables (m1/m2)</b>	<b>Synchronous spectrum <math>\Phi</math> (m1, m2)</b>	<b>Asynchronous spectrum <math>\Psi</math> (m1, m2)</b>	<b>Sequential order of product ion formation over applied perturbation excitation time (ET) range</b>
134/91	+	+	m/z134 occurs at lower ET than m/z91
134/92	+	+	m/z134 occurs at lower ET than m/z92
134/105	+	+	m/z134 occurs at lower ET than m/z105
134/119	+	+	m/z134 occurs at lower ET than m/z119
119/91	+	-	m/z91 occurs at lower ET than m/z119
119/92	+	-	m/z92 occurs at lower ET than m/z119
119/105	+	-	m/z105 occurs at lower ET than m/z119
105/91	+	-	m/z91 occurs at lower ET than m/z105
105/92	+	-	m/z92 occurs at lower ET than m/z105
92/91	+	+	m/z92 occurs at lower ET than m/z91

It can be observed from Table 6 that the sequence in which product ions were formed as a result of varying excitation time is slightly different from that formed as a result of varying CID energy. The product ion  $m/z$  92 is formed at the lowest excitation time, followed by  $m/z$  91, 105 and 119, respectively. Thus, we see that for both sets of mass spectral intensities where the

applied perturbations were varying CID energy at constant excitation time and varying excitation time at constant CID energy, the product ion  $m/z$  92 was formed at the lowest perturbation range, followed by other product ions. The slight deviation in the sequential order of product formations in varying excitation times compared to varying CID energy may be attributed to the fact that different perturbation types result in different amounts of internal energy deposited into the precursor ion upon activation<sup>23, 33</sup>.

The coherence spectrum for varying excitation time is similar to that obtained by varying CID energy. The coherence spectrum for varying excitation time, represented by Figure 19 (d), shows four intense peaks corresponding to precursor-product ion pairs (134/119, 134/105, 134/92, 134/91). The peaks observed at 134/105 and 134/119 are almost equal in intensity; however, the peaks at 134/92 and 134/91 have unequal intensities as compared to the other precursor-product ion pairs. It should be noted that product ion  $m/z$  92 is also referred to as an intermediate product ion in this research. In that context it can be observed that the precursor-intermediate ion pair 134/92 is relatively less intense and the peak at 134/91 is comparatively more intense than the other peaks. Thus, the coherence spectrum for varying excitation time resembles the coherence spectrum of the mixed like-parallel dissociation kinetic model, where the peak corresponding to the precursor-intermediate ion pair was the smallest. These observations are in agreement with Frisch's work for mixed dissociation models.

#### 4.2: 2DCOS Analysis of Kinetic Model

In this section, the results from the 2DCOS analysis of the kinetic model simulating the dissociation pathway of n-butylbenzene are presented. Recall that the kinetic modelled data was generated in MS-Excel and based on the first-order kinetic equations for unimolecular dissociation.

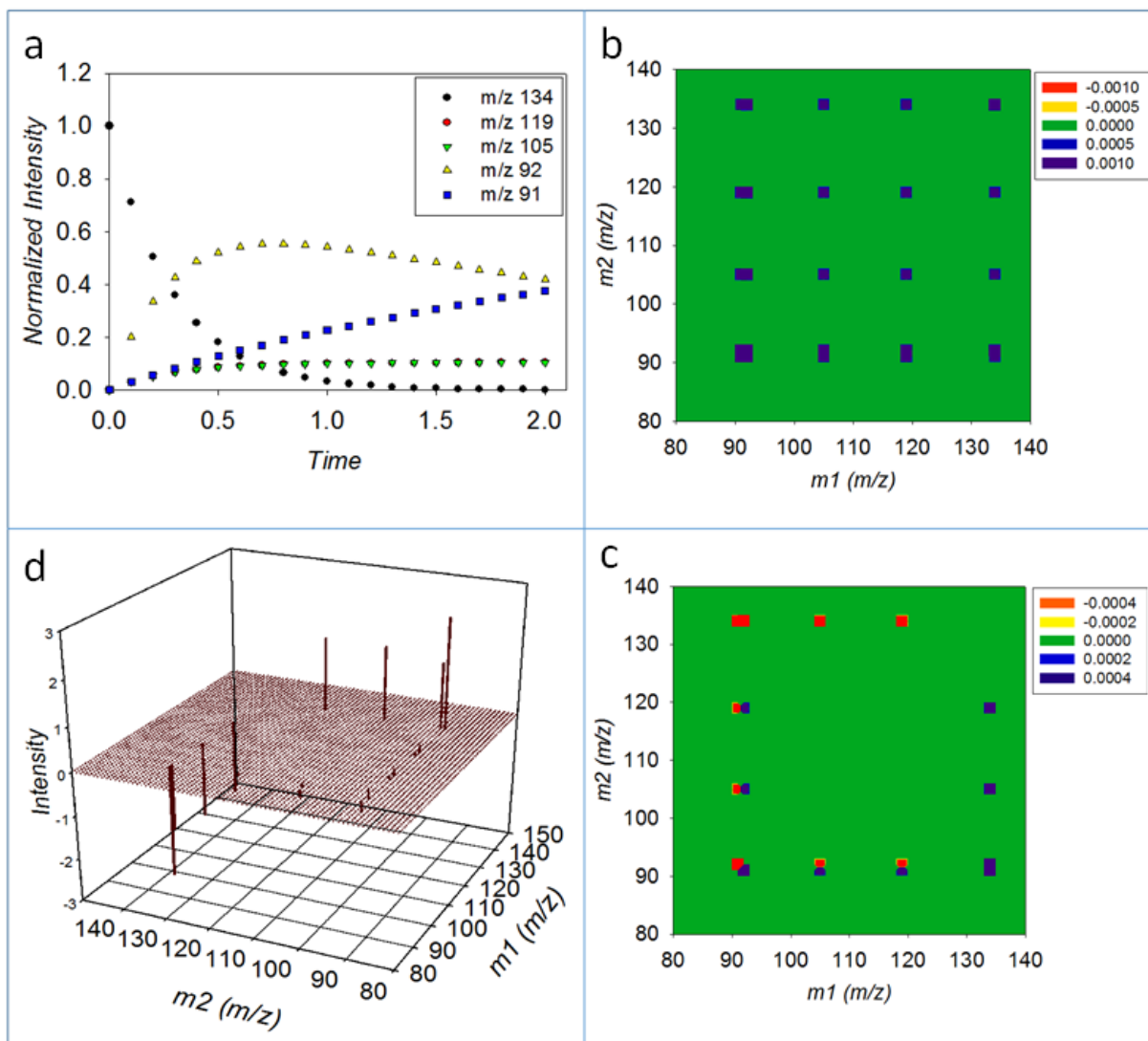


Figure 20: 2DCOS analysis of kinetic model: (a) breakdown curve of normalized intensity vs time (ms); (b) synchronous spectra; (c) asynchronous spectra; (d) coherence spectra.

For the kinetic modelled data, letters A to E were initially assigned to represent the precursor and product ions, respectively, where A denotes the precursor ion and the remaining letters denote product ions. However, for the purpose of interpretation, the letters representing precursor and product ions were replaced by  $m/z$  ratios instead of letters (see Figure 16). The formation of

product ions with the decay of the precursor ion for the kinetic modelled data is pictorially represented in the form of breakdown (see Figure 20 (a)). The breakdown curve for the modelled data resembles the breakdown curve obtained for the experimental data sets.

The synchronous spectrum for the modelled data is represented by Figure 20 (b). It shows characteristic auto-peaks along the diagonal. At the off-diagonal positions, synchronously correlated cross-peaks representing the correlation between precursor-product ion pairs (134/119, 134/105, 134/92, 134/91) are observed. Also observed are peaks corresponding to product-product ion pairs (119/91, 119/92, 119/105, 105/91, 105/92), including the intermediate-product ion pair peak corresponding to 92/91. The signs of all the auto-peaks and cross-peaks take positive values due to the use of a zero reference spectrum.

The asynchronous spectrum represented by Figure 20 (c) for the modelled data is different from the asynchronous spectra of the experimental data. As expected, it lacks the characteristic auto-peaks at the diagonal positions. Along the off-diagonal positions, the cross correlated peak corresponding to 119/105 observed in the asynchronous spectra of the experimental data is absent in the asynchronous spectrum of the modelled data. The absence of the cross-peak at 119/105 in the asynchronous spectrum was expected, as the kinetic model was simulated to form product ions  $m/z$  119 and 105 via parallel dissociation of the precursor ion.

Recall from section 1.2.2 that the absence of a cross-peak in the asynchronous spectrum implies that the spectral intensity change observed at the two spectral variables occurs at the same

perturbation. However, the asynchronous spectrum for the experimental data set exhibits a weak peak at 119/105. The presence of this weak peak at 119/105 for the experimental data may be attributed to instrumental noise. As for the sequence of product formation based on the signs of cross-peaks observed in the asynchronous and synchronous spectra for the modelled data, product ion  $m/z$  92 was formed at the lower perturbation range, product ions  $m/z$  119 and 105 at the same intermediate perturbation level, and  $m/z$  91 at the higher perturbation range. The sequence of product-ion formation for the modelled data as per Noda's sequential order rules is summarized in Table 7.

Table 7: Noda's Sequential Order Rules to Determine Product-Ion Formation as a Function of Applied Perturbation for Modelled Data

<b>Cross-Peaks observed at spectral variables (m1/m2)</b>	<b>Synchronou s spectrum <math>\Phi</math> (m1, m2)</b>	<b>Asynchronous spectrum <math>\Psi</math> (m1, m2)</b>	<b>Sequential order of product ion formation over applied perturbation (time) range</b>
134/91	+	+	m/z 134 occurs at lower ET than m/z 91
134/92	+	+	m/z 134 occurs at lower ET than m/z 92
134/105	+	+	m/z 134 occurs at lower ET than m/z 105
134/119	+	+	m/z 134 occurs at lower ET than m/z 119
119/91	+	+	m/z 119 occurs at lower ET than m/z 91
119/92	+	-	m/z 92 occurs at lower ET than m/z 119
119/105	+	0	m/z 119 and m/z 105 occurs at the same perturbation
105/91	+	+	m/z 91 occurs at lower ET than m/z 105
105/92	+	-	m/z 92 occurs at lower ET than m/z 105
92/91	+	+	m/z 92 occurs at lower ET than m/z 91

The coherence spectrum of kinetic modelled data resembles the coherence spectra of the experimental data sets. The peak corresponding to precursor-product ion pairs 134/119 and 134/105 are of equal intensity as expected, since they were simulated to fragment via parallel



dissociation. The peaks representing the precursor-product ion pairs at 134/92 and 134/91 are of unequal intensity as expected, with 134/92 representing the precursor-intermediate ion pair having the smallest intensity and 134/91 having the largest intensity as compared to other peaks. Thus, the coherence spectra of the modelled data, which was simulated to yield product ion  $m/z$  91 resulting from the dissociation of  $m/z$  134 and also from the dissociation of  $m/z$  92, resembles the coherence spectra for the experimental data, suggesting that n-butylbenzene may undergo mixed dissociation, depending upon the amount of internal energy deposited into the precursor ion.

## CHAPTER 5: CONCLUSIONS

### 5.1. Significance

In this research, the technique of 2DCOS was applied to study the fragmentation pathway of n-butylbenzene as a function of increasing amounts of CID energy and excitation time as applied perturbations. Application of 2DCOS resulted in two 2D correlation spectra: synchronous and asynchronous. The signs of the correlated peak intensities observed in the synchronous and asynchronous spectra suggested that formation of product ion  $m/z$  92 is favored at a lower energy, and formation of product ion  $m/z$  91 is favored at relatively higher energy. Further, the coherence spectral intensities of the peak corresponding to precursor-product ion pairs, a precursor-intermediate ion pair, and a product-product ion pair were useful in demonstrating that at higher energy intermediate product ion  $m/z$  92 can undergo further fragmentation to yield product ion  $m/z$  91.

To corroborate the results obtained from the 2DCOS analysis of the experimental data of n-butylbenzene, a simple kinetic model simulating the fragmentation of n-butylbenzene was created in MS-Excel. The spectral intensities of the modelled data were treated similarly prior to analyzing them with 2DCOS, and the results were compared with the 2DCOS results of the experimental data. It was found that the fragmentation of n-butylbenzene follows a mixed dissociation pathway that resembles a like-parallel dissociation scheme.

To further validate the results of the experimental data from the n-butylbenzene experiment and modelled data, the results were compared with the 2DCOS analysis of simple kinetic models from Frisch's work and were found to be in agreement. While the results observed in this research are in agreement, the primary objective was to demonstrate the application of 2DCOS to study fragmentation pathways of gaseous molecular ions in a quadrupole ion trap.

## 5.2. Future Work

For future work, 2DCOS can be applied to study the dissociation pathways of more complex molecules. For the present research, 2DCOS analysis of the experimental and kinetic modelled data was based on zero reference spectra. Additionally other reference spectra can be explored to obtain the dynamic spectra. For this purpose it would be imperative that the molecules investigated should be established molecules whose dissociation pathways have been studied by other methods so that the results can be compared. For validation of results, other analytical techniques, such as double resonance, and other instruments, such as triple quadrupole, can be incorporated in the study.

**PROJECT 2: INVESTIGATIVE STUDY OF FORMATION OF  
PYROLYSIS PRODUCTS FROM CONTROLLED BURNS TO AID IN  
FIRE DEBRIS ANALYSIS**

## CHAPTER 6: INTRODUCTION

### 6.1. Overview of Fire Debris Analysis

Fire debris analysis involves collection of debris from the fire scene followed by laboratory examination and interpretation of chromatographic results obtained from the analysis of debris<sup>34</sup>. The primary objective of the analysis is to test the presence of ignitable liquid residues (ILR) that may be present within the sample. The debris serving as evidence is very complex due to interfering products. The presence of ILR in fire debris samples therefore may not necessarily be correlated to the use of an ignitable liquid<sup>35</sup>. Interfering products usually refers to substrate background products and products formed due to combustion and pyrolysis. Fire debris analysis is complex because interfering products can mask the pattern of compounds of interest, rendering the interpretation of chromatographic results extremely difficult<sup>36</sup>. Therefore, in order to reach the correct interpretation of chromatographic results it is imperative to have a prior knowledge of these interfering products and how are they formed<sup>36-37</sup>.

### 6.2. Overview of Interfering Products

Interfering products may originate from any of the three sources as mentioned above: substrate background products, products formed due to partial combustion, and products formed from pyrolysis. Substrate background products may either be a naturally occurring product or may have been induced during the manufacturing process or due to contamination. An example of a naturally occurring interfering product would be terpenes found in wood<sup>38</sup>. Similarly, some rubber may contain high boiling point hydrocarbons<sup>35b</sup>. Some ignitable liquids may find their

way into finished products as part of the procedure adopted during manufacturing, for example, the use of petroleum solvents for coating wooden floors<sup>39</sup> and the use of kerosene as a solvent during the ink manufacturing process<sup>40</sup>. Substrates may also get contaminated via direct or indirect contacts and may interfere during the debris analysis. For example, the vehicle floor mat may get contaminated via direct contact with gasoline contaminated shoes<sup>41</sup>, or contamination can occur via indirect contact during aerial transportation of the contaminated sample to a clean substrate<sup>42</sup>.

The second sources of interfering product are those that are released due to combustion of substrates. Formation of combustion products are condition dependent and may yield a mixture of completely oxidized and reduced products usually accompanied by the production of CO<sub>2</sub> and H<sub>2</sub>O. For complete combustion to take place the conditions should be ideal; however, in reality in the presence of an oxidizer, substrates do not undergo complete combustion and may release products that are neither completely oxidized nor completely reduced<sup>35b, 43</sup>. Pyrolysis products make up the third important category of interfering products that are released by the substrate as a result of decomposition of materials under the influence of heat alone. The rate at which pyrolysis occurs depends upon the amount of heat that is provided. More heat results in faster pyrolysis, and the presence of an oxidant such as oxygen results in flaming fire.

### 6.3. Overview of Pyrolysis

As mentioned above, interfering products—in particular, pyrolysis products—pose a major concern in fire debris analysis. Although the presence of pyrolysis products in fire debris is well

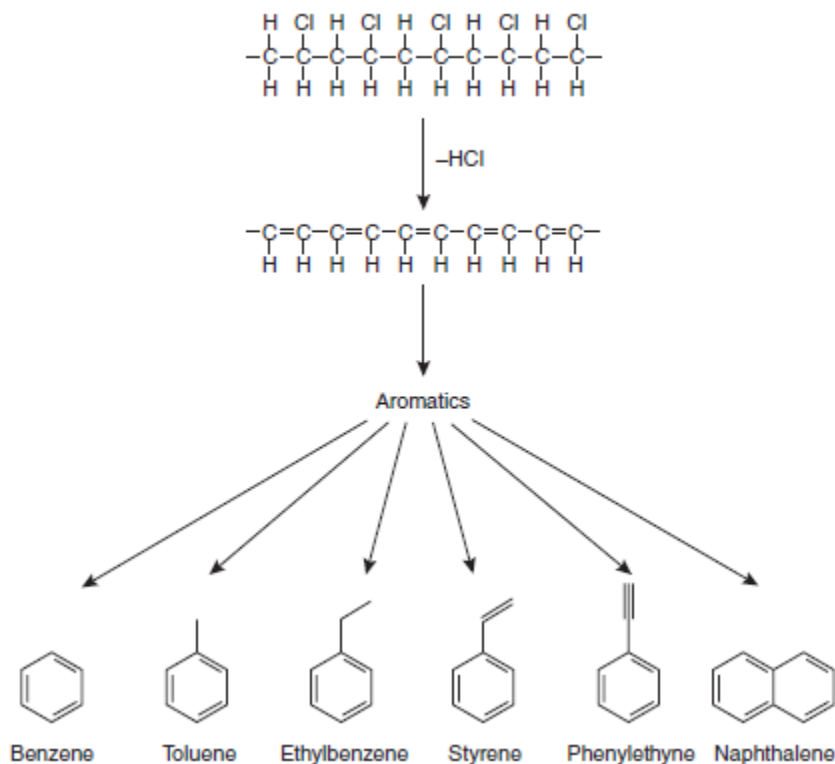
known, it is not clear how these products are formed. Several published reports describe the pyrolysis process; however, the most common definition was reported by Stauffer: a process in which chemical compounds, regardless of their physical states, undergo degradation of their constituents to yield smaller volatile molecules under the influence of heat and without the interaction of oxygen or any other oxidant<sup>36</sup>. The temperature range at which pyrolysis typically occurs is 500-800° C. From 100 to 300° C, the process is termed thermal degradation instead of pyrolysis. From 300 to 500° C the process is termed mild pyrolysis, and anything beyond 800° C is termed vigorous pyrolysis<sup>36</sup>. Although environmental conditions and the nature of the substrates influence the pyrolysis process, the breakdown of chemicals compounds into smaller volatile molecules occurs via following three mechanisms.

#### *6.3.1. Random Scission*

Random scission proceeds through formation of a free radical due to breaking of a polymer backbone. In addition to backbone breaking, the mechanism may involve C-H bond cleavage and formal 1,3-hydrogen-shifts, yielding a series of smaller repeating structures with different carbon chain lengths.





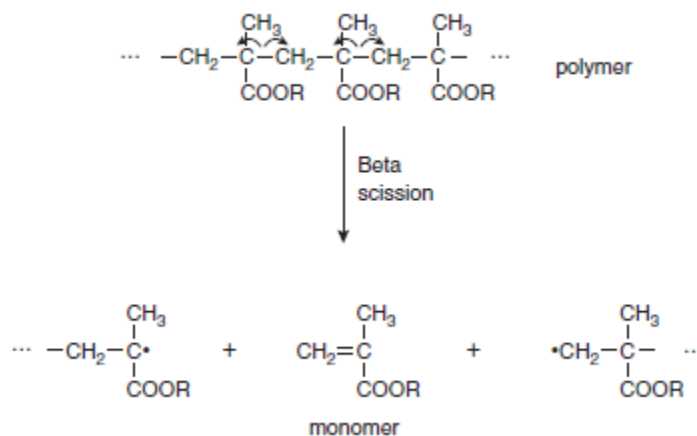


(Adapted from the journal article titled “Concept of pyrolysis for fire debris analysts” by E. Stauffer, 2003, Science & Justice. with copyright permission from Elsevier, see appendix)

Figure 22: PVC representing side-group scission mechanism

### 6.3.3. Depolymerisation

Depolymerisation involves degradation of a polymer via a free radical mechanism, yielding a monomer that make up the polymer<sup>44</sup>. This mechanism is also referred to as monomer reversion<sup>36</sup>. Several polymeric molecules undergo degradation via this mechanism, which proceeds through the formation of a free radical on the polymer backbone. This causes the polymer to undergo scission to yield small unsaturated molecules and then propagate to the free radical on the polymer backbone<sup>45</sup>. Figure 19 represents the depolymerisation mechanism of polymethacrylate.



(Adapted from the journal article titled “Concept of pyrolysis for fire debris analysts” by E. Stauffer, 2003, Science & Justice. with copyright permission from Elsevier; see Appendix)

Figure 23: Polymethacrylate undergoing depolymerisation to yield monomer

#### 6.4. Purpose of Research

Once a building structure catches fire, regardless of whether the fire was intentional as in arson or unintentional, the fire’s destructive nature causes extreme damage to property and human lives. In the case of an arson investigation, the challenge is to find a link between the debris and ignitable liquid that may have been used to set the fire. As part of the investigation, the preliminary steps involve collection of debris from the fire scene, followed by their laboratory analysis and interpretation of the chromatographic result. The objective of the laboratory analysis is to identify traces of ILR; however, the presence of interfering products complicates the process and calls into question the reliability of the analysis. For the correct interpretation of

chromatographic results, it is therefore imperative to distinguish interfering products from the compounds that are characteristic of ignitable liquids.

Among the several factors that may have an influence on the chromatographic results, the crucial one is the method adopted for separation of ILR from fire debris samples. A method widely used by the forensic community is known as passive headspace concentration. This method is based on recommendations of the American Society for Testing and Materials (ASTM E 1412) and uses an activated charcoal strip to adsorb the vapors from the samples upon heating<sup>46</sup>. One of the major concerns pertaining to using a charcoal strip is saturation of adsorption sites, which can further lead to displacement of chemical components<sup>47</sup>. These concerns can eventually have an overall impact on the interpretation of chromatographic results. Thus, in order to reach the correct interpretation of the results, it is beneficial to have prior knowledge of the interfering products, especially the pyrolysis products. Thus, the primary objective of this research was to investigate the formation of pyrolysis products.

For this purpose, commonly used substrates such as polystyrene (PS), polyvinylchloride (PVC), nylon-carpet, padding, and yellow-pine used in residential and commercial constructions were subjected to controlled burns in the laboratory using a tube and propane torch as heat source. Paint cans, and flat pans were used to contain the substrates. The burnt samples were then subjected to passive headspace adsorption as described in ASTM E1412 and analyzed using gas-chromatography mass spectrometry. For quantitative analysis of pyrolysis products, yellow pine and a combination of nylon carpet and padding were subjected to controlled burns in the

presence of ignitable liquids represented by of n-alkanes ranging from octane to undecane. The major products formed during the controlled burns were quantified by constructing a calibration plots employing 2,3-dimethylheptane as an internal standard.

## CHAPTER 7: FIRE DEBRIS ANALYSIS

As mentioned in the previous chapter, the preliminary steps involved in the investigation of fire debris analysis are collection of debris from the fire scene, extraction of ignitable liquid from the debris and lastly, laboratory analysis to test the presence of ignitable liquids. The challenge here is the proper identification of ILR which depends upon the correct interpretation of the chromatographic result obtained from the laboratory analyses. Chemical analysis of fire debris requires appropriate skill and knowledge pertaining to both the nature of ignitable liquids and scientific instrumentation<sup>48</sup>. This chapter will discuss methods that are frequently employed by the forensic community for fire debris analysis.

### 7.1. Collection of Fire Debris.

Collection of fire debris samples may seem trivial nevertheless it is one of the most crucial steps of the investigation. When considering the volatile nature of ignitable liquid, the timely collection and preservation of this liquid is crucial. Another factor is the location inside the burnt structure from where the samples are collected. Ignitable liquids tend to get absorbed by these substrates and may be retained at different levels depending upon their packing, porosity and thickness. In general there is no standard procedure for collection of debris as they may vary depending upon their nature. The procedure that is commonly used in the United States involves collection of debris samples in paint-cans. These cans are available commercially in different sizes with sealable lids that are not completely leak-proof and puncture resistant<sup>48</sup>. In some European countries, other than paint-cans, nylon bags, kapak bags, laminated bags and mason

jars<sup>49</sup> have been used for collection of debris, however some of them were found to leak certain chemical compounds after a week<sup>48</sup>.

## 7.2. Extraction of ILR

Once the fire debris has been collected in an appropriate container, it is transported to the laboratory where it is subjected to extraction. The objective of this step is to isolate ILR that may be adsorbed onto to the substrate surface. Several methods have been utilized for extraction of ILR from the debris some of them are discussed as follows.

### *7.2.1. Solvent Extraction*

It is one of the earliest techniques utilized for extraction of ILR from a non-absorbent surface, such as glass<sup>50</sup>. This is essentially a destructive technique and therefore must be employed only when the fire-debris sample can be reused for future analysis. This technique involves soaking the sample in a beaker containing volatile organic solvents. The time for which the samples are soaked may vary depending upon the size and nature of the sample. Finally, the samples are removed from the solvent followed by concentration of the solvent by evaporation. Though this technique offers several advantages in terms of simplicity and fast recovery, it can contribute to the complexity of the analysis due to contamination. In this case the solvent used for extraction may be similar to one of the products corresponding to ILR. Another issue is that low-boiling products may be lost during evaporation. Hence, solvent extraction technique is mainly suited for extraction of high-boiling chemicals<sup>50</sup>.

### *7.2.2. Dynamic Headspace Concentration*

This technique involves heating the sample in a closed container resulting in vaporization of volatiles. This technique requires a tube containing an adsorbent, such as activated charcoal. Headspace of the container can either be withdrawn through this adsorbent tube by continuous suction utilizing vacuum or the headspace can be pushed through the adsorbent tube by applying positive pressure with an inert gas. For desorption of the volatiles, an appropriate solvent such as carbon disulfide is used. One of the major advantages of this technique is better recovery efficiency of the volatiles. The disadvantage of utilizing this technique is that since almost all the volatiles are extracted from the sample, it is considered a destructive technique based on ASTM E1413-95 which is a standard practice for separation of ILR from fire debris<sup>51</sup>. Also there is a possibility of contamination due to usage of an external inert gas.

### *7.2.3. Passive Headspace Concentration*

This technique is based on ASTM E1412-00, a standard practice for separation of ILR from fire debris widely used by the U.S. forensic community. It primarily utilizes an activated 10 mm x 20 mm charcoal strip as adsorbent, oven for heating and a temperature measuring device as shown in Figure 24.

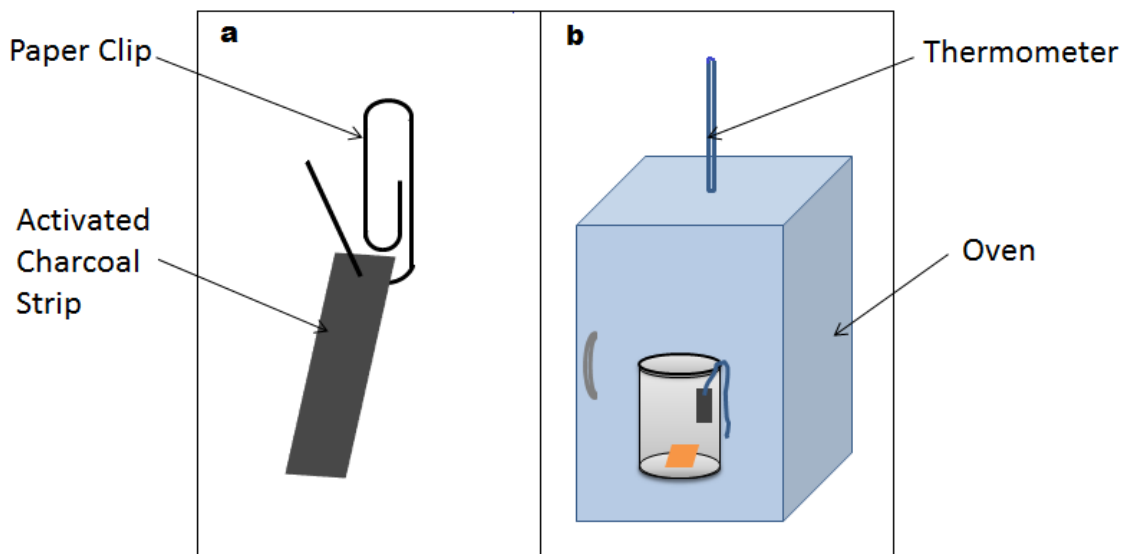


Figure 24: Passive headspace adsorption (a) paper clip holding activated charcoal strip; (b) heating device for adsorption of volatiles onto charcoal strip

In this technique, an activated charcoal strip pierced through a paperclip is suspended into the headspace of the container containing the fire debris samples<sup>52</sup>. The container is then sealed with a new solid lid and activated by placing into an oven for about 16 to 18 hours. During the activation period, fire debris samples release the volatiles which are adsorbed onto the surface of the charcoal strip. After approximately 16 hours of activation, the container is removed from the oven and cooled to attain room temperature. Once the container is sufficiently cooled, the charcoal strip is then eluted with a suitable solvent such as carbon disulfide or diethyl ether. This technique is considered non-destructive as the charcoal strip is placed into the headspace of the container. Another advantage is that only a portion of this charcoal strip can be used for desorption of volatiles and the remaining portion of the strip can be archived for reuse<sup>47</sup>.



#### *7.2.4. Headspace Concentration Using Solid Phase Micro Extraction (SPME)*

This technique involves coating a SPME fiber with a suitable adsorbent for extraction of ignitable liquids from the evidence container. The adsorbents that are commonly used for coating the SPME fiber are polymers such as polydimethylsiloxane (PDMS), polyacrylate and Carboxen<sup>47</sup>. Furthermore, choice of adsorbent and its thickness onto the fiber can also affect the adsorption of analytes. For example, ignitable liquids in the range of C<sub>10</sub>-C<sub>25</sub> were efficiently adsorbed by using a SPME fiber coated with 100 µm thick PDMS layer. Similarly, for adsorption of ignitable liquids in the range of C<sub>1</sub>-C<sub>10</sub>, a SPME fiber coated with 85 µm thick polyacrylate layer was recommended. In this technique, the evidence container's lid is punctured and a septum is inserted into the hole for allowing the SPME needle to pierce through the septum and into the headspace of the container. For extraction of ILR, the evidence container is then placed into oven for approximately 30 minutes between the temperatures of 60°C and 80°C. This temperature results in the vaporization of ignitable liquids into the headspace of evidence container. After 30 minutes, the container is removed from the oven and the SPME fiber which is held within the needle is inserted through the septum and into the headspace of the container to allow adsorption of ILR onto the polymeric coating. Once the fiber is exposed into the headspace for about 5 to 15 minutes, it is retracted into the needle and immediately inserted into the injection port of GC<sup>53</sup>.

Thus we see that several techniques have been used for extraction of ILR from fire debris samples and each technique has their own merits and demerits. One of the main objectives behind the selection of a particular technique is recovery efficiency and sensitivity. In this

research project, for extraction purposes, passive headspace concentration method was utilized throughout. Though this technique is relatively time consuming considering the activation time in oven which is approximately 16 hours, the recovery of the volatiles are sufficiently high and it is non-destructive.

### 7.3. Detection of ILR

After extraction of ILR, the next step involves their analysis by suitable analytical instrumentation. As mentioned in the previous section, the ILR may be extracted into a solvent or as headspace. Therefore it is essential that the analytical instrumentation used must be capable of analyzing the samples in both liquid and gas phase. For this purpose gas chromatography-mass spectrometry (GC-MS) is the obvious choice in forensic labs. Other than a mass spectrometer (MS), flame ionization detector (FID) has also been explored as a detector. However, hyphenation of GC to MS offers more in terms of chemical information and sensitivity. In the research presented here all the samples and standards were analyzed by GC-MS.

#### *7.3.1. Gas Chromatography-Mass Spectrometry (GC-MS).*

Chromatography is a technique in which components of a mixture are partitioned between a stationary phase and a mobile phase. In GC, the stationary phase can either be a solid or liquid coated on a solid support while mobile phase is usually a gas. The mobile phase in GC is often referred to as carrier gas. Though nitrogen, hydrogen and helium may be used as a carrier gas, for research purposes use of helium has been predominant. As the name suggests the function of

carrier gas is to carry the analytes through a heated column. The GC column is basically a fine capillary tube made up of glass, the inner walls of which consist of immobile liquid coated onto the surface of an inert solid. A pictorial representation of GC-MS instrumentation is shown in figure 25.

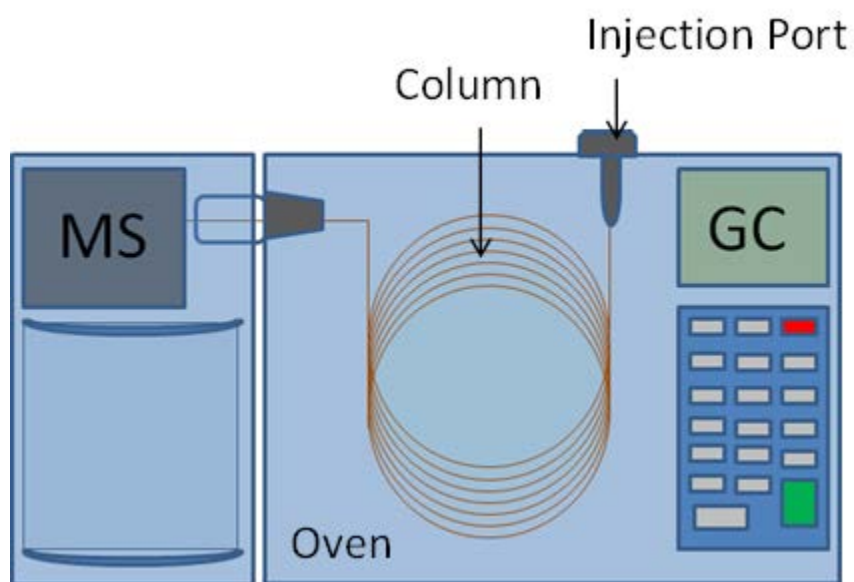


Figure 25: Pictorial representation of gas chromatography mass spectrometry (GC-MS)

The GC column in different dimensions and inner coatings may be obtained as per project requirements. For the analysis, the analyte molecules in the gas phase or liquid phase are injected into the GC column through a heated zone known as injection port. Since the analysis requires the analyte molecules to be in gas phase, the temperature at the injection port is maintained higher than the boiling point of the analytes. As the analytes pass through the heated capillary column under the influence of the carrier gas, they are partitioned between stationary phase and carrier gas. The interaction of different analytes for the same stationary phase is based on

polarity. This interaction between analytes and stationary phase causes the analytes to migrate at different rates within the column resulting in their separation.

Once the gaseous analytes elute from the GC column they enter the ionization source of the mass spectrometer. In the ionization source, the gaseous neutral analyte molecules are bombarded with high energy electron beam emitted from an electrically heated filament. The energy associated with the electron beam is approximately 70 eV. However, the ionization potential required to convert a neutral molecule into a radical cation is approximately 15 eV. This method of ionization is known as electron ionization (EI) and is the preferred ionization method due to its reproducibility. The ionized molecules then accelerate into the mass analyzer where they may collide with bath gas molecules, usually helium, resulting in fragmentation. Under the influence of an applied electric field, these fragment ions can be separated based on their  $m/z$  ratio as they reach the detector.

For the analysis of fire debris samples, forensic laboratories generally employ mass spectrometers equipped with quadrupole and/or ion-trap instruments. In this section however, only quadrupole mass spectrometer has been discussed as it was used throughout this research. Quadrupole mass spectrometer consists of a set of four cylindrical rods arranged to have a hyperbolic cross section. Alternative potentials can be applied at the rods so that if one pair of opposite rods has a positive potential then the other opposite rods will be at negative potentials and vice-versa. The applied potential is a combination of direct current (D.C) voltage and alternating current (A.C), voltage being represented by “U” and “ $V\cos(\omega t)$ ” respectively. As a result of these alternating potentials the trajectory of the ions is affected such that for a given

direct current D.C and A.C voltages, only ions of a certain  $m/z$  ratio will travel radially and reach the detector while the other ions lose their trajectory before they reach the detector. Thus, by varying the applied voltages on the rods, ions of different  $m/z$  ratios can be obtained to yield a mass spectrum.

### *7.3.2. Interpretation of Results*

In fire debris investigation, interpretation of results obtained from the GC-MS analysis of fire debris samples is very crucial. The challenge here is to distinguish the samples containing ILR from the samples that do not contain ILR.<sup>37</sup> However, this process of identification of ILR from the fire debris samples can be intricate for several reasons. First, the numbers of ignitable liquids that are available commercially are enormous. Furthermore, each of these liquids are comprised of hundreds of chemical compounds. The complexity arises when some of these compounds present in ignitable liquids are also found in pyrolysis products in fire debris. Such compounds are referred to as target compounds<sup>54</sup> and the extraction of target compounds from the fire debris samples therefore may not necessarily indicate that ignitable liquids were present since they can also be resulting from pyrolysis. Among other factors that can contribute to the complexities are differential evaporation also referred to as weathering and deterioration of the ignitable liquids. During weathering certain low-boiling point compounds will evaporate faster than higher-boiling point compounds considering the high temperature that is reached during fire conditions<sup>55</sup>. Deterioration involves degradation of ignitable liquids. For example, microorganisms present in the soil can breakdown the chemical compounds thereby modifying the composition of gasoline<sup>56</sup>. In forensic laboratories, extraction of ILR from the fire debris is commonly effected utilizing

activated charcoal strips as described in passive headspace concentration (see section 7.2.3). However studies utilizing charcoal strips have demonstrated that less volatile and high molecular weight compounds can preferentially adsorb over relatively more volatile and low molecular weight compounds<sup>47</sup>. In this case the resultant chromatogram is more likely to resemble the chromatogram of a weathered sample<sup>57</sup>.

Thus in order for the correct identification of ILR in fire debris samples, the American Society for Testing and Materials (ASTM) listed methods which involves visual comparisons of total ion chromatograms (TICs), extracted ion profiling (EIP) and target compound analysis (TAC). These methods are based on pattern recognition in which TICs corresponding to a fire debris sample is compared to that of a known reference or standard. Pattern recognition further involves identification of specific chemical compounds and their appropriate ratios. Identification based on visual comparisons can be challenging due to the weathering effect as discussed above and considering the complex matrix involved in fire debris samples. Additionally factors such as variations in laboratory conditions and instrumental parameters may yield inherent noise that can mask the patterns of compounds of interest. Therefore interpretation of chromatographic results based on pattern recognition requires an analyst to have experience in analyzing fire debris samples and appropriate knowledge pertaining to the nature of ignitable liquids<sup>58</sup>.

Other methods that have been utilized for determining the presence and classification of ILR are based on statistical analysis involving Total ion spectrum (TIS) instead of TIC. Total ion spectrum was generated for each sample by taking the sum of mass spectral intensities associated

with each  $m/z$  ratio across the length of the chromatographic time to obtain a one dimensional data set. The advantage of TIS over TIC is that it does not depend on instrumental parameters which influence retention-times. For this reason comparisons of TIS are convenient. However sampling methods, analysis methods and weathering effect can cause distortions of TIS inducing complications in the classification of ILR<sup>58-59</sup>. Experimental approaches have also been undertaken by forensic scientists to aid in the correct interpretation of chromatographic results. These methods involve controlled burns of substrates commonly used in residential and commercial settings. Several studies on controlled burns performed in laboratories have been reported and are discussed in the next chapter.

## CHAPTER 8: CONTROLLED BURNS

As discussed in the previous chapter, interpretation of results obtained from the GC-MS analysis of fire debris samples can be extremely complex. The major factor contributing to the complexities is the presence of pyrolysis products that can interfere in the proper identification of ILR. In order to increase the confidence in the correct identification of ILR, it is imperative to understand the process by which pyrolysis products are formed. One of the approaches to investigating the formation of pyrolysis products is subjecting the substrates to controlled burns in the laboratory and analyzing the resulting pyrolysis products. In a study done by Ettl and Adams, they attempted to char a wide variety of materials such as wood, newspaper magazines and sheets of different fabrics. The materials were burned separately in a muffle furnace with and without gasoline at 600 °C and analyzed by gas chromatography equipped with flame ionization detector (GC-FID). The objective of the study was to determine the type and amount of hydrocarbons that can be extracted from the charred materials. The authors concluded that the amount of hydrocarbons extracted from organic materials were greater than when they were charred both with and without gasoline samples. The study however did not attempt to identify the pyrolysis products. The method used for quantification of hydrocarbons was not also reported<sup>60</sup>.

In another study done by Howard and McKague, charred carpet debris, recovered from the fire scene for a suspected arson case, was analyzed. Headspace of the carpet debris was drawn using a small pump and trapped onto a charcoal containing sampling tube. The trapped organic vapors were then eluted with carbon disulfide and analyzed by GC-FID. Benzene and toluene were



some of the compounds identified based on matching retention times, which also happens to be components of gasoline. Styrene, a known combustion product of carpet containing polystyrene copolymers was found to be the major peak. The authors did not rule out the possible use of ignitable liquid based on the presence of styrene from the charred material and decided to carry out controlled burns of copolymer of styrene and butadiene in a test tube with a side arm. The organic vapors resulting from the pyrolysis of the copolymer sample were collected and trapped in a similar way as carried out for the carpet debris. The authors found the chromatograms obtained from the analysis of carpet debris and styrene/butadiene copolymer to be virtually identical and further concluded that the hydrocarbons extracted from charred carpet debris was a result of combustion of carpet and not from addition of ignitable liquid<sup>61</sup>.

DeHaan and Bonarius performed experiments where they burned substrates like nylon carpet, polyurethane pads and floor covering in a simulated structure. The substrates were burned both in the absence and presence of ignitable liquid. The objective was to study the volatiles released during burning and whether their presence can cause any interference in the identification of ignitable liquids. The authors concluded by offering some solutions to distinguish the chromatograms of pyrolysis products from that of ignitable liquids<sup>50</sup>.

Sigman et al employed Konex steel containers for setting up large scale burns. The interior of the container was built to simulate an apartment or home, with a door and window to allow ventilation. Substrates used for burns included wood laminate, vinyl tile, furniture, magazines, clothing, shoes, curtains, carpet and padding. Ignitable liquids were poured on some portion of

the room to initiate burns. Temperature inside the container was recorded for the entire duration of the burns by utilizing thermocouples connected to computers. After the set time for burns, the fire was extinguished with water by professional fire fighters. Once the containers were sufficiently cooled, the debris samples were collected in clean unused gallon-sized metal cans and further analyzed by GC-MS<sup>58</sup>.

Bertsch, burned samples of new and old carpet and padding in a clean unused metal can by heating them with an open flame. The carpet and padding samples were burned separately such that in some of the carpet and padding samples, a small amount of gasoline was spiked. The objective was to create comparison samples of pyrolysis products to aid in the interpretation of chromatograms of fire debris samples. The samples were heated in a controlled manner to obtain samples with different degree of burns<sup>62</sup>. Controlled experiments involving heating of substrates in clean unused metal cans have also been employed by other authors to generate pyrolysis products. Stauffer burned a variety of building materials in metal cans for characterization and identification of pyrolysis products. The author concluded that the degradation mechanism is complex and a large number of products resulted from the pyrolysis of polymers. Toluene, Ethylbenzene, Phenylethyne, Styrene and Naphthalene were some of pyrolysis products that were found to be intense compared to other interfering products resulting from combustion and from substrate background. In another study, Castelbuono developed a modified destructive distillation methodology based on the method provided by Florida Bureau of Forensic Fire and Explosive Analysis for generating interfering products. The method involved heating the substrates in quart sized paint cans by applying heat to the bottom of the can with propane torch.

Substrates such as carpet, carpet blends, hardwoods, softwoods, vinyl and linoleum floorings were heated in paint cans and the post burn samples were analyzed by GC-MS<sup>63</sup>.

Sandercock, demonstrated a simple reproducible method for generating pyrolysis products. The method involved heating different substrates in culture tubes which was then inserted into a temperature programmable pre-heated steady state-tube furnace. This method was developed with the aim to create pyrolysates similar to those found in debris samples recovered at the fire scene. The author also used this method for proficiency tests and for creating a library of pyrolysates<sup>64</sup>.

Thus, so far several methodologies have been developed by forensic scientists for the purpose of investigating pyrolysis products. The most commonly employed method for preparing pyrolysis reference samples involves heating the substrates in metal cans. However, there are several factors that may influence the reproducibility of the results such as size of the substrate, time for which substrate was heated and temperature and heating methods such as heating the substrate with an open flame versus heating with a propane torch. The dissertation research presented here also aims to investigate the formation of pyrolysis products by subjecting commonly used building materials to controlled burns in a laboratory. To carry out controlled burns, new methodologies have been developed involving heating the substrates in a furnace and steel pans in addition to the modified destructive distillation method. These methodologies have been discussed in detail in the next chapter. Substrates utilized in this research were polymers like polystyrene, polyvinylchloride, polybutadiene, as well as yellow pine, nylon carpet and padding.

To further investigate the influence of ignitable liquids on the formation of pyrolysates, yellow pine, and a combination of nylon carpet and padding were heated separately in the presence of hydrocarbon mixtures ranging from octane to undecane. For analysis of the samples, Passive headspace concentration method was utilized for the analysis of the samples.

## CHAPTER 9: MATERIALS AND METHODS

### 9.1: Controlled Heating in Furnace:

In this chapter, the methods developed for generating pyrolysis products are presented. The first method involved heating the substrate samples in a 40 mL capacity Pyrex vial that was then inserted into the ceramic work tube of the furnace (Carbolite, Model: MTF 10/25/130). Figure 26 represents the schematic of the experimental setup for generating pyrolysis products using the furnace.

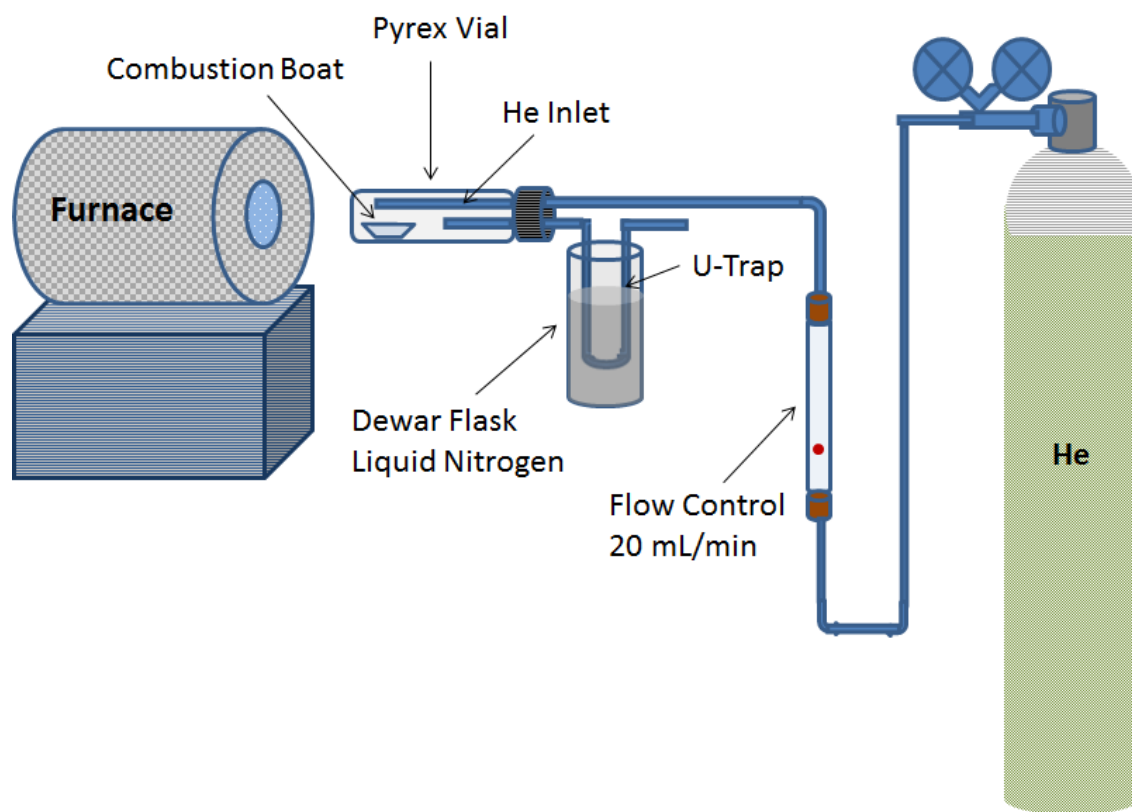


Figure 26: Schematic representation of experimental setup for generating pyrolysis reference samples using a tube furnace

The assembly for the pyrolysis experiment involving a furnace consisted of a Pyrex vial, two steel tubes with an internal diameter of 3.175 millimeter (mm), and a porcelain combustion boat with dimensions of length, width, and height equals to 17.0, 6.0 and 4.0 mm, respectively. In order to eliminate any residual oxygen inside the Pyrex vial prior to heating the substrate sample, the interior of the vial was purged with an inert gas by connecting one of the steel tubes to a helium source (tank). While this tube connected to the helium source served as an inlet for helium, the other steel tube inside the vial served as a cold trap for the vapors (pyrolysates). Trapping of pyrolysates was implemented by bending a section of the steel tube outside the vial into a “U” shape as shown in Figure 26, which was then immersed into a Dewar flask containing liquid nitrogen. For the purpose of establishing a controlled environment, the helium flow rate was maintained constant at 20 mL/min by connecting the helium inlet steel tubing via a flow controller.

For the experiments, substrate samples and combustion boats were weighed separately, and their masses were recorded. Prior to heating the substrates, the furnace was preheated to a target temperature of 450 °C. The combustion boat carrying the substrate samples was then placed into the vial and introduced into the preheated furnace. In this research, the substrates were heated separately at three time intervals: one, five, and eight minutes. The objective was to investigate the formation of pyrolysis products as a function of time under a given set of experimental conditions. After the desired time of heating, the vial containing the pyrolyzed sample was allowed to cool for approximately 60 seconds by moving the furnace away from the hot Pyrex

vial while the U shaped cold trap was still immersed into the Dewar flask containing liquid nitrogen.

For analysis of pyrolysates, the trap was removed from the Dewar flask and allowed to warm for approximately 10 seconds. The pyrolysates inside the cold trap were then eluted with 2 mL of n-pentane (99+ % pure, Acros Organics) and collected into a new clean vial labelled “Vapors” for further analysis by GC-MS (see Figure 27).

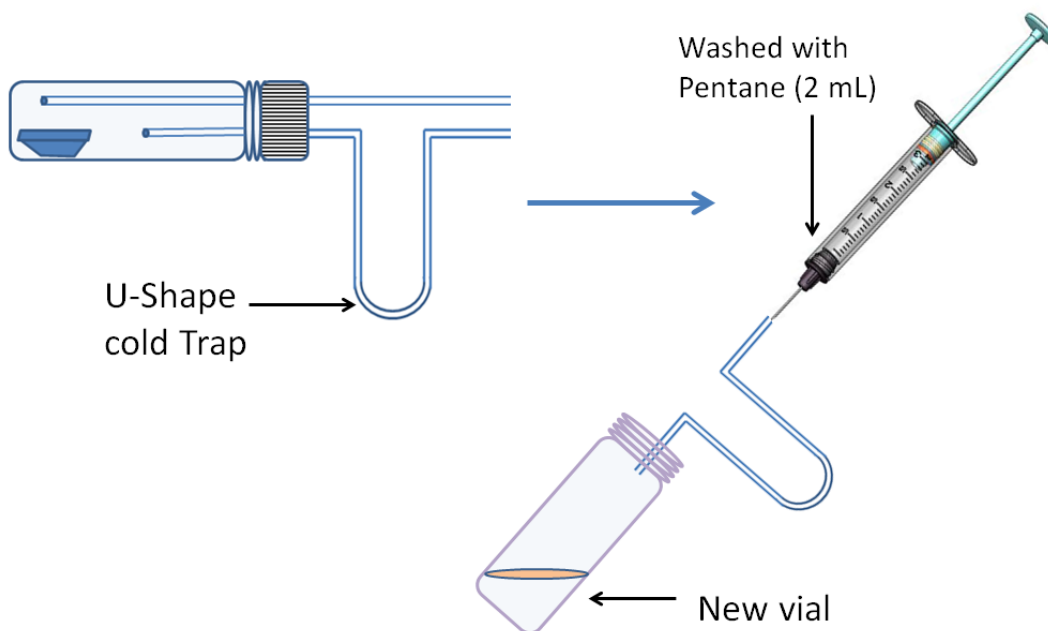


Figure 27: Elution of vapors (pyrolysates) with pentane for GC-MS analysis

For analysis of residues, that is, the remains of substrates on the combustion boat after it was subjected to heating, the combustion boat was removed from the Pyrex vial, avoiding any contact with the walls of the Pyrex vial (see Figure 28) and transferred into a new clean vial labelled

“Residue.” The passive headspace concentration method as described in Section 7.2.3 was employed for adsorption of analytes from the residues which were then extracted into 500 microliter (uL) of carbon disulfide for GC-MS analysis

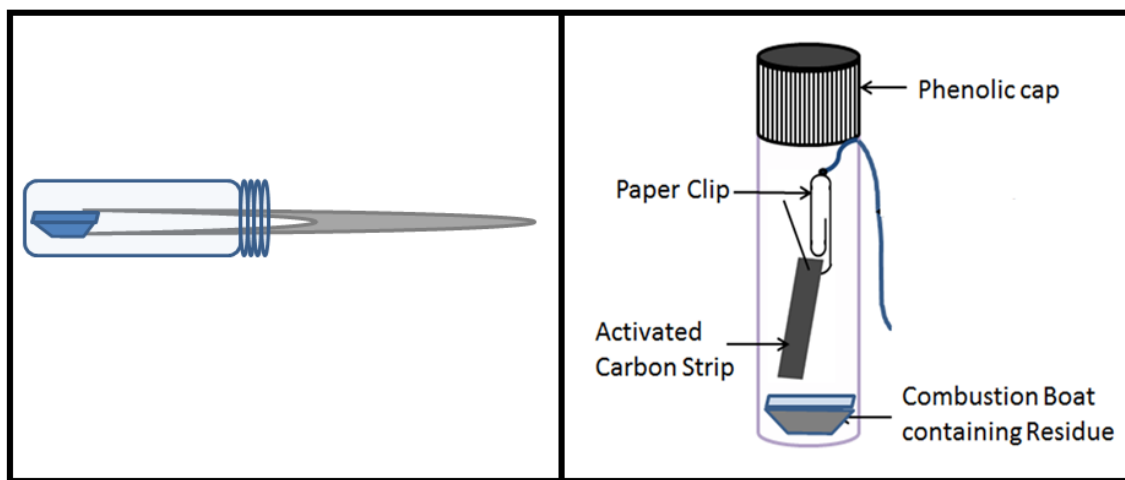


Figure 28: Residue analysis

Since the front end of the Pyrex vial near the phenolic cap was exposed to atmosphere, the temperature at the front end was relatively lower than the remaining portion of the vial which was covered by the hot ceramic tube. As a result, some vapors produced during heating of substrates condensed near the front end of the Pyrex vial, as seen in Figure 29. The condensed vapors were referred to as condensates. For the analysis of condensates, the original Pyrex vial was washed with 2 mL of n-pentane and the condensates collected in another new clean vial labelled “Condensate” and analyzed by GC-MS. It should be noted that prior to washing the original Pyrex vial for condensate analysis, the combustion boat containing residue was removed and transferred to another new clean vial as discussed above for residue analysis.





Figure 29: Pyrex vial with vapors condensed at the front end

#### *9.1.1. Investigation of New Products Formed from Co-Pyrolysis*

For this study, two sets of polymeric substrates were subjected to heating in two separate experiments: one-boat and two-boat. The first set of polymers comprised polystyrene (PS) and polyvinylchloride (PVC), while the second set comprised PS and polybutadiene (PB). The primary objective of these experiments was to investigate the products formed when samples from different substrates were heated together in the same Pyrex vial by placing them in contact and when placed separately

For this purpose the experiment was performed in two ways. In the first experiment, substrate samples from the same set of polymers were heated together in the Pyrex vial by placing them in contact in one combustion boat, referred to as the one-boat (1B) experiment in Figure 30 (a). In the second experiment, substrate samples from the same set of polymers were heated by placing

them separately in two combustion boats and inserted into the same Pyrex vial, referred to as the two-boat (2B) experiment in Figure 30 (b).

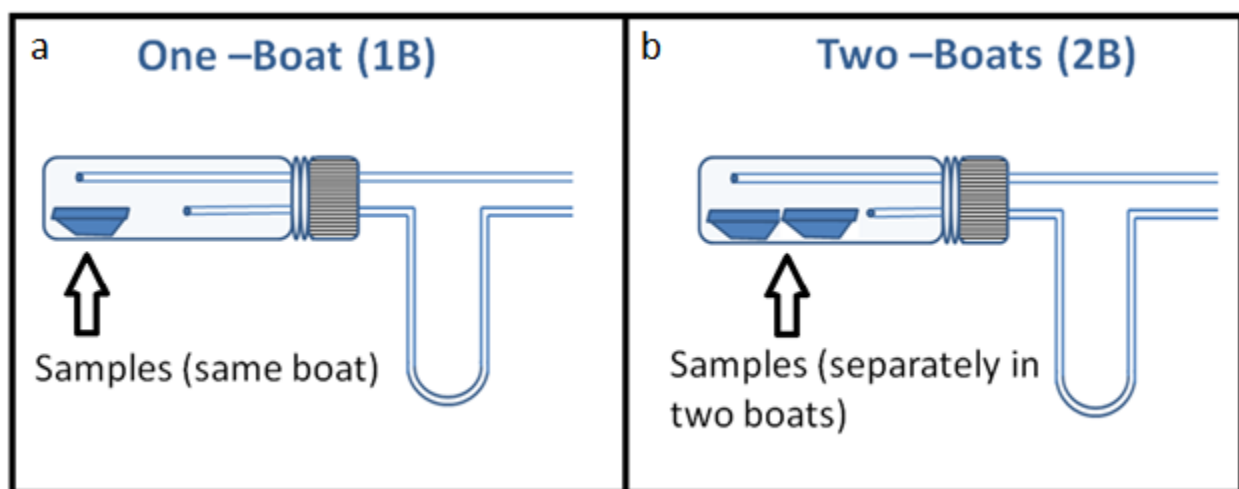


Figure 30: Pictorial representation of one-boat and two-boat experiments

Thus, for the two sets of polymers involving substrates PS, PVC, and PB, two 1B experiments were performed in the tube furnace. In the first 1B experiment, PS and PVC were placed in one combustion boat and inserted into the Pyrex vial for heating. In the second 1B experiment, PS and PB were placed in one combustion boat and inserted into the Pyrex vial for heating. As mentioned above, the heating of substrates was performed for 1-, 5-, and 8-minute periods. The vapors produced from the heating of substrates, along with residue and condensates corresponding to each time interval, were collected and further analyzed by GC-MS.

Similarly for the 2B experiments, the same set of polymers involving PS, PVC, and PB were subjected to heating in the tube furnace. In the first 2B experiment, substrates PS and PVC were

placed separately in two combustion boats and inserted into one Pyrex vial for heating. In the second 2B experiment, PS and PB were placed separately in two combustion boats and inserted into another Pyrex vial for heating. The substrates sets were heated for 1-, 5-, and 8-minutes, respectively. The analysis of vapors and condensate corresponding to each time interval was similar to the one-boat experiment except for the residues. For residue analysis resulting from the 2B experiment, the two combustion boats from the Pyrex vial were removed (see Figure 31) and transferred into two new clean vials and labelled appropriately. The passive headspace concentration method as described in Section 7.2.3 was used to extract analytes from the residue, which was further analyzed by GC-MS along with vapors and condensate.

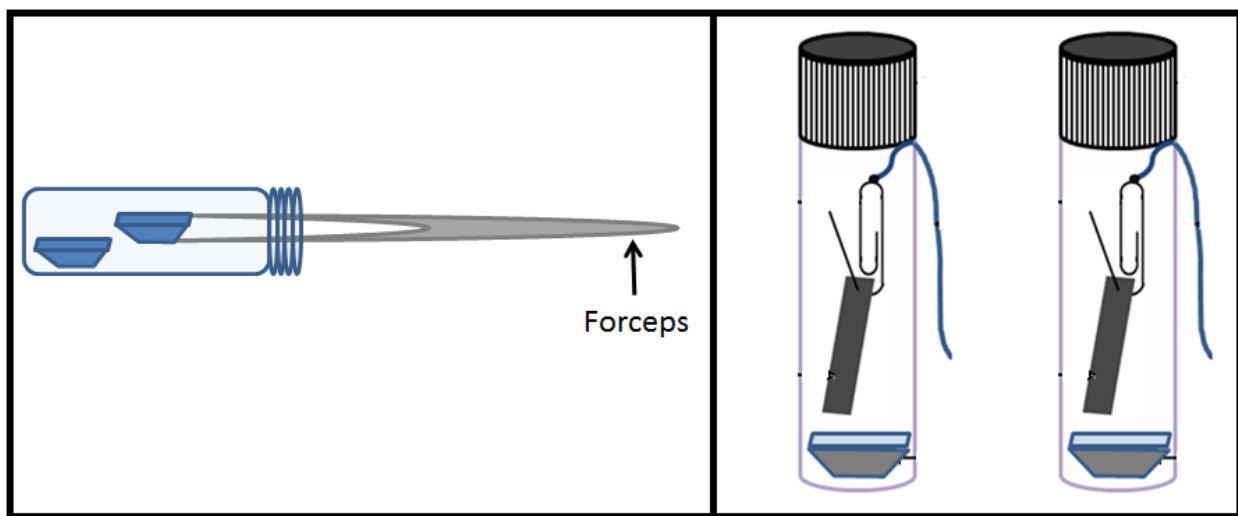


Figure 31: Analysis of residues from 2B experiment

## 9.2: Controlled Heating in Paint Cans

For controlled burns of substrates to generate interfering products using paint cans, substrate samples were heated by two methods. The first method involved heating the substrate as per the modified destructive distillation methodology, which was originally provided by the Florida Bureau of Forensic Fire and Explosive Analysis<sup>63</sup>. It should be noted that for the present research, the above method was referred to as the normal destructive distillation method (NDDM)

### *9.2.1: Normal Destructive Distillation Method (NDDM)*

In the NDDM, pyrolysis products were generated by placing a known mass of substrate upside down in a clean quart-sized paint can with a loosely placed lid with nine holes. The holes were approximately 5 mm in diameter and served as ventilation. Heating was implemented by placing the paint can on a ring stand approximately 4 cm above the nozzle of the propane torch, as shown in Figure 32. Substrates were then heated until distinct white smoke was observed above the lid. Once white smoke appeared, heating was continued for 2 additional minutes before the heat was removed. Once the heat was removed, the lid containing holes was immediately replaced with a new and clean solid lid to prevent escaping of vapors from the hot can. The hot paint can was then allowed to cool to attain room temperature, after which an activated charcoal strip was suspended into the headspace of the paint can for adsorption of analytes by the passive headspace concentration method (see Section 7.2.3). The analytes adsorbed onto the charcoal strip were then desorbed using 500 uL of carbon disulfide for GC-MS analysis.

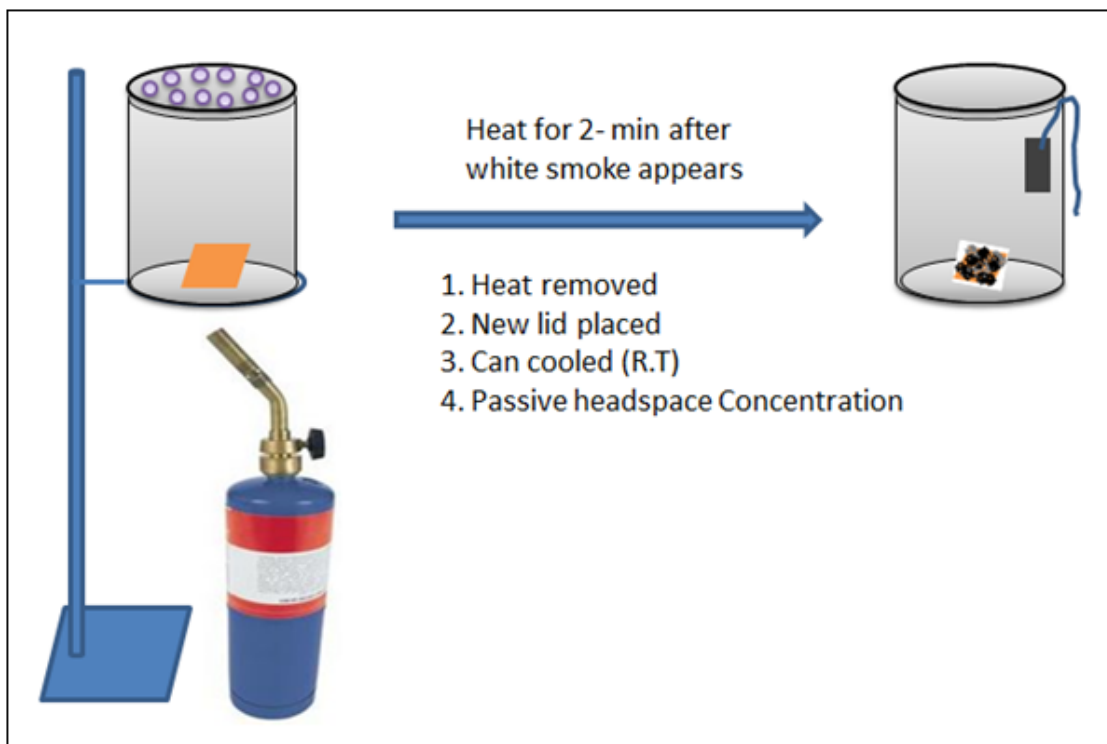


Figure 32: Normal destructive distillation method

Although controlled burns of substrates by NDDM were effective for generating pyrolysis products, there were some shortcomings. In NDDM, since the paint cans were heated at the bottom, the temperature at the top of the can, especially near the brim and on the inside walls, was relatively lower than at the bottom, which had been directly exposed to the flame from the propane torch. Consequently, a large quantity of vapors produced during heating condensed more at the brim and onto the walls of the container. Another possibility was that the vapors may condense back on the surface of the substrate remains after it was subjected to heating. It should be noted that in the present research, the remains of the substrate after heating is referred to as “Residue”. Thus condensation of vapors may cause distortion of the chromatographic profile due to displacement of low-molecular-weight compounds by compounds having relatively higher

molecular mass. Therefore, in order to minimize condensation, NDDM was slightly modified and subsequently referred to as the destructive distillation no condensate method (DDMNC), which is described in the next section.

### 9.2.2: Destructive Distillation No Condensate Method (DDNCM)

The method described in this section is similar to that of NDDM in which known mass of substrates was placed upside down inside the paint-can and heated with a loosely placed lid at the top. The lid contained nine holes with approximately the same diameter. Substrates were heated by placing a propane torch at the bottom of the paint-can until white smokes were observed above the perforated lid. Once white smokes appeared, heating was continued for additional 2 minutes before the heat was removed.

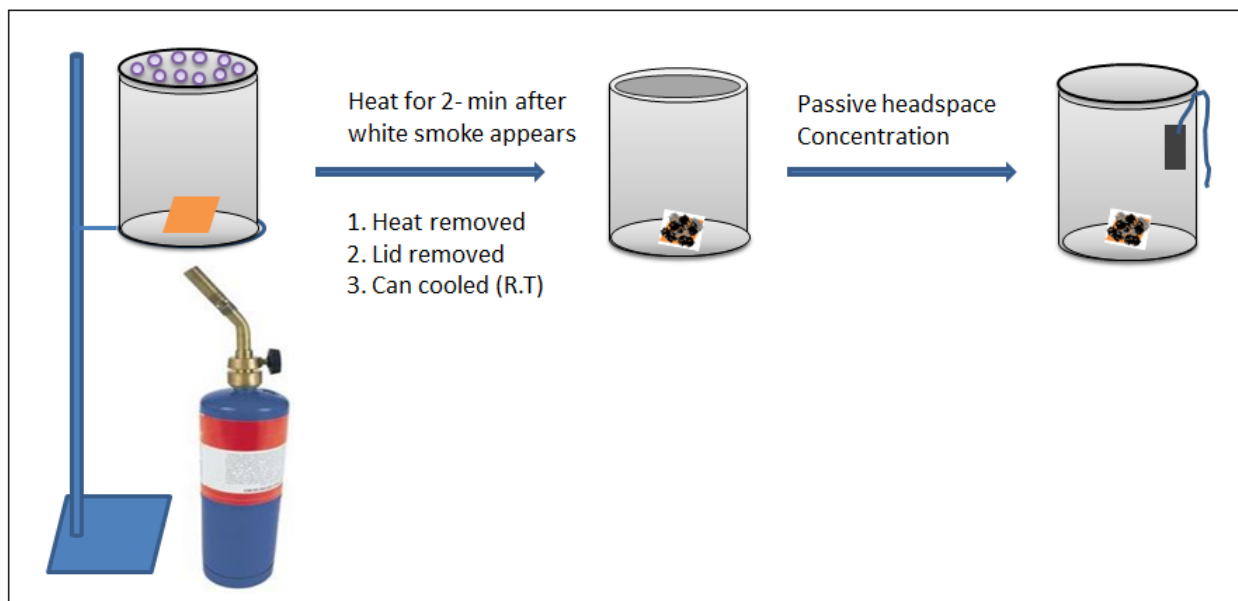


Figure 33: Destructive Distillation No Condensate Method (DDNCM)

Upto this point, the two methods were same. However after this point, a slight modification was introduced in DDNCM by removing the perforated lid from the hot paint-can. This allowed some vapors to escape from the hot can as it cooled simultaneously. Once the paint-can was cooled to room temperature, an activated charcoal strip was suspended into the headspace of the can for passive headspace concentration and sealed with a new solid lid as shown in figure 33. After 16 hours of activation in oven at, the cans were cooled and the charcoal strip was extracted with 500 uL of carbon disulfide for GC-MS analysis.

### *9.2.3: Residue and Condensate Analysis*

While DDNCM was primarily developed to eliminate the condensation of vapors, some vapors were still getting condensed especially at the brim of the paint-can. Also in DDNCM method, removal of the perforated lid after the additional 2 minutes of heating may possibly result in loss of low boiling compounds. Therefore in order to curtail the possible loss of low boiling compounds and to investigate the products released from the residue, additional experiments were performed to investigate the condensate and residue separately. For this purpose, substrates with known mass were heated as described in NDDM. After the heat was removed, the residue from the hot paint-can was transferred into a new paint-can. New solid lids were then placed onto the paint-cans containing the residue and the original paint-can which was subjected to heating. The two paint-cans, that is the original paint-can which was heated and the new paint-can containing the residue were then labelled as “Condensate” and “Residue” respectively. Charcoal strips were then suspended into the headspace of the two paint-cans for passive

headspace concentration (see section 7.2.3). The schematic representation for condensate and residue analysis is shown in figure 34 below.

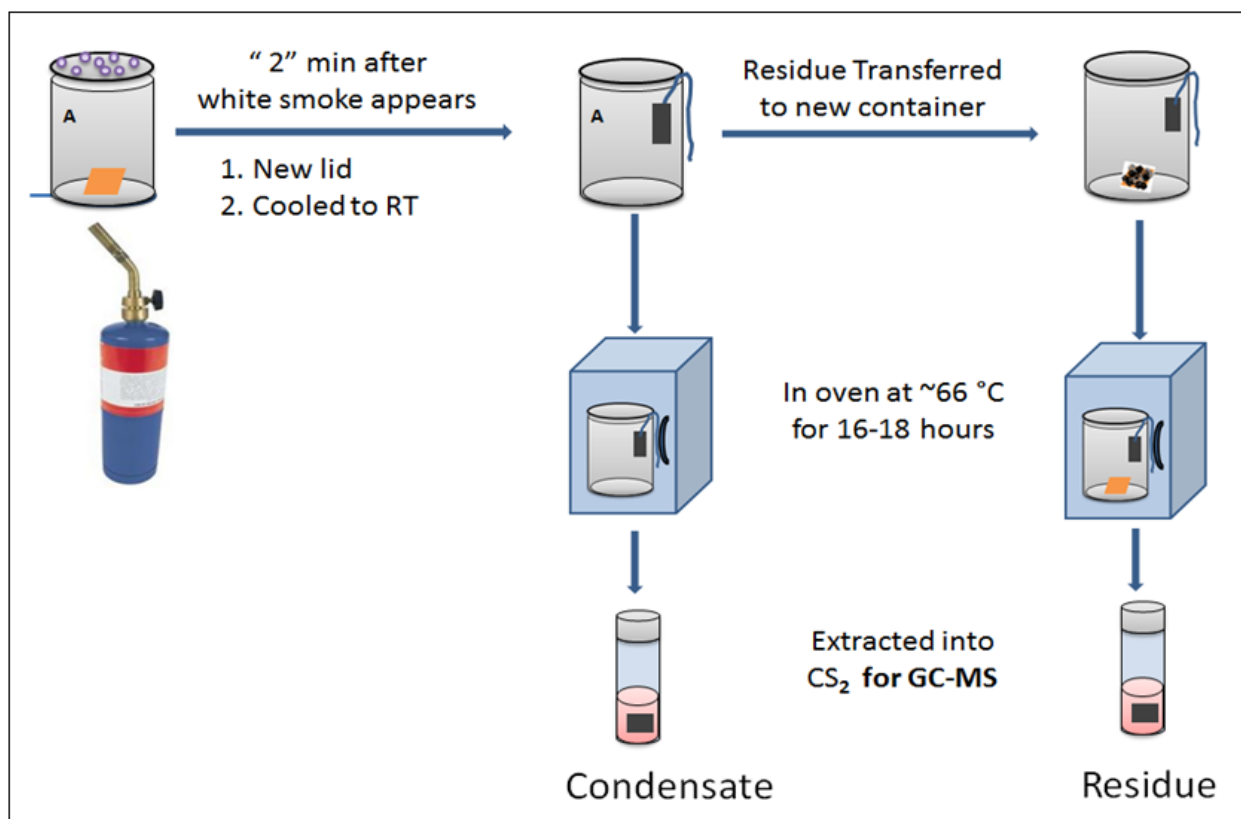


Figure 34: Schematic representation of Condensate and Residue Analysis

In this research, for investigating the formation of pyrolysis products by NDDM and DDNCM, the substrates PS and PVC were subjected to controlled burns in paint-cans. It should be noted that, the substrates were placed on a custom made aluminum boat and then introduced into the paint-cans for heating. Incorporation of aluminum boats for heating the substrates in paint-cans made it convenient for transferring the residue into other paint-can.



For the controlled experiments, the substrates were heated in two ways. In one experiment, samples of PS and PVC were placed on two separate aluminum boats and heated by NDDM and DDNCM each. In another experiment, samples of PS and PVC were placed on the same aluminum boat similar to one-boat experiment and heated by NDDM and DDNCM respectively. Thus a total of six paint-cans were generated, three from NDDM and the remaining three from DDNCM for PS, PVC and PS and PVC combined as shown in figure 35.







METHOD	SUBSTRATES		
	PS	PVC	PS+PVC
NDDM			
DDNCM			

Figure 35: Pictorial representation of paint-cans containing residues generated by NDDM and DDNCM

For the analysis of condensates and residues, the above experiments were repeated by NDDM method only. For condensate and residue analysis after the 2 additional minutes of heating, heat was removed and the aluminum boat containing the residue was transferred into a new paint-can for each substrate sample when heated individually and when they were heated together in the

same aluminum boat. Thus a total of six paint-cans were obtained from the experiments, three for condensates and the other three for residues as shown in figure 36.



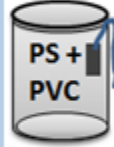



	SUBSTRATES		
METHOD	PS	PVC	PS+PVC
CONDENSATE			
RESIDUE			

Figure 36: Pictorial representation of paint-cans containing condensates and residues investigated separately

For extraction of analytes, activated charcoal strips were suspended into the headspace of all the twelve paint-cans and sealed for passive headspace concentration (see section 7.2.3). After approximately sixteen hours of activation at 66 °C, the cans were removed from the oven and cooled to attain room temperature after which the charcoal strips were extracted with 500 uL of carbon disulfide for GC-MS analysis.

In this work, when PS and PVC were subjected to heating by NDDM and DDNCM, it was observed that most of the samples were melted leaving small quantity of residue on the aluminum boat after the completion of heat. This was probably due to the nature and quantity of

substrate subjected to heating. For example, PS utilized in this research was in the form of small solid pellets and PVC was in fine crystalline powder. The chemicals were purchased from Sigma-Aldrich and for the controlled experiments the average weight of the substrates utilized was approximately 0.3 grams. Therefore in this research a solid substrate such as yellow-pine was purchased from a local home depot store and was subjected to controlled burns by NDDM and DDNCM. Yellow-pine used for the controlled burns was cut in the form of square with each side approximately 1.0 inch long and about 4.0 mm thick. The chromatographic results obtained from the controlled burns of the above substrates by NDDM and DDNCM has been presented in the next chapter.

### 9.3: Controlled Heating in Flat Steel Pans

As discussed in the previous section, although heating the substrates by DDNCM significantly reduced the condensation of vapors onto the inside walls of the paint-cans, some of the vapors however were still getting condensed at the brim of the paint-cans. Also in the above two methods (NDDM and DDNCM), the substrates were heated indirectly by heating the bottom of the paint-can with propane torch. In real fire however, the substrates commonly found in the building structures may have been directly exposed to fire. Therefore in this research, two additional heating methods were developed in an attempt to prepare pyrolysis reference samples that would be more representative of what might be obtained from real fire scene. These methods has been discussed in detail in the next section.

### 9.3.1: Top-Heat Pan

The top heat method discussed in this section involves placing the substrate sample on a flat steel pan and heating it directly with a propane torch. The experimental setup for the top heat method primarily consist of a ring stand to hold the propane torch in a horizontal position, a screw jack and a flat steel pan (see figure #).

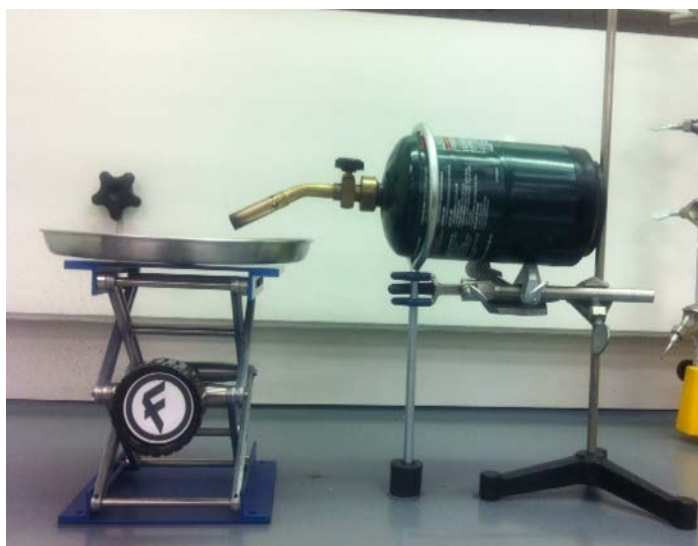


Figure 37: Experimental setup for controlled burns by Top-Heat method utilizing steel pan

It should be noted that for the Top-Heat method, the substrates were placed on a customized aluminum boat and then placed onto the steel pan for heating. For the purpose of heating the substrates under controlled conditions, the distance between the nozzle and substrate was maintained constant. This was executed by placing the steel pan on a screw jack and adjusting the height of the steel pan so that the substrate and nozzle were approximately 4 centimeters (cm)

apart. Also in the Top-Heat method, substrates were placed normally unlike in NDDM and DDNCM where the substrates were placed upside down inside the paint-cans



Figure 38: Aluminum boat carrying nylon carpet and padding for Top-Heat method.

For the controlled burns, known mass of the substrate was placed at the center of the steel pan and heated directly by placing the flame on top of the substrate for 2 minutes. After the 2 minute period, heat was removed from the substrate and cooled until very little smokes were observed. In this research the average time for which the substrates were cooled was 90 seconds. The cooling time may vary depending upon the type and size of the substrate. Once the substrates were sufficiently cooled, they were transferred into a new and clean quart size paint-can along with the aluminum boat. For extraction of analytes, activated charcoal strip was then suspended into the headspace of the paint-can containing the residue for passive headspace adsorption as described in section 7.2.3. After 16 hours of activation in oven, the paint-can was removed from the oven and cooled to attain room temperature. Once the paint-cans were sufficiently cooled, the

charcoal strips were eluted with 500  $\mu\text{L}$  of carbon disulfide for GC-MS analysis. In this research, the substrates that were subjected to controlled burns by Top-Heat method were yellow pine and a combination of nylon carpet and padding. Yellow pine used for the burns were cut into small square blocks with each side approximately 1 inch long and about 5mm thick. As for nylon carpet and padding, they were cut into medium size piece with each side approximately 2.5 inches long and were placed above each other with nylon carpet on the top (see figure 38).

### *9.3.2: Bottom-Heat Pan*

The Bottom-Heat method presented here is very similar to NDDM except that the substrates were subjected to controlled burns by heating them in steel pan instead of paint-cans. In NDDM since the substrates were heated in paint-cans, most of the vapors produced during heating were condensing on to the walls and at the brim of the paint-cans. Therefore one of the objectives for developing the bottom heat method was to reduce the condensation of vapors to a minimum. For this purpose in this method, the substrates were subjected to heating in a steel pan. The substrates were placed on a customized aluminum boat and then placed onto the steel pan for heating. The experimental setup for the Bottom-Heat method as shown in figure 39 (a) consists of ring stand, propane torch and steel pan. For the controlled burns, known mass of the substrate were placed upside down on steel pan and heated from the bottom. It should be noted that in Bottom-Heat method, the same substrates that is yellow pine and combination of nylon carpet and padding were subjected to controlled burns. In case of carpet and padding, nylon carpet was placed at the bottom and padding was placed above it on the aluminum boat as shown in figure 39 (b).

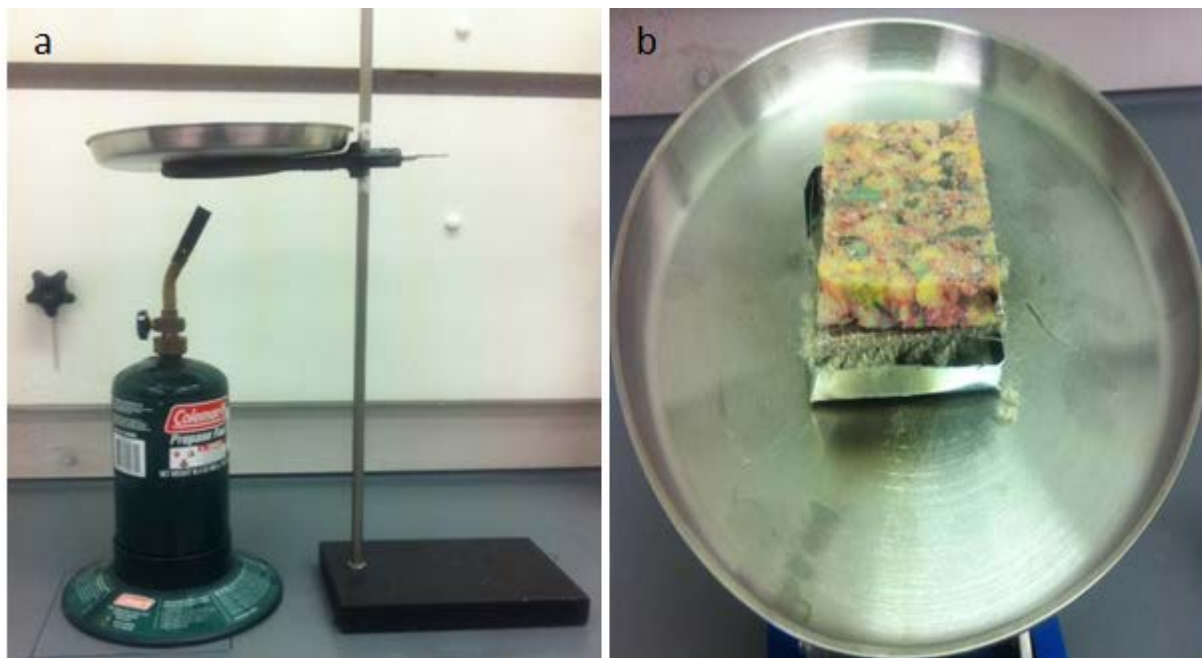


Figure 39: (a) Experimental setup for controlled burns by Bottom-Heat method utilizing steel pan; (b) Nylon carpet and padding on aluminum boat for Bottom-Heat method

The substrates were then heated till white smokes were observed. Once white smokes appeared heating was continued for additional 2 minutes before removing the heat away. Once the heat was removed, the residue was cooled to room temperature and then transferred into a clean quart sized paint-can. Activated charcoal strip was then suspended into the headspace of the paint-can for passive headspace concentration (see section 7.2.3) and the can was sealed with a new solid lid and placed into oven for activation. After approximately 16 hours of activation, the paint-can was removed and allowed to cool to room temperature. Once cooled, the charcoal strips were removed from the paint-cans and extracted with 500  $\mu\text{L}$  of carbon disulfide for GC-MS analysis.

#### 9.4: Time Study of Pyrolysis Products.

In fire debris analysis, interpretation of chromatographic results can be challenging due to the interference of pyrolysis products in the correct identification of ILR. The complexity involved is that pyrolysis products can mask the compounds of interest thereby making chromatographic results interpretation extremely difficult. Therefore in order to investigate the influence of IL on the formation of pyrolysis products, substrates yellow pine and a combination of nylon carpet and padding were subjected to controlled heating by NDDM, Top-Heat and Bottom-Heat methods in the presence of hydrocarbons (HC) mixture representing ignitable liquids. The hydrocarbons mixture representing ignitable liquids were n-alkanes comprising of octane (C<sub>8</sub>), nonane (C<sub>9</sub>), decane (C<sub>10</sub>) and undecane (C<sub>11</sub>). For the controlled experiments, equivalent molar solution of HC mixture were prepared and 100 μL of it was spiked on top of the substrate. After the HC mixture was spiked, the substrates were allowed to sit for 30 seconds to allow HC mixture to diffuse through the substrate surface. After 30 seconds, the substrates were then placed into the paint-can as in NDDM or on steel pan as in Top and Bottom heat methods for the controlled heating. Note that for controlled heating by NDDM and Bottom-Heat method, since substrates were heated indirectly by heating the bottom of the paint-can (NDDM) and steel pan (Bottom-Heat), the spiked surface of the substrates were placed upside down.

For the time study experiments, the spiked substrates were heated by NDDM, Top-Heat and Bottom-Heat method separately in the range of 0 to 10 minutes at every 2.5 minute interval. The primary objective here was to investigate the influence of ignitable liquids in the formation of pyrolysis products when substrates were subjected to controlled burns over a period of time. In



this study, thus a total of five burns were performed for each method and fifteen burns overall from all the three methods for yellow pine and repeated the same for nylon carpet and padding combined. The pictorial representation of the time study experiment for yellow pine and combination of nylon and padding is shown in figure 40 and 41 respectively.
















		Yellow Pine		
Time\Method		NDDM (Paint-Can)	Top-Heat (Steel Pan)	Bottom-Heat (Steel Pan)
0.0	min			
2.5	min			
5.0	min			
7.5	min			
10.0	min			

Figure 40: Pictorial representation of time study experiments for yellow pine.
















		Nylon Carpet + Padding		
Time\Method		NDDM (Paint-Can)	Top-Heat (Steel Pan)	Bottom-heat (Steel Pan)
0.0	min			
2.5	min			
5.0	min			
7.5	min			
10.0	min			

Figure 41: Pictorial representation of time study experiments for nylon carpet and padding

### 9.5: Time Study and Quantitative Analysis

For quantification of pyrolysis products and IL, internal standard calibration method was employed. The internal standard (IS) used in this study was 2, 3 dimethylheptane (Sigma-Aldrich, USA, 98%). 2,3-dimethylheptane did not interfere with any of the analyte of interest investigated in this research. For quantification of pyrolysis products and IL from the time study experiments, the charcoal strips used for passive headspace concentration were extracted with 500  $\mu$ L of 6.0 mM internal standard solution prepared in carbon disulfide. The standards corresponding to four major peaks identified in the chromatograms of yellow-pine and combination of nylon carpet and padding were purchased. The standards of the major peaks observed in the chromatographic results from yellow-pine and combination of nylon carpet used for quantification is shown in Figure 42.

	Standards	Company	Purity (%)
<b>Hydrocarbon</b>	Octane	Sigma-Aldrich	98
	Nonane	Sigma-Aldrich	99
	Decane	Sigma-Aldrich	99
	Undecane	Sigma-Aldrich	99
<b>Yellow Pine</b>	Alpha-Pinene	Acros-Organics	98
	Beta-Pinene	Acros-Organics	98
	Alpha-Terpineol	Acros-Organics	97
	4-Allylanisole	Acros-Organics	98
<b>Nylon Carpet and padding</b>	Styrene	Sigma-Aldrich	98
	Benzaldehyde	Sigma-Aldrich	99.5
	Alpha-Methylstyrene	Sigma-Aldrich	99
	caprolactam	Sigma-Aldrich	99

Figure 42: List of standards used for quantification

For calibration curve of hydrocarbons, a series of standard mixtures comprising of equimolar solution of octane, nonane, decane, and undecane were prepared. For the calibration curves of yellow pine, a series of standards mixtures comprising of equimolar solution of alpha-pinene, beta-pinene, alpha-terpineol and 4-allylanisole were prepared and for calibration curves of nylon carpet and padding, a series of standard mixtures comprising of equimolar solution of styrene, benzaldehyde, alpha-methylstyrene, and caprolactam were prepared. All the standard mixture solutions were prepared in carbon disulfide containing 6.0 mM 2,3 dimethylheptane as an internal standard. All the standard mixtures were run in triplicates. The limit of quantitation (LOQ) for all the standard mixtures corresponding to hydrocarbon mixture, yellow-pine and

combination of nylon carpet and padding were determined from the lowest concentration by using equation 9.1.

$$LOQ = \frac{10 s}{m} \quad (9.1)$$

Where  $s$  denotes the standard deviation obtained from the triplicate runs and  $m$  denotes the slope. For quantification of the pyrolysis products and IL, calibration curves were constructed by plotting the peak area ratio corresponding to analyte and internal standard versus its corresponding concentration.

#### 9.6: GC-MS analysis.

The analysis of samples and standards in this study was carried out in 7890A gas chromatograph coupled to a 5975C mass spectrometer from Agilent Technologies, USA. The gas chromatographic separation was performed on a 30 m Rtx-5MS column with an internal diameter of 0.25 mm and 0.25  $\mu$ m film thickness. 1.0  $\mu$ L of the sample was injected with the injection port temperature at 250 °C in split mode with a split ratio of 50:1. The initial temperature of oven was 50 °C which was held constant for 5 minutes and then ramped at a rate of 10 °C/minute to 100 °C held for 0 minutes and then ramped again at 25 °C/minute to a final temperature of 280 °C and held for 2 minutes. Helium was used as the carrier gas with a constant flow rate of 1.0 mL/minute. The temperature of transfer line was 280 °C. The source temperature was 230 °C and the MS quad temperature was 150 °C.

## **CHAPTER 10: RESULTS AND DISCUSSIONS**

### 10.1: Controlled Burns in Furnace

In this section, results from the pyrolysis of substrates performed in tube furnace are presented. Recall that substrates were heated separately at three time intervals of 1, 5 and 8 minutes. The substrates were heated individually and also in conjunction with other substrates in the furnace. Once the substrates were heated for the set time, the vapors (pyrolysates), condensate and residue were analyzed by GC-MS. This section presents the chromatographic results obtained from the GC-MS analysis of vapors, condensate and residues corresponding to the substrates PS, PVC and PB when they were heated separately in a furnace at 450 °C with a continuous flow of helium. It should be noted that, in this research, all the peaks observed in the chromatographic results were identified based on National Institute of Standards and Technology (NIST.98) library search and confirmed by matching the retention times and mass spectra of the known standards.

10.1.1: Pyrolysis of PS at 1, 5, and 8 Minutes

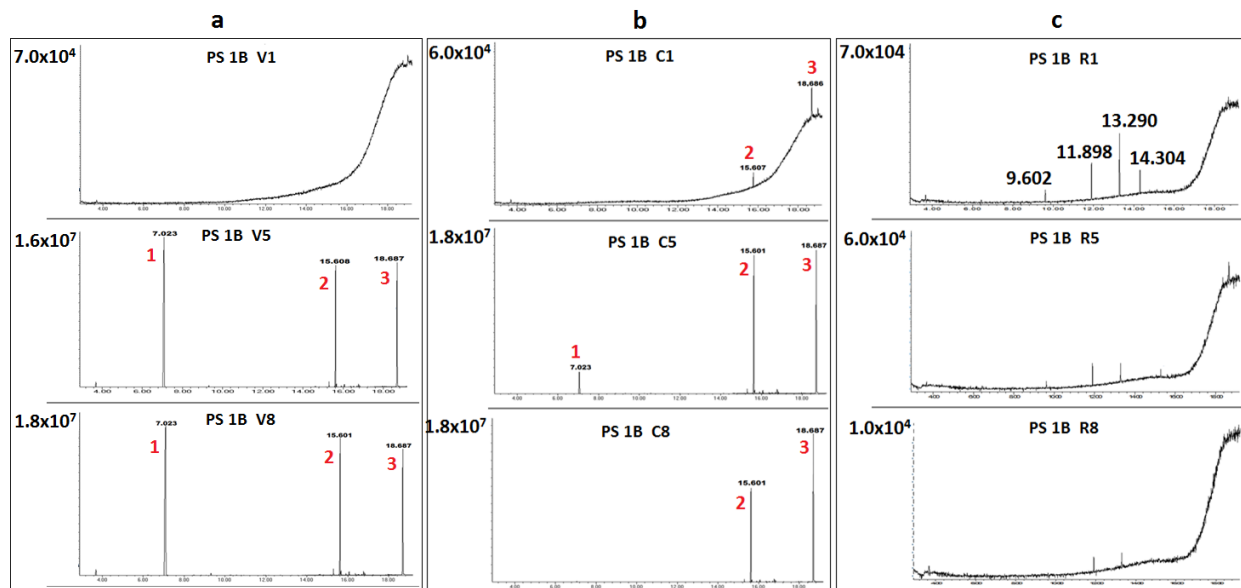


Figure 43: Chromatographic results of PS (a) Vapors, (b) Condensate, (c) Residue.

Table 8: Compounds and Their Retention Times from Pyrolysis of PS in Furnace

Peak number	Retention Time (Rt) minutes	compounds
1	7.096	Styrene monomer
2	15.612	Styrene dimer
3	18.676	Styrene trimer

The chromatograms of PS vapors are shown in figure 43 (a). Based on the library search and retention time match, the peaks observed in the chromatograms of PS vapors, condensate and residue at 1, 5 and 8 minutes are listed in table 8. It can be observed in the chromatogram of PS

vapors at 1 minute represented by (PS 1B V1), there are no significant peaks indicating that at 1 minute, very little pyrolysis occurred. However, the chromatogram of PS vapors at 5 and 8 minute represented by (PS 1B V5) and (PS 1B V8) shows three intense peaks characteristic of styrene monomer ( $m/z$  104), dimer ( $m/z$  208) and trimer ( $m/z$  312) respectively. It should be noted that in this research, the vapors at 1,5 and 8 minutes are denoted by V1, V5 and V8 respectively. Similarly, condensates at 1, 5 and 8 minutes are denoted by C1, C5 and C8, while residues at 1, 5 and 8 minutes are denoted by R1, R5 and R8 respectively.

The chromatograms of PS condensates are shown in figure 43 (b). At 1 minute chromatogram represented by (PS 1B C1), two weak peaks corresponding to styrene dimer and trimer were observed. Comparing this chromatogram with (PS 1B V1) chromatogram, it can be inferred that very little vapors were produced resulting from heating of PS. Furthermore these vapors did not enter the cold trap however they condensed at the front end near the neck of the Pyrex vial which was at a lower temperature (approximately 130 °C) compared to the remaining portion of the vial which was concealed inside the hot ceramic tube which was at 450 °C. The chromatograms at 5 and 8 minutes represented by (PS 1B C5) and (PS 1B C8) show two intense peaks characteristic of styrene dimer and trimer respectively further indicating that at 5 and 8 minutes, more pyrolysis occurred producing more vapors which not only entered the cold trap but were also condensed onto the walls at the front end of the Pyrex vial. It can be observed that at higher times, compounds with high molecular mass are condensed and low molecular mass compounds are not observed.

The chromatograms of PS residue are shown in figure 43 (c). At 1 minute, the chromatogram of the residue represented by (PS 1B R1) shows a few weak peaks. The peaks observed here do not match any of the characteristics peaks that were observed in the chromatograms of PS vapors and condensates. However when a charcoal strip was suspended into the headspace of a vial carrying a new and clean combustion boat for passive headspace adsorption and analyzed by GC-MS, similar peaks were observed in the chromatogram of the new combustion boat (blank). The retention times of the observed peaks matched the retention times of peaks observed in the chromatogram of PS residues. However, when a library search was performed on these peaks, the peaks were not identified. It should be noted that PS used in this research were purchased from Sigma-Aldrich. For the controlled experiments in furnace, approximately 0.058 grams of PS was placed in the combustion boat for heating



10.1.2: Pyrolysis of PVC at 1, 5, and 8 Minutes

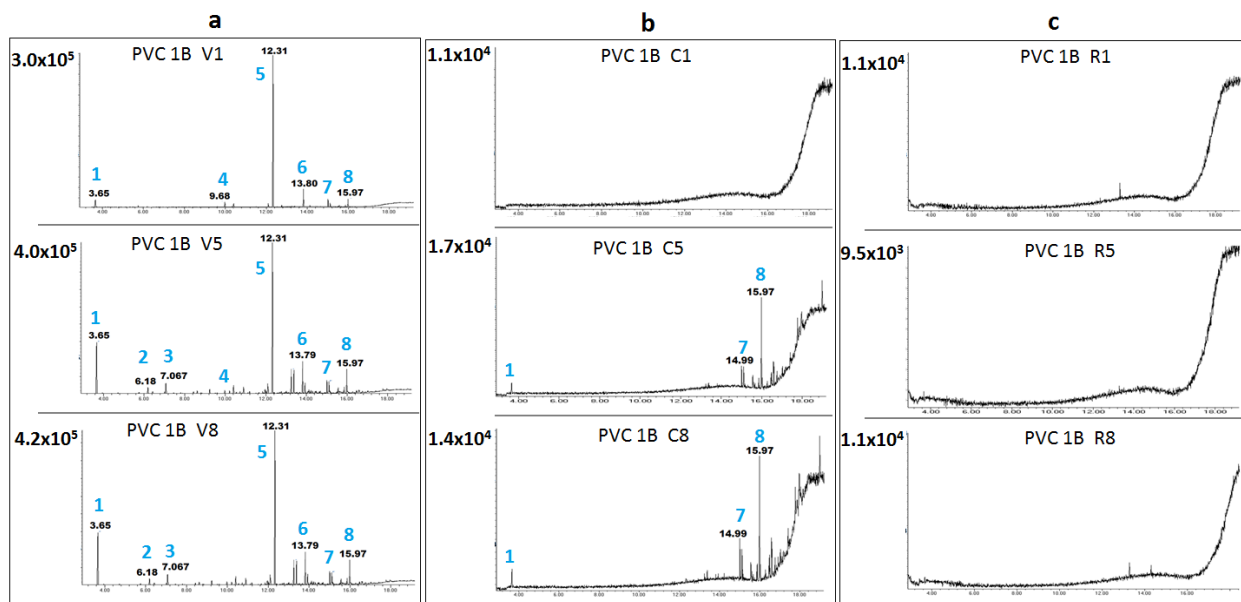


Figure 44: Chromatographic results of PVC (a) Vapors, (b) Condensate, (c) Residue.

Table 9: Compounds and Their Retention Times from Pyrolysis of PVC in Furnace

<b>Peak number</b>	<b>Retention Time (Rt) minutes</b>	<b>compounds</b>
<b>1</b>	3.65	Toluene
<b>2</b>	6.17	Ethylbenzene
<b>3</b>	7.06	1,2-dimethylbenzene
<b>4</b>	9.68	Benzylchloride
<b>5</b>	12.31	Naphthalene
<b>6</b>	13.79	Biphenyl
<b>7</b>	14.99	Fluorene
<b>8</b>	15.97	Anthracene

The chromatogram of PVC vapors is shown in figure 44 (a). Based on the library search and retention time match, the peaks observed in the chromatograms of PVC vapors, condensate and residue at 1, 5 and 8 minutes are listed in table 9. At 1 minute, the chromatogram of PVC vapors represented by (PVC 1B V1) shows a few weak peaks with one relatively intense peak at Rt of 12.31 minutes (peak number 5). The intense peak was identified as naphthalene. The chromatograms of PVC vapors at 5 and 8 minutes represented by (PVC 1B V5) and (PVC 1B V8) were identical with two additional peaks (peak number 2 and 3) identified as ethylbenzene and 1,2-dimethylbenzene respectively. As observed in the chromatogram (PVC 1B V1), the peak

corresponding to naphthalene was most intense in the chromatograms of PVC vapors at 5 and 8 minutes. The peak at Rt of 3.65 minutes identified as toluene, was present in the PVC vapor chromatograms at all times (1, 5 and 8 minutes). Comparing the three PVC vapors chromatograms, it can be inferred that, pyrolysis of PVC occurred more at 5 and 8 minutes producing more vapors as compared to 1 minute.

The chromatograms of PVC condensates are shown in figure 44 (b). At 1 minute chromatogram represented by (PVC 1B C1), no peaks were observed. The PVC condensate chromatograms at 5 and 8 minutes were identical with one intense peak (peak number 8), which was identified as anthracene. The other peaks observed were relatively weak and identified as toluene (peak number 1) and fluorene (peak number 7) respectively. Once again the chromatograms of condensates indicate that higher molecular mass compounds show a tendency to condense as compared to relatively low molecular mass compounds.

The chromatograms of PVC residue are shown in figure 44 (c). No significant peaks were observed in the PVC residue chromatograms at all times (1, 5 and 8 minutes). PVC used in this study was in the form of fine crystalline powder. It was observed that at higher times, PVC substrate completely melted leaving a yellow colored stain on the inside walls of the Pyrex Vial in which the substrates were heated.

10.1.3: Pyrolysis of PB at 1, 5, and 8 Minutes

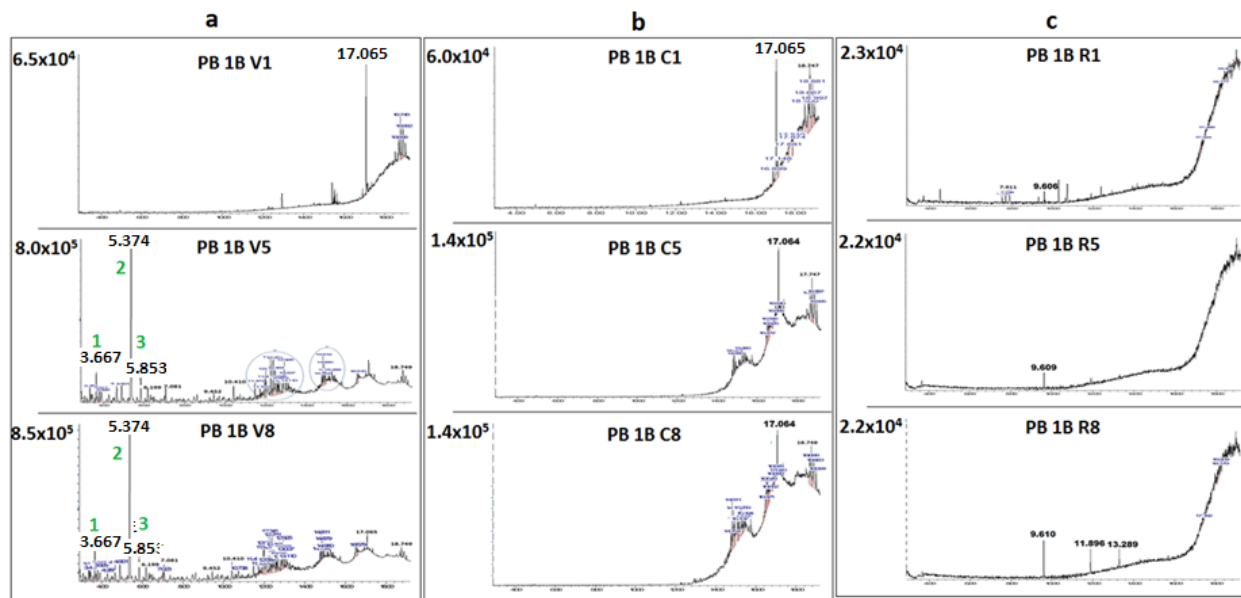


Figure 45: Chromatographic results of PB (a) Vapors, (b) Condensate, (c) Residue

Table 10: Compounds and Their Retention Times from Pyrolysis of PB in Furnace

Peak number	Retention Time (Rt) minutes	Compounds
1	3.665	Toluene
2	5.374	4-ethenylcyclohexene
3	5.853	4-ethylcyclohexene

The chromatogram of PB vapors is shown in figure 45 (a). Based on the library search and retention time match, the peaks observed in the chromatograms of PB vapors, condensate and residue at 1, 5 and 8 minutes are listed in table 10. At 1 minute, the chromatogram of PB vapors represented by (PB 1B V1) shows a few weak peaks. Library search for these peaks did not return any significant match. The chromatograms of PB vapors at 5 and 8 minutes were identical with one intense peak at Rt of 5.374 (peak number 2) which was identified as 4-ethenylcyclohexene. Also observed were complex set of peaks in the 5 and 8 minutes chromatograms at higher retention times. These complex peaks lacked resolution and library search did not return any significant match.

The chromatograms of PB condensates are shown in figure 45 (b). The chromatograms of PB condensate at 1, 5 and 8 minutes are represented by (PB 1B C1), (PB 1B C5) and (PB 1B C8) respectively. In all the three chromatograms, no significant peaks were observed.

The chromatograms of PB residue at 1, 5 and 8 minutes is shown in figure 45 (c). Although a few weak peaks were observed in the chromatogram of PB residue at 8 minutes, they were identical to the chromatogram of the blank combustion boat.

#### *10.1.4: Co-Pyrolysis of PS and PVC*

In this section, chromatographic results from the co-pyrolysis of PS and PVC are presented. Recall from chapter 9, co-pyrolysis experiments were performed in two ways namely one-boat (1B) and two-boat (2B). In 1B experiments, the substrates subjected to co-pyrolysis were placed

in one combustion boat and introduced into the Pyrex vial for heating. While in 2B experiment, the substrates were placed separately in two combustion boats and introduced into the Pyrex vial for heating. The primary objective of co-pyrolysis experiments were to investigate whether any new products are formed when these substrates are placed in close proximities (in contact) and when they are placed separately (not in contact).

#### 10.1.4.1. Co-Pyrolysis of PS and PVC One-Boat (1B) Experiment

In PS and PVC 1B experiment, an equivalent amount of PS and PVC was placed in one combustion boat. The average amount of PS and PVC used for heating was approximately 0.030 grams. The chromatograms of vapors from PS and PVC 1B experiment are shown in figure 46 (a). Based on library search and retention time match, the peaks observed in the chromatograms of vapors, condensate and residue at 1, 5 and 8 minutes are listed in table 11.

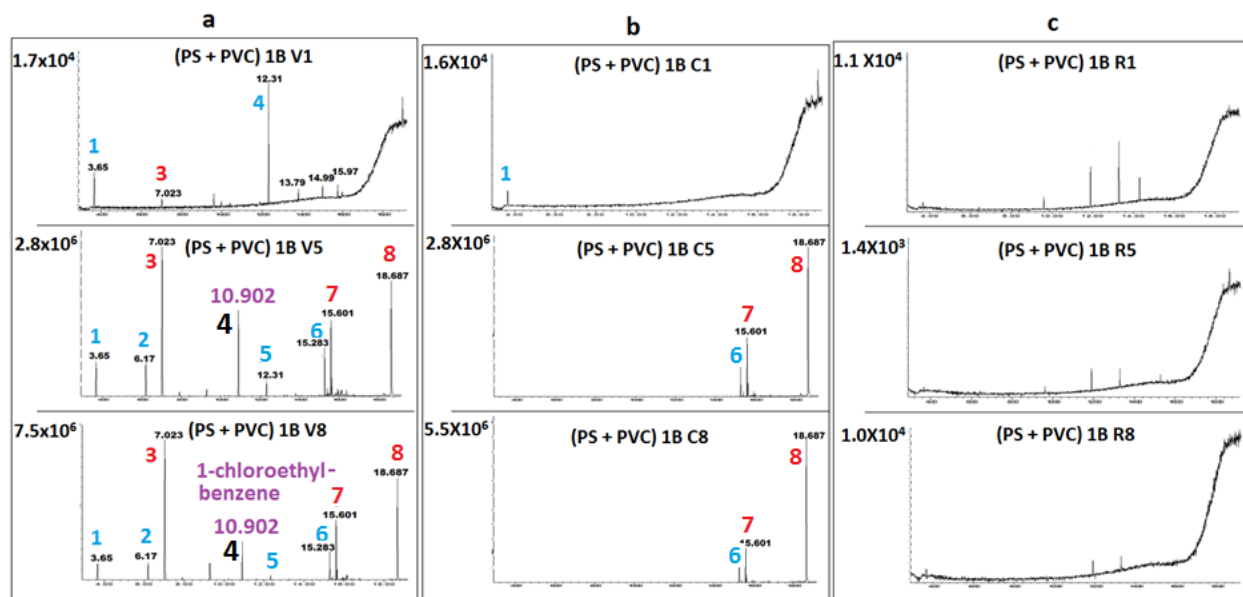


Figure 46: Chromatographic results from PS and PVC (1B) experiment (a) Vapors, (b) Condensate, (c) Residue.

Table 11: Compounds and Their Retention Times from Pyrolysis of PS and PVC 1B Experiment in Furnace

Peak number	Retention Time (Rt) minutes	Compounds
1	3.65	Toluene
2	6.17	Ethylbenzene
3	7.023	Styrene
4	10.902	1-chloroethylbenzene
5	12.31	naphthalene
6	15.283	1,1'-(1,3-propanediyl)bis benzene
7	15.601	Styrene dimer
8	18.687	Styrene trimer

At 1 minute, the chromatogram of vapors represented by [(PS+PVC) 1B V1] shows an intense peak at Rt of 12.31 minute (peak number 5) corresponding to naphthalene. Also observed was a weak peak at Rt of 7.023 minutes (peak number 3) which is characteristic of PS. Other peaks in the chromatogram, not listed in table 11 were weak and were also observed in the chromatogram of PVC vapors at 1 minute. Thus it can be observed that at 1 minute, when PS and PVC were placed in the same combustion boat and heated, PVC produced more vapors as compared to PS. At 5 and 8 minutes chromatograms represented by [(PS+PVC) 1B V5] and [(PS+PVC) 1B V8], a significant contribution from both PS and PVC were observed. The characteristic peaks of PS corresponding to styrene monomer, dimer and trimer were observed (peak number 3, 7 and 8).

Also observed were peaks corresponding to PVC peak number (2, 5 and 6). Toluene was observed in the vapor chromatograms at all times (1, 5 and 8 minutes). The peaks corresponding to PS were relatively more intense as compared to the characteristics products corresponding to PVC. A new peak (peak number 4) identified as 1-chloroethylbenzene was observed at Rt of 10.902 minutes in the chromatogram of 5 and 8 minute indicating that a free radical reaction occurred between PS and PVC. This peak was not observed in the chromatograms of PS and PVC when they were subjected to controlled heating individually.

The chromatograms of condensates from PS and PVC 1B experiment is shown in figure 46 (b). At 1 minute condensate chromatogram represented by [(PS+PVC) 1B C1)], no significant peaks were observed. The condensate chromatograms at 5 and 8 minutes were identical with two intense peaks corresponding to styrene dimer and trimer (peak number 7 and 8) and a weak peak corresponding to PVC (peak number 6).

The chromatograms of residue from PS and PVC 1B experiment are shown in figure 46 (c). Although few weak peaks were observed in the chromatograms at 1, 5 and 8 minutes, these peaks were weak and resembled the peaks from blank combustion boat.



#### 10.1.4.2. Co-Pyrolysis of PS and PVC Two-Boat (2B) Experiment

The chromatograms of vapors from PS and PVC 2B experiment are shown in Figure 47 (a). Based on library search and retention time match, the peaks observed in the chromatograms of vapors, condensate and residue at 1, 5 and 8 minutes are listed in Table 12.

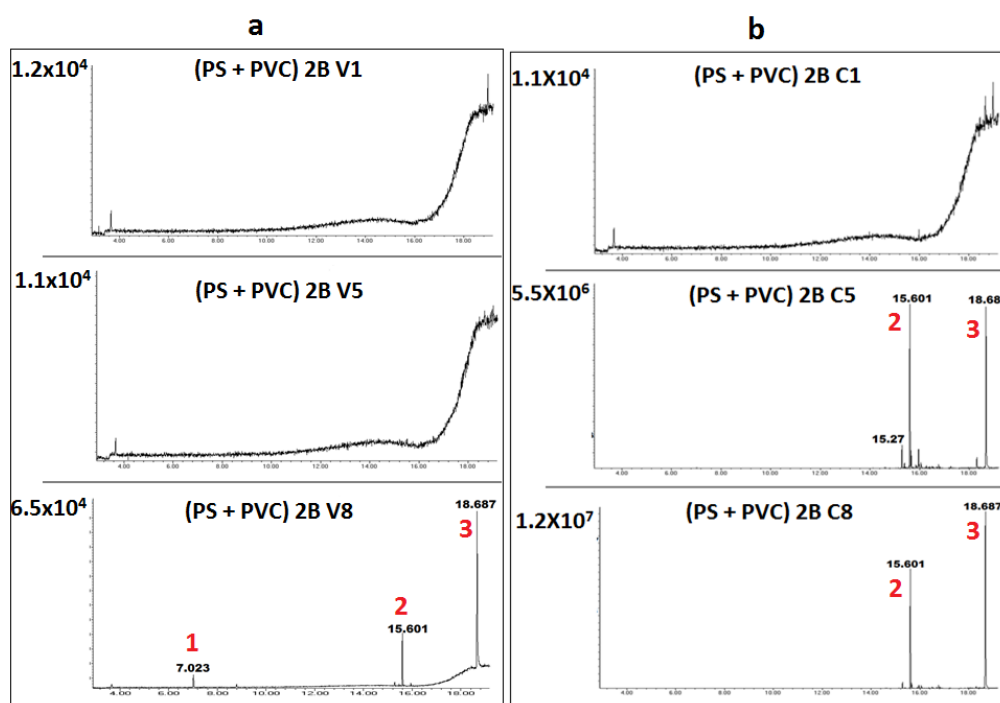


Figure 47: Chromatographic results from PS and PVC (2B) experiment (a) Vapors, (b) Condensates.

Table 12: Compounds and Their Retention Times from Pyrolysis of PS and PVC 2B Experiment in Furnace

<b>Peak number</b>	<b>Retention Time (Rt) minutes</b>	<b>compounds</b>
<b>1</b>	7.023	Styrene monomer
<b>2</b>	15.601	Styrene dimer
<b>3</b>	18.687	Styrene trimer

At 1 and 5 minute vapor chromatogram represented by [(PS+PVC) 2B V1)] and [(PS+PVC) 2B V5)], no significant peaks were observed. However at 8 minute chromatogram represented by [(PS+PVC) 2B V8)], the characteristic peaks from PS were observed. Peak number 3 corresponding to styrene trimer was the most intense as compared to other peaks. No peaks characteristic of PVC were observed in all the three chromatograms.

The chromatograms of condensate from PS and PVC 2B experiment are shown in figure 47 (b). At 1 minute condensate chromatogram represented by [(PS+PVC) 2B C1)], no significant peaks were observed. Comparison of 1 minute condensate chromatogram to [(PS+PVC) 2B V1)] chromatogram indicates that the two substrates did not undergo pyrolysis in one minute. However the 5 and 8 minute condensate chromatograms represented by [(PS+PVC) 2B C5)] and [(PS+PVC) 2B C8)] had two significant peaks corresponding to PS (peak number 2 and 3) and a weak peak from PVC at Rt 15.278 identified as 1,1'-(1,3-propanediyl)bis benzene.

The chromatograms of residue from PS and PVC 2B experiment are shown in figure 48. Recall from 1B experiment, since the two substrates PS and PVC were placed in one combustion boat they were in contact. However in 2B experiment since PS and PVC were placed separately in two combustion boats they were not in contact. For the residue analysis in 2B experiment the two combustion boats containing residues were extracted separately by passive headspace concentration separately.

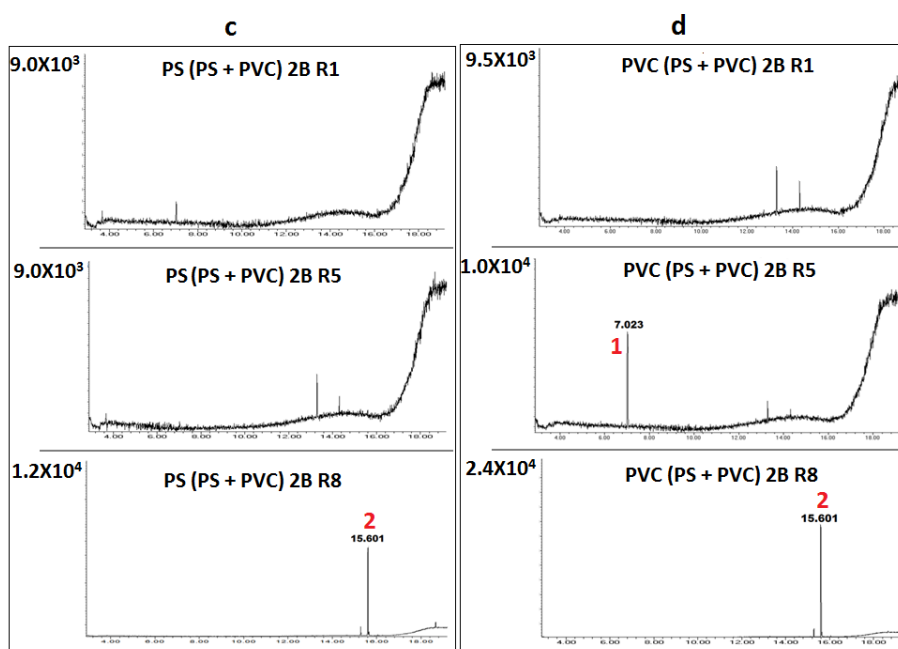


Figure 48: Chromatographic results from PS and PVC (2B) experiment (a) PS residue from PS and PVC 2B experiment (b) PVC residue from PS and PVC 2B experiment

The chromatograms of PS residue from PS and PVC 2B experiments are shown in figure 48 (a). At 1 and 5 minute chromatograms, no significant peaks were observed. At 8 minute chromatogram, a weak peak corresponding to styrene dimer (peak number 2) was observed. No peaks corresponding to PVC were observed at any times. The PVC residue chromatograms from the 2B experiment at 1, 5 and 8 minutes are shown in figure 48 (b). It can be observed from the 1

minute chromatogram, no significant peaks were observed. However at 5 minutes, peak corresponding to styrene monomer was observed. At 8 minute chromatogram, peak corresponding to styrene dimer peak was observed. Thus in the PVC residue chromatogram from 2B experiment, no characteristic peaks corresponding to PVC were observed. Comparing the chromatographic results from 1B and 2B experiments, it can be inferred that the results may vary depending upon whether the substrates are in contact or they are placed separately.

#### *10.1.5: Co-Pyrolysis of PS and PB*

In this section, the chromatographic results from 1B and 2B experiments of PS and PB are presented. The primary objective of these experiments were the same as that for PS and PVC 1B and 2B experiments, That is to investigate whether new products are formed when different substrates are heated together. In one boat experiment, approximately 0.025 grams of PS and PB each were placed on one combustion boat and heated.

### 10.1.5.1. Co-Pyrolysis of PS and PB One-Boat (1B) Experiment

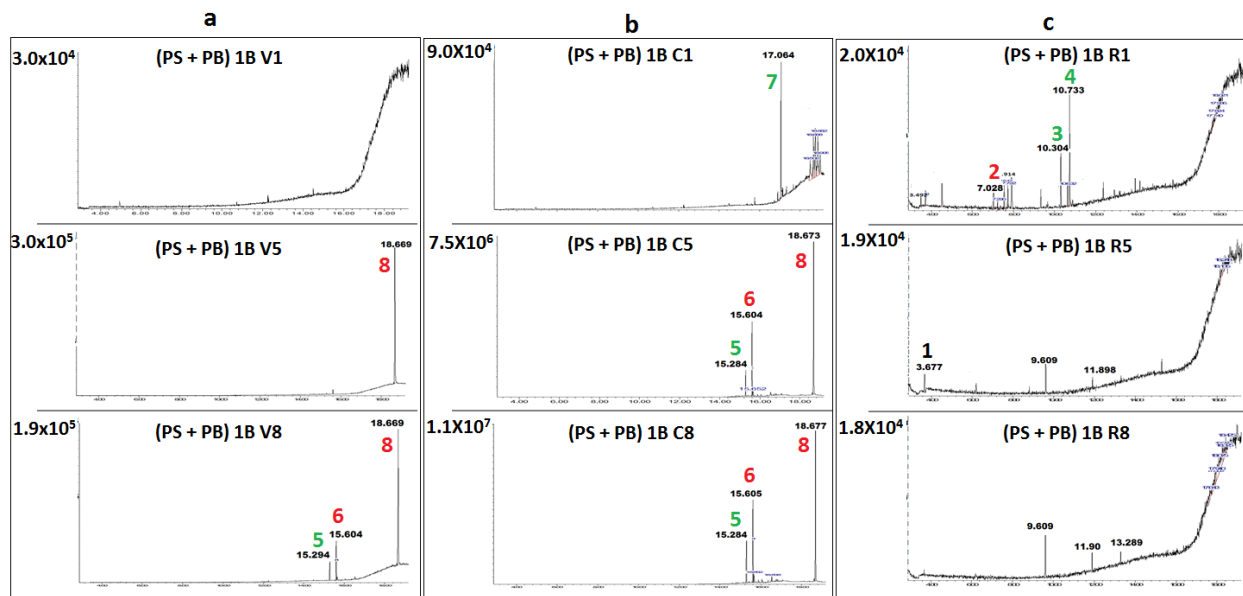


Figure 49: Chromatographic results from PS and PB (1B) experiment (a) Vapors, (b) Condensate, (c) Residue

Table 13: Compounds and Their Retention Times from Pyrolysis of PS and PB 1B Experiment in Furnace

Peak number	Retention Time (Rt) minutes	Compounds
1	3.65	Toluene
2	7.023	Styrene monomer
3	10.304	3-ethyl-2-hexene
4	10.733	2-methyl-2-butene
5	15.294	Benzene,1,1'-(1,3-propanediyl)bis
6	15.604	Styrene dimer
7	17.064	Cyclohexene, 1,5-diethenyl-3-methyl-2-methylene
8	18.687	Styrene trimer

The chromatograms of vapors from PS and PB 1B experiment are shown in figure 49 (a). Based on library search and retention time match, the peaks observed in the chromatograms of vapors, condensate and residue at 1, 5 and 8 minutes are listed in table 13. At 1 minute vapor chromatogram represented by [(PS+PB) 1B V1], no significant peaks were observed. The 5 minute vapor chromatogram represented by [(PS+PB) 1B V5)] had one peak characteristic of PS (peak number 8) corresponding to styrene trimer. At 8 minutes vapor chromatogram represented by [(PS+PB) 1B V8)], two peaks (peak number 6 and 8) corresponding to styrene dimer and trimer and one relatively weak peak (peak number 5) corresponding to PB were observed.

The chromatograms of condensates from PS and PB 1B experiment are shown in figure 49 (b). At 1 minute condensate chromatogram represented by [(PS+PB) 1B C1)], one peak (peak number 7) corresponding to PB were observed. The chromatograms of condensates at 5 and 8 minutes represented by [(PS+PB) 1B C5)] and [(PS+PB) 1B C8)], were identical with two intense peaks (peak number 6 and 8) corresponding to styrene dimer and trimer and one weak peak (peak number 5) corresponding to PB was observed.

The chromatograms of residues from PS and PB 1B experiment are shown in figure 49 (c). At 1 minute residue chromatogram represented by [(PS+PB) 1B R1)], two relatively intense peaks corresponding to PB (peak number 3 and 4) and one weak peak corresponding to styrene monomer (peak number 2) was observed. The 5 and 8 minute residue chromatograms represented by [(PS+PB) 1B R5)] and [(PS+PB) 1B R8)] did not have any significant peaks except for a weak peak of toluene at 5 minutes. The weak peaks observed in the residue chromatograms at 5 and 8 minutes were also observed in the chromatograms of blank combustion boat used for heating.

#### 10.1.5.2. Co-Pyrolysis of PS and PB Two-Boat (2B) Experiment

In PS and PB 2B experiment, PS and PB were placed separately on two combustion boats and heated in the same Pyrex vial. The average amount of PS and PB used in this study was 0.055 grams. The chromatograms of vapors and condensate from PS and PB 2B experiment are shown in figure 50 (a) and 50 (b) respectively.

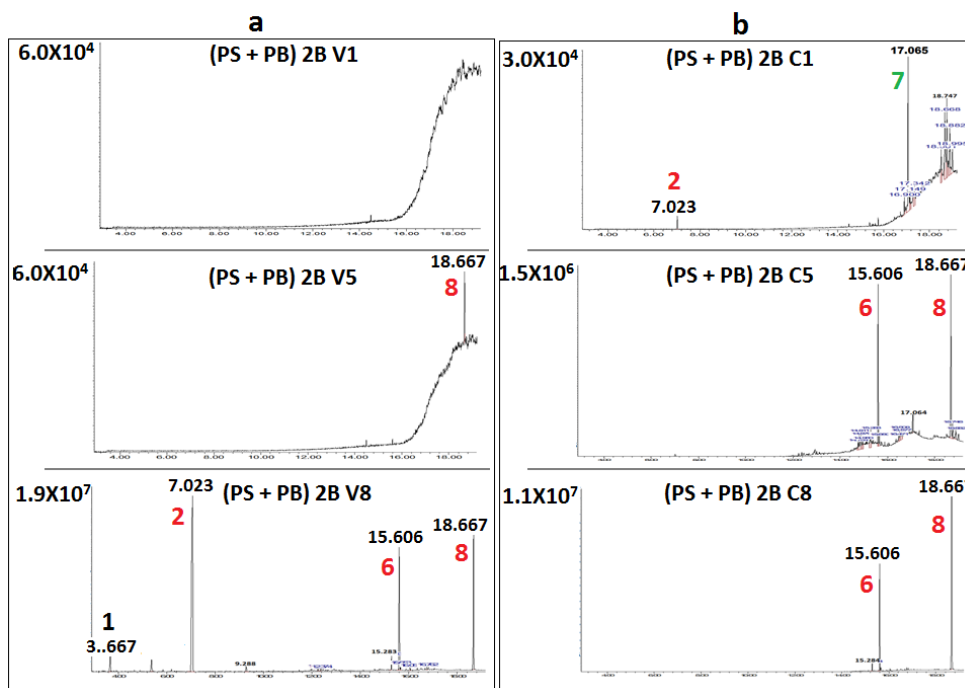


Figure 50: Chromatographic results from PS and PB (2B) experiment (a) Vapors, (b) Condensate

At 1 minute vapor chromatogram represented by [(PS+PB) 2B V1], no significant peaks were observed. At 5 minute vapor chromatogram represented by [(PS+PB) 2B V5], a weak peak corresponding to styrene trimer was observed. The 8 minute vapor chromatogram represented by [(PS+PB) 2B V8], had three intense peaks corresponding to styrene monomer, dimer and trimer. Also observed in the chromatogram was a weak toluene peak. Thus the vapor chromatograms from PS and PB 2B experiment had only vapors from PS (peak number 2, 6 and 8) and almost no peaks corresponding to PB (see table 13).



The condensate chromatograms of PS and PB 2B experiment are shown in figure 50 (b). At 1 minute condensate chromatogram represented by [(PS+PB) 2B C1)], a weak peak corresponding to styrene monomer and another weak peak (peak number 7, table 13) corresponding to PB was observed. The condensate chromatogram at 5 and 8 minutes represented by [(PS+PB) 2B C5)] and [(PS+PB) 2B C8)] were similar with two intense peaks corresponding to styrene dimer and trimer and no peaks corresponding to PB. The chromatograms of vapors and condensates from PS and PB 1B and 2B experiments indicate that PB did not undergo pyrolysis when placed with PS in both 1B and 2B experiment.

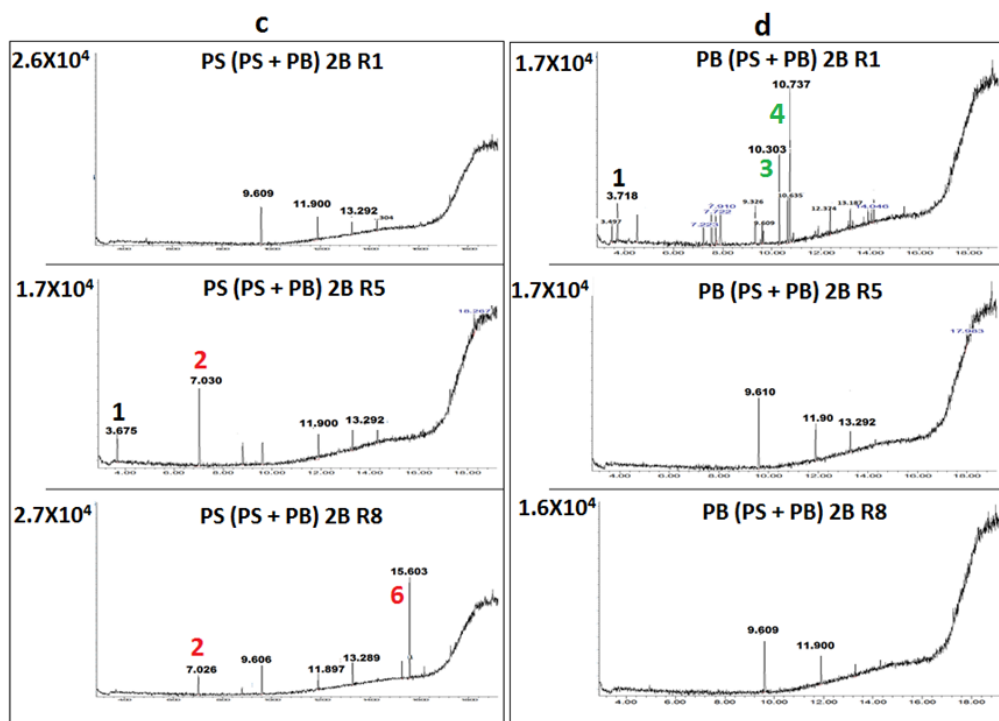


Figure 51: Chromatographic results from PS and PB (2B) experiment (c) PS residue from PS and PB 2B experiment (d) PB residue from PS and PB 2B experiment

The chromatograms of PS residue from PS and PB 2B experiment are shown in figure 51 (c). At 1 minute PS residue chromatogram represented by [PS(PS+PB) 2B R1)], no significant peaks corresponding to PS or PB were observed. At 5 minute PS residue chromatogram, only one weak peak characteristic of PS (styrene monomer) was observed and at 8 minute PS residue chromatogram, two characteristic peaks corresponding to styrene monomer and dimer were observed. In the PS residue chromatograms at all times, no peaks characteristic of PB were observed although both the substrates were heated in the same Pyrex vial but placed in separate combustion boats.

The chromatograms of PB residue from PS and PB 2B experiment are shown in figure 51 (d). At 1 minute PB residue chromatogram represented by [PB(PS+PB) 2B R1)], two significant peaks corresponding to PB (peak number 3 and 4, table 13) were observed. The 5 and 8 minute PB residue chromatogram represented by [PB(PS+PB) 2B R5)], and [PB(PS+PB) 2B R8)] did not have any significant peaks characteristic of PB or PS.

#### *10.1.6: Summary of 1B and 2B Experiments from (PS+PVC) and (PS+PB)*

Based on the observations from 1B and 2B experiments of PS and PB, no new products were observed. However, when PS and PVC were subjected to heating in 1B experiment, a new product identified as 1-chloroethylbenzene was observed based on library match. In (PS+PVC) 2B experiment when PS and PVC were subjected to controlled heating by placing them separately in two combustion boats, the peak corresponding to 1-chloroethylbenzene was not observed. Thus based on these observations from 1B and 2B experiment for both sets of

substrates (PS+PVC) and (PS+PB), it can be inferred that, pyrolysis product formation not only depends upon the nature of the substrates, but may also depend upon whether the substrates are in contact or not. In case of halogenated compounds such as PVC, there may be a possibility of free radical reaction resulting in new products. Therefore in order to investigate other factors that may influence pyrolysis product formation, PS and PVC were subjected to controlled heatings by new methodologies involving paint-cans for comparison

### 10.2: Controlled Burns in Paint Cans

In this section chromatographic results from the controlled burns of substrates carried out in paint-cans by NDDM and DDNCM method are presented. Also presented are the chromatographic results from the separate analysis of condensate and residue.

### 10.2.1: Pyrolysis of PS in Paint Can

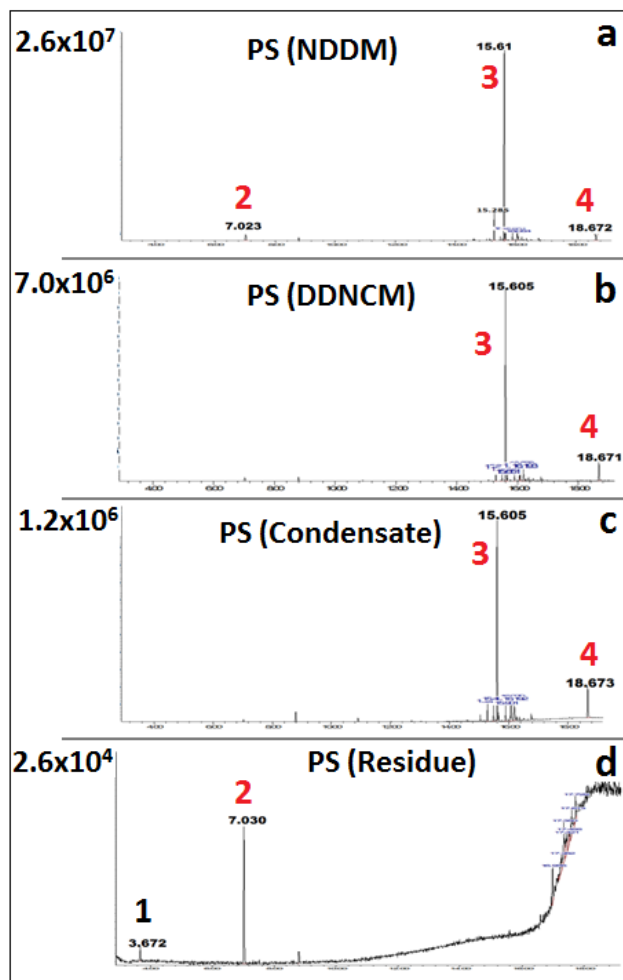


Figure 52: Chromatographic results of PS from (a) NDDM (b) DDNCM, (c) Condensate (d) Residue

The chromatographic results from controlled heating of PS by NDDM and DDNCM are shown in Figure 52 (a) and (b) and the chromatographic result of PS condensate and residue are shown in figure 52 (c) and (d) respectively. Based on library search and retention time match, the peaks observed in the chromatograms of PS are listed in table 14. The average weight of one PS pellet used in this study was 0.021 grams and for the controlled heating 11 pellets were used.

Table 14: Identified Compounds and Their Retention Times from Controlled Heating of PS Using Paint Cans.

Peak number	Retention Time (Rt) minutes	Compounds
1	3.65	Toluene
2	7.023	Styrene monomer
3	15.604	Styrene dimer
4	18.687	Styrene trimer

The chromatographic result from the pyrolysis of PS by NDDM shows three characteristic peaks. The peak corresponding to styrene dimer (peak number 3) was intense while the peaks corresponding to styrene monomer (peak number 2) and trimer (peak number 4) were relatively weak. The chromatograms of PS from DDNCM and condensate were identical with an intense peak at Rt of 15.604 minute corresponding to styrene dimer (peak number 3) and a weak peak at Rt of 18.667 minute corresponding to styrene trimer (peak number 4). The peaks corresponding to styrene monomer were not observed in both the chromatograms. In the PS residue chromatogram however only the peak corresponding to styrene monomer was observed with a weak peak of toluene at Rt of 3.65 minute.

10.2.2: Pyrolysis of PVC

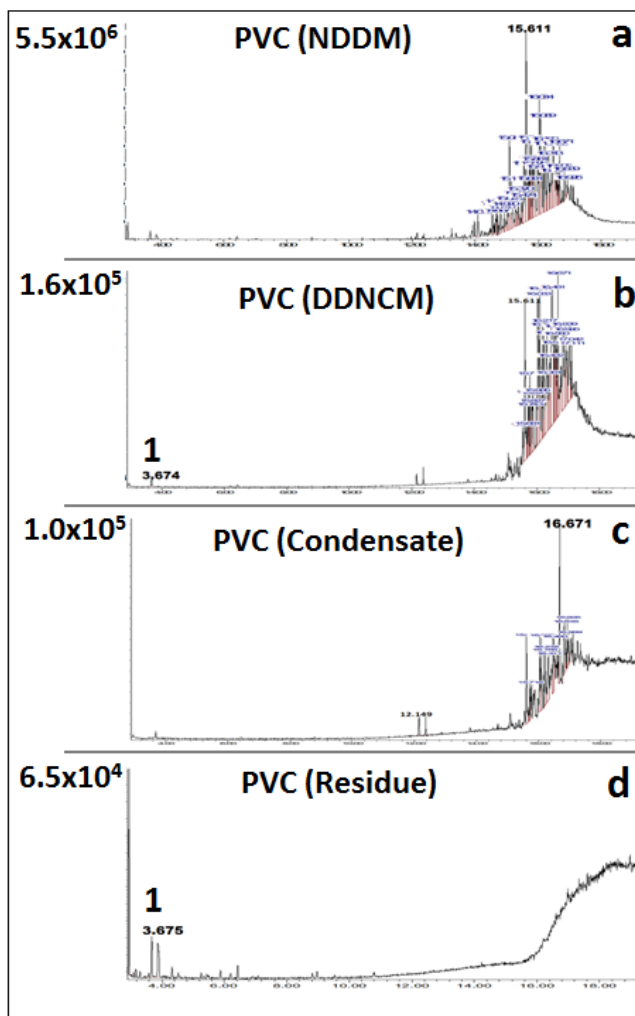


Figure 53: Chromatographic results of PVC from (a) NDDM (b) DDNCM, (c) Condensate (d) Residue

The chromatographic results from controlled heating of PVC by NDDM and DDNCM are shown in Figure 53 (a) and (b) and the chromatographic result of PVC condensate and residue are shown in figure 53 (c) and (d) respectively. Based on library search and retention time match, the

peaks observed in the chromatograms of PVC are listed in table 15. For the controlled heating, the weight of PVC used was approximately 0.3 grams.

Table 15: Identified Compounds and Their Retention Times from Controlled Heating of PVC Using Paint Cans

Peak number	Retention Time (Rt) minutes	Compounds
1	3.674	Toluene
2	14.00-18.00	Complex set of peaks

No significant peaks were observed in any of the chromatograms from the controlled heating of PVC in paint-cans. The chromatograms of PVC from NDDM, DDNCM and condensate were identical. A complex set of peaks in the range of 14.00 to 18.00 minutes were observed. Library search for these peaks did not return any significant matches. In the PVC residue chromatogram, only a weak peak of toluene at Rt of 3.674 minute was observed.

### 10.2.3: Co-Pyrolysis of PS and PVC

In this section, chromatographic results from the controlled heating of PS and PVC 1B experiments in paint-cans are presented. The experiment is similar to PS and PVC 1B performed in a furnace. The primary objective was to investigate whether any new products are formed since they were observed when PS and PVC were heated in 1B experiment using the furnace.

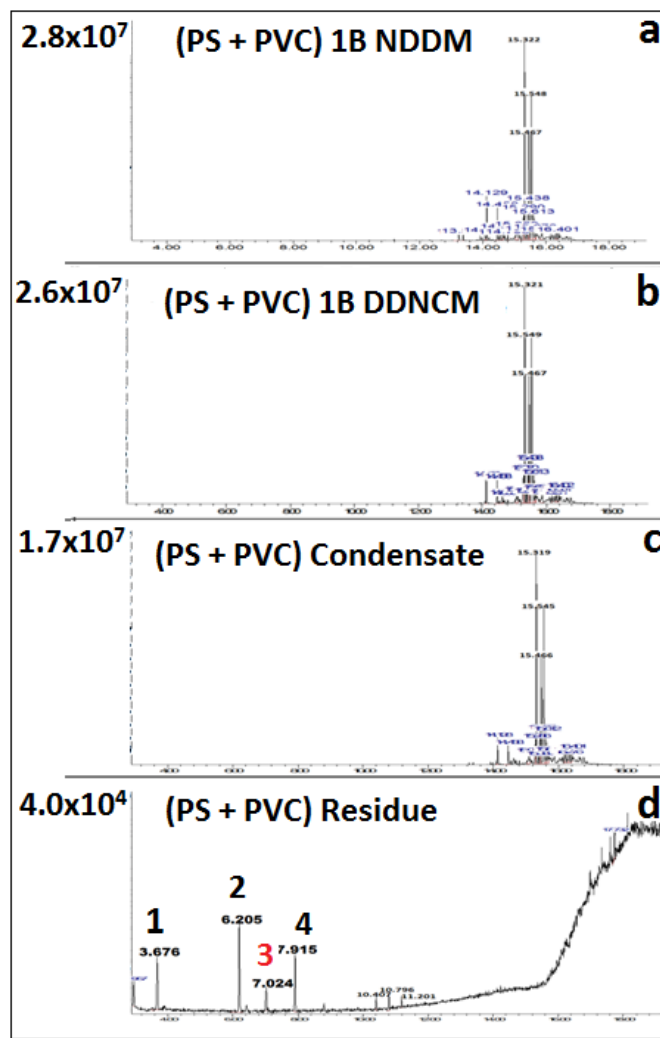


Figure 54: Chromatographic results of PS and PVC 1B from (a) NDDM (b) DDNCM, (c) Condensate (d) Residue

The chromatographic results from PS and PVC 1B experiment by NDDM and DDNCM are shown in Figure 54 (a) and (b) and the chromatographic result of (PS+PVC) 1B condensate and residue are shown in figure 54 (c) and (d) respectively. Based on library search and retention time match, the peaks observed in the chromatograms are listed in table 16. For the controlled



heating, equal amounts of PS and PVC each weighing approximately 0.231 grams were subjected to heating.

Table 16: Identified Compounds and Their Retention Times from Controlled Heating of PS and PVC 1B Experiment Using Paint Cans

<b>Peak number</b>	<b>Retention Time (Rt) minutes</b>	<b>Compounds</b>
<b>1</b>	3.65	Toluene
<b>2</b>	6.202	Ethylbenzene
<b>3</b>	7.024	Styrene monomer
<b>4</b>	18.687	1-methylethylbenzene

The chromatograms of PS and PVC 1B experiments by NDDM, DDNCM and condensate were identical. No characteristic peaks from PS were observed except for a complex set of peaks between 14 and 18 minutes retention time. At this retention time range, a similar set of complex peaks were observed in the PVC chromatogram. In the residue chromatogram, a weak peak corresponding to styrene monomer (peak number 3) and two peaks (peak number 2 and 4) corresponding to PVC was observed. New products were not observed when PS and PVC were subjected to heating in paint-cans.

#### *10.2.4: Comparison of PS and PVC 1B Experiments from Furnace and Paint Can*

The chromatographic results from the controlled heating of PS and PVC 1B carried out in furnace and paint-can was expected to resemble, however the results were slightly different. In the PS and PVC 1B experiment carried out in furnace, characteristic peaks corresponding to both PS and PVC were observed in the vapor chromatograms. However when PS and PVC were subjected to heating in paint-cans, characteristics peaks corresponding to PS were not observed except for a weak styrene monomer peak in the residue chromatogram. The dissimilarities in the chromatographic results may be attributed to several factors, such as quantity of substrates subjected to heating with respect to the volume of the container in which they are heated. Other factors that may be attributed to the difference in chromatographic results would be heating time and nature of the substrates. For example, when PS and PVC were heated in paint-cans they were completely melted and almost no residue was left on the aluminum boat. Another factor observed was condensation of vapors onto the walls of paint-cans and Pyrex vials. Therefore in this study, another substrate that may leave some solid residue and not completely melt like PS or PVC after heating was explored. For this purpose, yellow-pine purchased from a local home-depot store was cut into small square blocks with each side approximately 1 inch long and about 5 mm thick and heated in paint-cans by NDDM and DDNCM. The chromatographic results from these experiments are presented in the next section.

#### *10.2.5: Pyrolysis of Yellow Pine (YP)*

In this section, chromatographic results from the controlled heating of yellow-pine in paint-cans are presented. The chromatographic results from the pyrolysis of YP by NDDM and DDNCM

are shown in Figure 55 (a) and (b) and the chromatographic results of YP condensate and residue are shown in figure 55 (c) and (d) respectively.

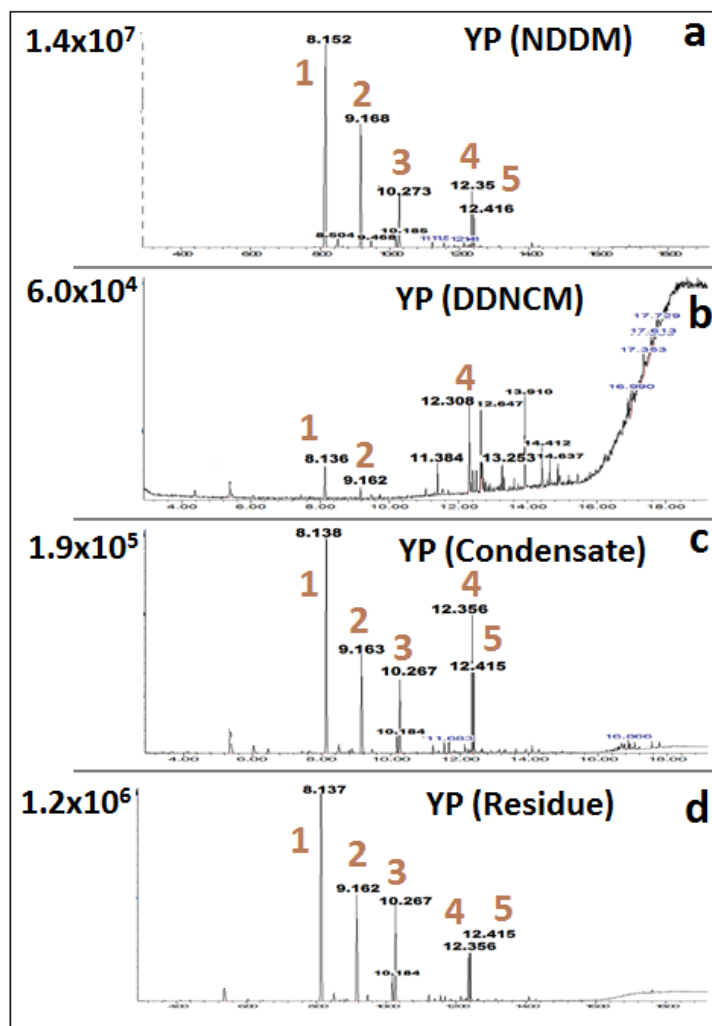


Figure 55: Chromatographic results of yellow-pine from (a) NDDM (b) DDNCM, (c) Condensate (d) Residue

Table 17: Identified Compounds and Their Retention Times from Controlled Heating of YP in Paint Cans.

Peak number	Retention Time (Rt) minutes	Compounds
1	8.152	Alpha-Pinene
2	9.155	Beta-Pinene
3	10.273	Cyclohexene,4-methylene-1-(1-methylethyl)
4	12.358	Alpha-Terpineol
5	14.10	4-Allylanisole

Based on library search and retention time match, the major peaks observed in the chromatograms of YP were identified (see table 17). From the chromatographic results, it can be observed that the chromatograms corresponding to the controlled heating of YP by NDDM, DDNCM and residue are identical. The chromatogram of YP from DDNCM was slightly different in terms of the number of peaks and their relative intensities. Recall from chapter 9 in DNNCM (section 9.2.2), Once the heat was removed after 2 additional minute of heating the paint-can containing the hot residue was allowed to cool without the solid lid unlike in NDDM where a solid lid was immediately placed once the heat was removed. Thus keeping the paint-can open may have resulted in loss of volatiles and hence the chromatogram of YP from DDNCM method may be different from the other chromatograms.

### 10.3: Controlled Heating in Steel Pans

As discussed in the previous sections involving controlled heating of substrates in paint-cans, condensation of vapors onto the walls of the paint-cans was a major concern. In this study, in addition to NDDM other heating methodologies involving paint-cans were also developed for the purpose of reducing condensation. However, the vapors were still getting condensed onto the walls and in some cases the low boiling compounds were not observed in the chromatograms probably due to their loss or displacement by higher molecular mass compounds. Therefore in an attempt to further minimize the condensation and to prepare pyrolysis reference samples which were more reflective of what may be obtained in a real fire, the substrates were subjected to controlled heating using flat steel pans. Recall from chapter 9, the substrates was heated in two ways namely Top-Heat (see section 9.3.1) and Bottom heat (see section 9.3.2). In this section, the chromatographic results from the controlled heating of substrates by Top-Heat and Bottom-Heat methods are presented. The substrates subjected to controlled heating by these methods were yellow pine and combination of nylon carpet and padding.

10.3.1: Pyrolysis of Yellow Pine

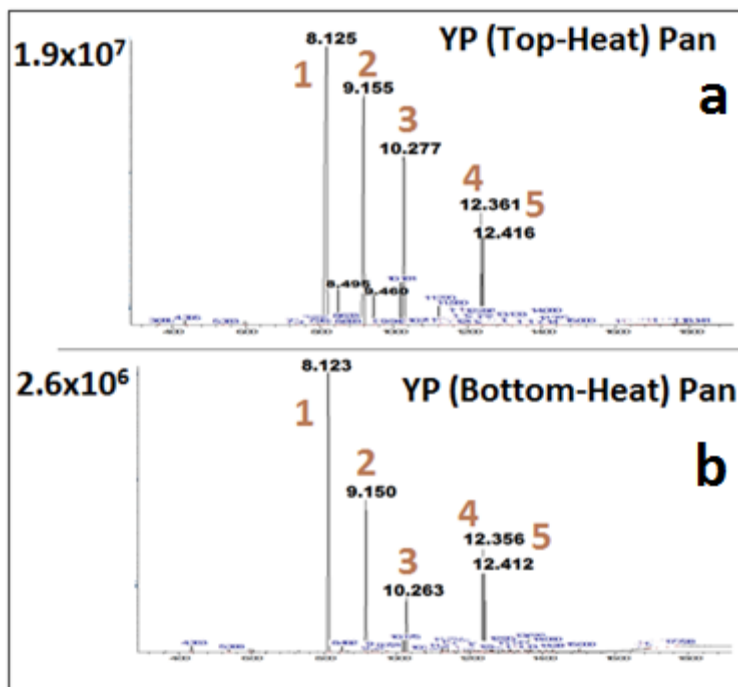


Figure 56: Chromatographic results of YP by (a) Top-Heat Method (b) Bottom-Heat method

Table 18: Identified Compounds and Their Retention Times from Controlled Heating of YP by Top-Heat and Bottom-Heat Methods

Peak number	Retention Time (Rt) minutes	Compounds
1	8.152	Alpha-Pinene
2	9.155	Beta-Pinene
3	10.273	Cyclohexene,4-methylene-1-(1-methylethyl)
4	12.358	Alpha-Terpineol
5	14.10	4-Allylanisole

The chromatograms from the controlled heating of YP by Top-Heat and Bottom-Heat methods are shown in figure 56. The major peaks identified based on library search and retention time match are listed in table 18. The chromatographic results from Top-Heat (figure 56.a) and Bottom-Heat (figure 56.b) methods were similar. The same set of peaks was observed in the chromatograms of both methods except that in Top-Heat chromatogram, the peaks were comparatively more intense. Based on the comparison of chromatographic results of YP from Top-Heat and Bottom-Heat methods, it can be inferred that, the Top-Heat method produced more pyrolysis and partial combustion products as compared to Bottom-Heat. Also, since Top-Heat method involves heating the substrates directly by placing the flame on top of the substrate unlike in Bottom-Heat and other methods, where substrates were heated indirectly, the chromatographic results from Top-Heat method may be more representative of what may be observed in a real fire. In order to investigate whether similar results would be observed for more complex substrate than yellow pine, a combination of nylon carpet and padding were subjected to controlled heating by Top-Heat and Bottom-Heat methods in this research, the results of which are discussed in the next section.

10.3.2: Pyrolysis of Nylon Carpet and Padding

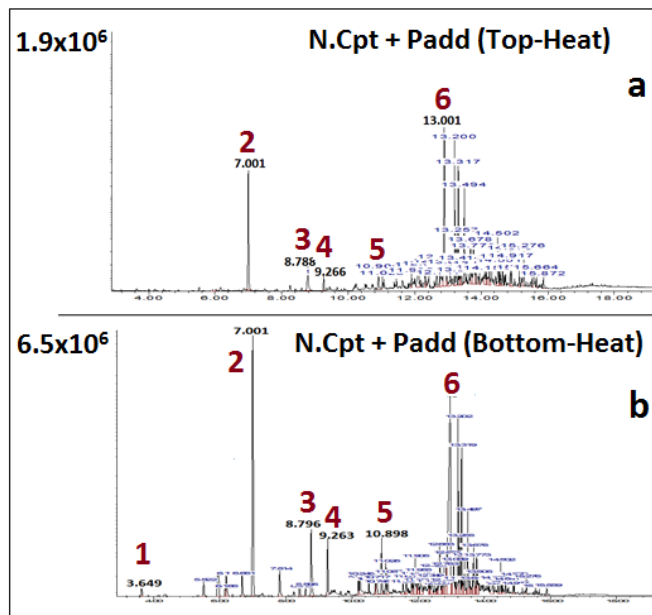


Figure 57: Chromatographic results of combination of nylon carpet and padding by (a) Top-Heat Method (b) Bottom-Heat method

Table 19: Identified Compound and Retention Times Match from Controlled Heating of Combination of Nylon Carpet and Padding from Top-Heat and Bottom-Heat methods.

Peak number	Retention Time (Rt) minutes	Compounds
1	3.649	Toluene
2	7.001	Styrene
3	8.796	Benzaldehyde
4	9.263	Alpha-methylstyrene
5	10.898	Acetophenone
6	13.001	Caprolactam



The chromatograms from the controlled heating of a combination of nylon carpet and padding by Top-Heat and Bottom-Heat methods are shown in figure 57. The major peaks observed in the chromatograms were identified based on library search and retention time match (see table 19). Based on the comparison of chromatographic results from Top-Heat and Bottom-Heat methods, it can be inferred that, controlled heating of nylon carpet and padding by Bottom-Heat method produced more pyrolysis products than in Top-Heat method. In bottom heat method, the peak at Rt of 7.001 corresponding to styrene was the most intense. Among other significant peaks, the peak corresponding to caprolactam (peak number 6) was intense in both the chromatograms. In Bottom-heat chromatogram, the peaks corresponding to benzaldehyde (peak number 3), alpha-methylstyrene (peak number 4) and acetophenone (peak number 5) were slightly more intense compared to that in Top-Heat chromatogram.

Thus in case of combination of nylon carpet and padding, bottom-heat method produced slightly more pyrolysis products than Top-Heat method, whereas in case of yellow-pine, Top-Heat method produced more pyrolysis products than in Bottom-Heat. Thus it was observed that, when substrates were subjected to controlled heating by Top-Heat and Bottom-Heat methods which utilizes flat steel pan, condensation of vapors is considerably reduced due to absence of walls in steel pans which may otherwise allow for condensation.

## 10.4: Time Study and Quantitative Analysis

In this section, chromatographic results from time study experiment and quantification results are presented. Recall from chapter 9, in time study experiment, the substrates were subjected to controlled heating in the presence of hydrocarbon mixture representing as ignitable liquids. The objective was to investigate the influence of IL on the formation or pyrolysis products over a period of time.

### 10.4.1: Yellow Pine with Hydrocarbons by NDDM

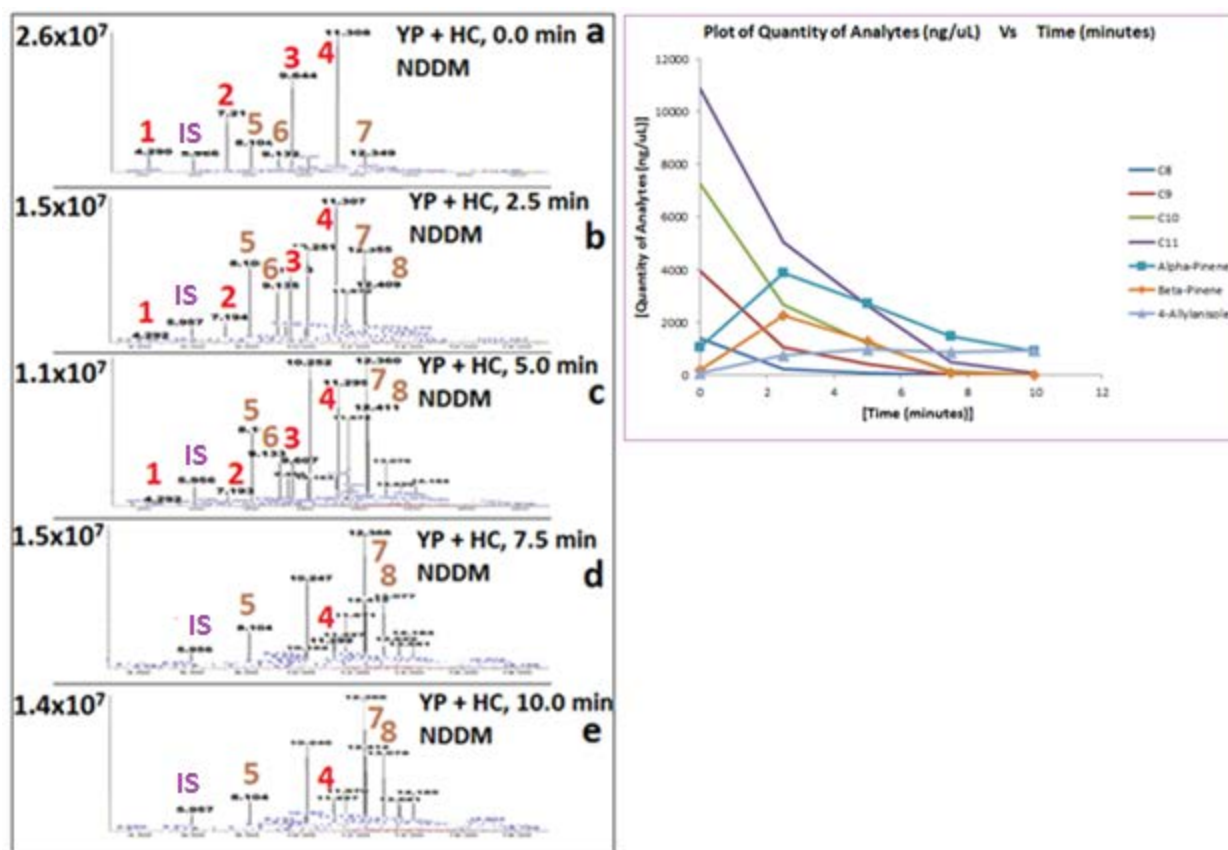


Figure 58: Chromatograms and quantification results from time study experiment of yellow-pine and HC mixture by NDDM

Table 20: Identified Compounds and Their Retention Times from Yellow-Pine and HC Mix

Peak number	Retention Time (Rt) minutes	Compounds
1	4.292	C8
2	7.194	C9
3	9.644	C10
4	11.308	C11
5	8.105	Alpha-pinene
6	9.132	Beta-pinene
7	12.349	Alpha-terpineol
8	12.410	4-allylanisole

The chromatographic results from the time study experiment of yellow-pine with hydrocarbon mixture by NDDM is shown in figure 58. The major peaks observed in the chromatograms were identified based on library match and retention match, (see table 20). As shown in figure 58, visual interpretation of chromatographic results may be difficult. However when the quantities of recovered pyrolysis products and ignitable liquids were plotted as a function of time, the effects of ignitable liquid on the formation of pyrolysis products were distinct. From the plot shown in figure 58, it can be observed, at higher times, the intensities of the peaks corresponding to hydrocarbons (peak 1 to 4, table 20) decreased. As a result at higher times the intensities of the peaks corresponding to the pyrolysis products appear intense. In case of yellow-pine, alpha-pinene was predominant as compared to other products.

### 10.4.2: Yellow Pine with Hydrocarbons by Top-Heat Method

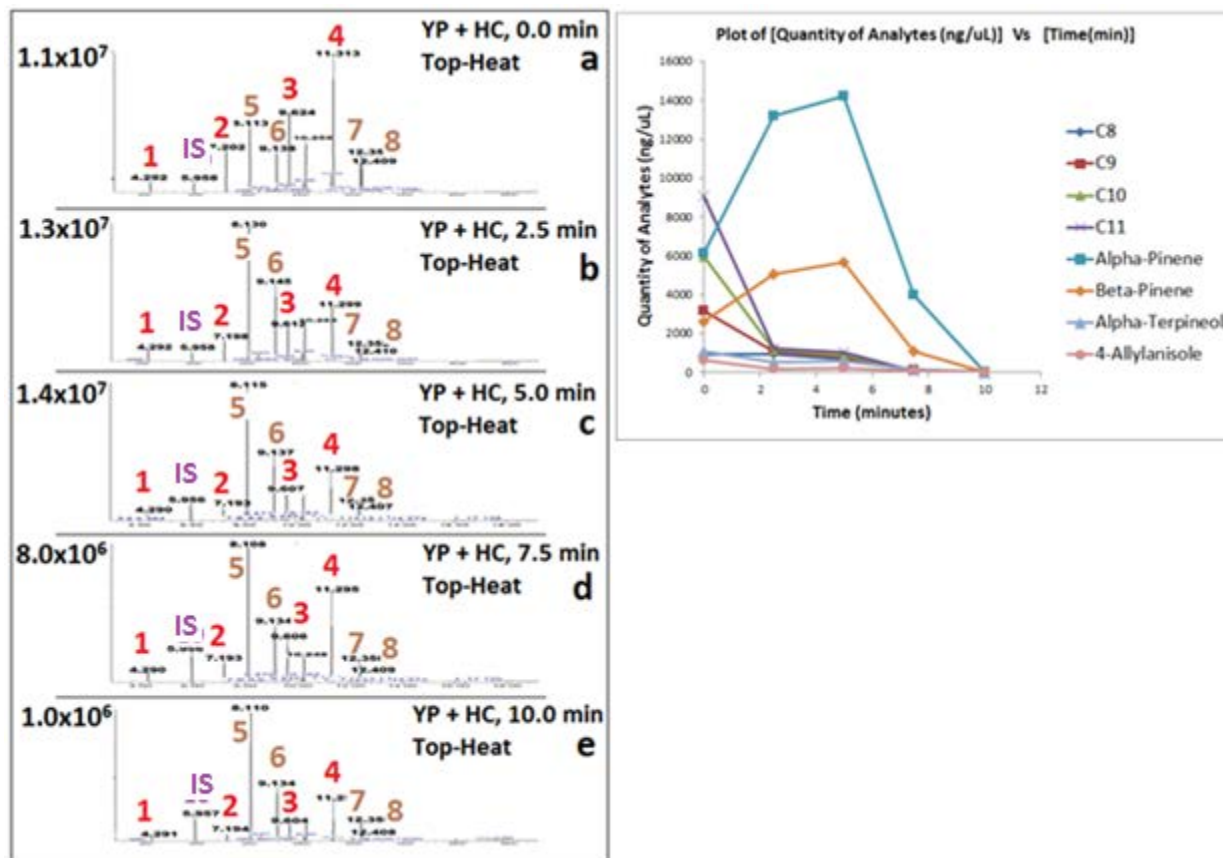


Figure 59: Chromatograms and quantification results from time study experiment of yellow-pine and HC mixture by Top-Heat method

The chromatographic results from the time study experiment of yellow-pine with hydrocarbon mixture by Top-Heat method is shown in figure 59. The major peaks observed in the chromatograms were identified based on library match and retention match, (see table 20). The chromatographic results from the time study experiments of yellow-pine with HC mix by Top-Heat method looks similar to the chromatographic results from NDDM. With time, the amount of hydrocarbons starts to decrease. At 10 minute chromatogram, hydrocarbons decreased

considerably. From the quantitation plot shown in figure 59, it can be inferred that, Top-Heat method produced more pyrolysis products compared to NDDM. Another significant observation was that in Top-Heat method, hydrocarbons decreased at a relatively faster rate. Alpha-pinene was once again predominant as compared to other products.

### 10.4.3: Yellow Pine with Hydrocarbons by Bottom-Heat Method

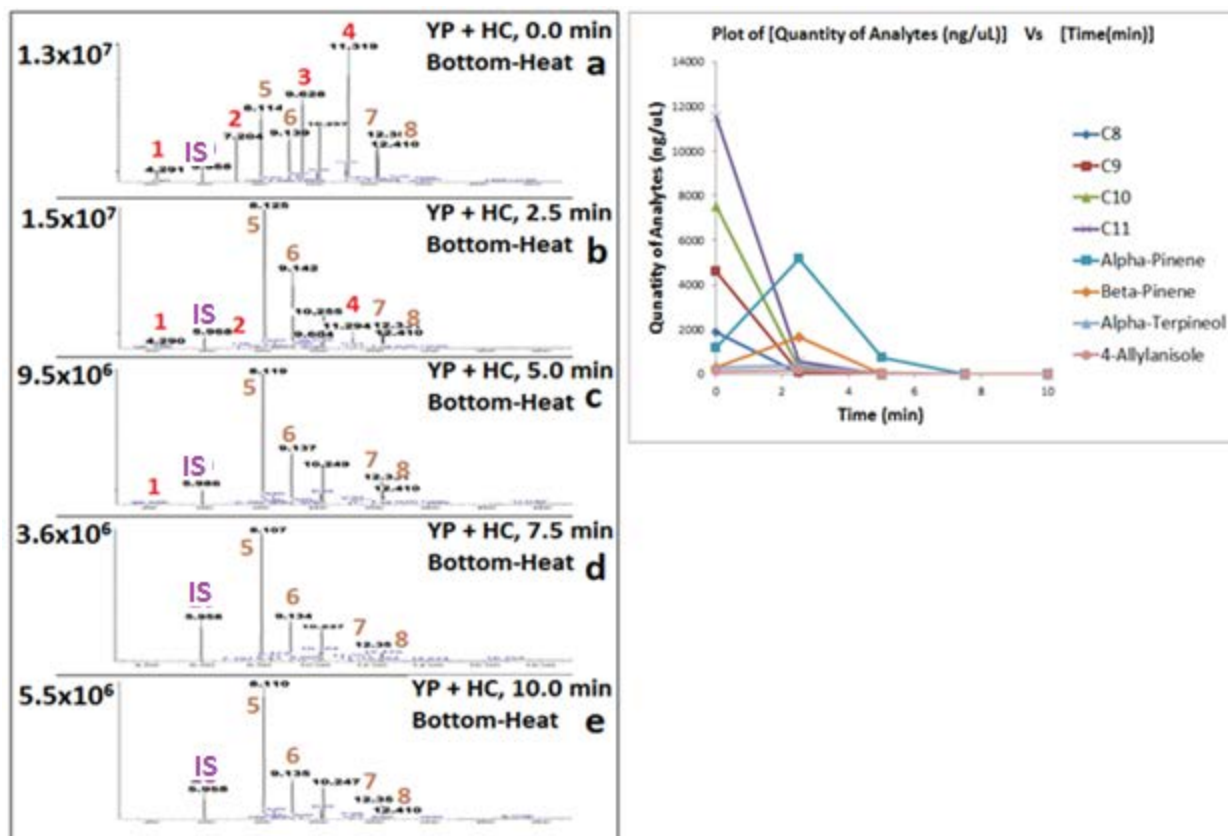


Figure 60: Chromatograms and quantification results from time study experiment of yellow-pine and HC mix by Bottom-Heat method

The chromatographic results from the time study experiment of yellow-pine with hydrocarbon mixture by Bottom-Heat method is shown in figure 60. The major peaks observed in the

chromatograms were identified based on library match and retention match, (see table 20). The chromatographic results from the time study experiment by Bottom-Heat method shows HC mixture decreasing at a faster rate. The amount of pyrolysis products was also less as compared to NDDM and Top-Heat method. Although alpha-pine was predominant in Bottom-Heat chromatogram, it was comparatively less intense than observed in the chromatograms of NDDM and Top-Heat method

10.4.4: Time Study of Nylon Carpet and Padding with Hydrocarbons

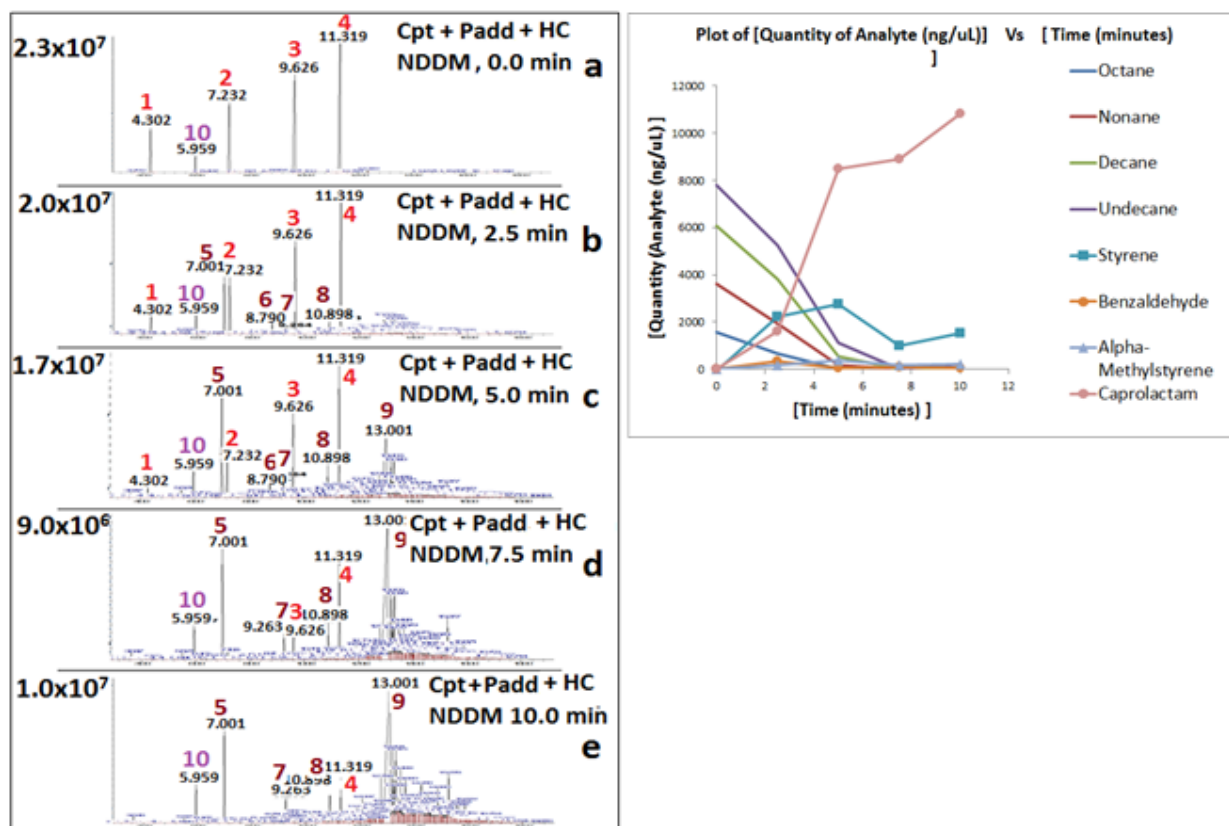


Figure 61: Chromatograms and quantification results from time study experiment of nylon carpet, padding and HC mix by NDDM

The chromatographic results from the time study experiment of combination of nylon carpet and padding with hydrocarbon mixture by NDDM is shown in figure 61. The major peaks observed in the chromatograms were identified based on library match and retention match, (see table 21).

Table 21: Identified Compound and Their Retention Times from Nylon Carpet, Padding, and HC Mix

<b>Peak number</b>	<b>Retention Time (Rt) minutes</b>	<b>Compounds</b>
<b>1</b>	4.302	C8e
<b>2</b>	7.232	C9
<b>3</b>	9.626	C10
<b>4</b>	11.319	C11
<b>5</b>	7.001	Styrene
<b>6</b>	8.790	Benzaldehyde
<b>7</b>	9.263	Alpha-methylstyrene
<b>8</b>	10.898	Acetophenone
<b>9</b>	13.001	Caprolactam

Based on the chromatographic results from time study experiment of combination of nylon carpet and padding with HC mixture, a decrease in the quantity of HC was observed as the heating time was increased. The peak corresponding to caprolactam (peak number 9) and styrene (peak number 5) were relatively more intense. Another significant observation was that even at 10 minute, caprolactam was most abundant and its quantity appeared to increase even more as

compared to other pyrolysis products. The next abundant peak corresponded to styrene (peak number 5). When nylon carpet and padding were heated by NDDM in the presence of HC mixture, it was observed that, the quantity of HC decreased at a moderate rate.

#### 10.4.5: Nylon Carpet and Padding with Hydrocarbons by Top-Heat Method

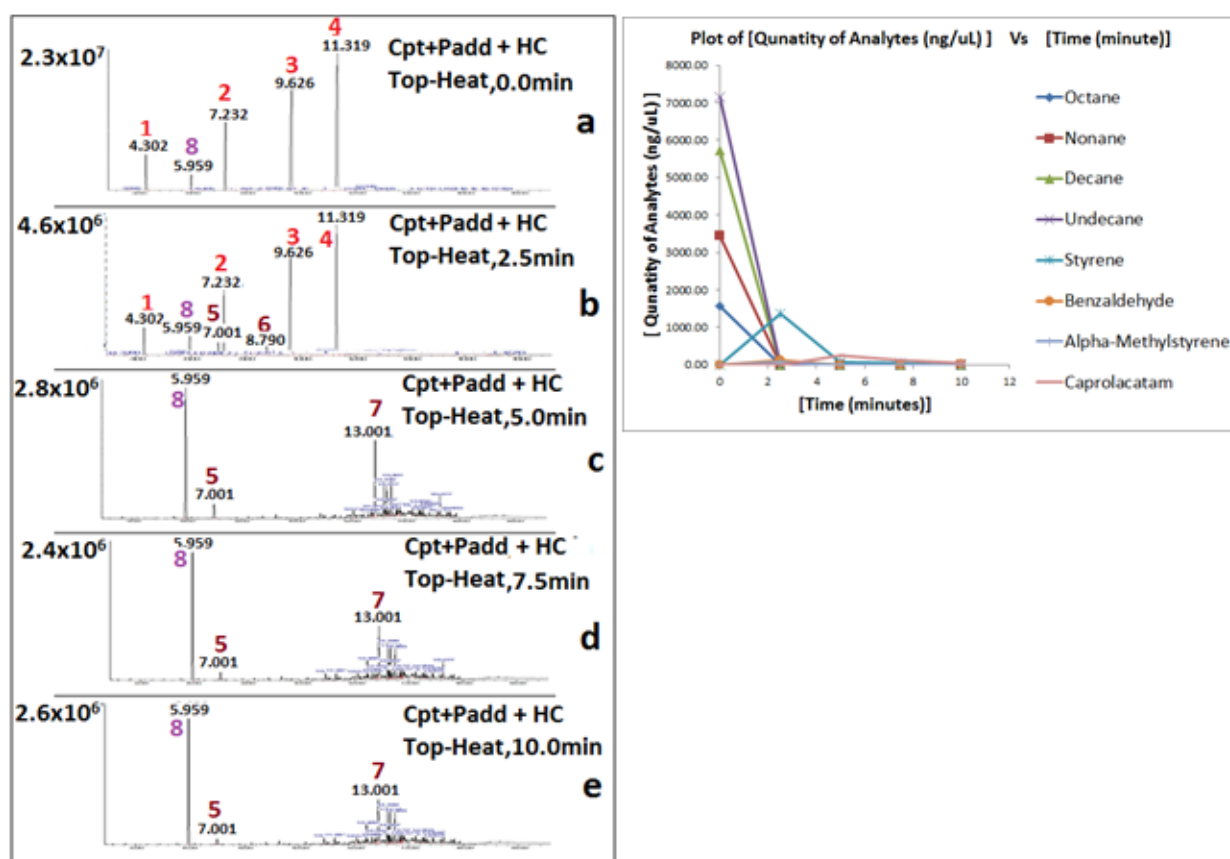


Figure 62: Chromatograms and quantification results from time study experiment of nylon carpet, padding and HC mix by Top-Heat method.

Based on the chromatographic results from Top heat method, it can be observed that HC mixture decreased at a faster rate compared to NDDM. When nylon carpet and padding were heated from



the top in the presence of HC, The peak corresponding to caprolactam was not observed. Only a weak peak corresponding to styrene was observed. The results from Top-Heat for nylon carpet and padding with HC were very different from NDDM with respect to the amount of caprolactam.

10.4.6: Nylon Carpet and Padding with Hydrocarbons by Bottom-Heat Method

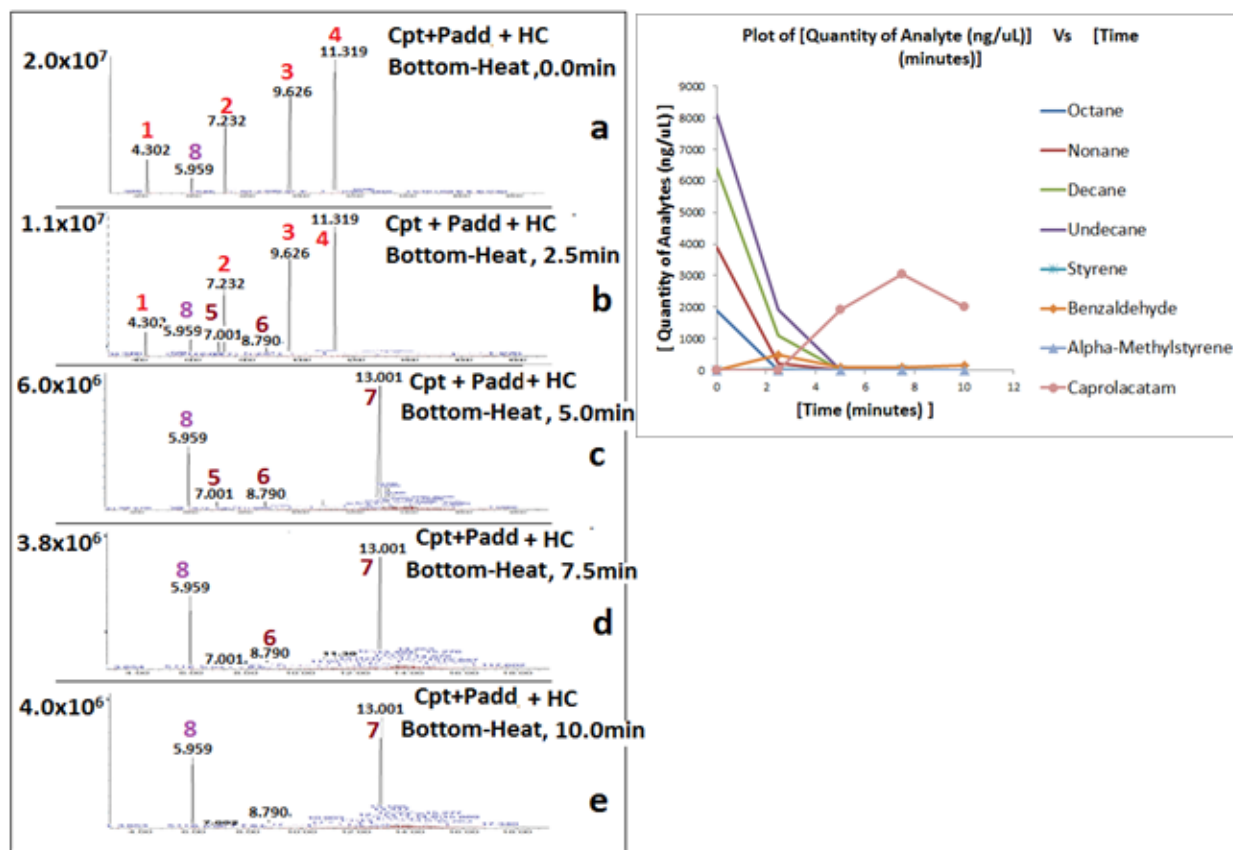


Figure 63: Chromatograms and quantification results from time study experiment of nylon carpet, padding and HC mix by Bottom-Heat method

The Bottom-Heat chromatographic result for the combination of nylon carpet and padding in the presence of HC mixture is similar to the results from NDDM. The peak corresponding to caprolactam was intense. Also the rate of decrease of HC with time is slow as compared to Top-Heat method.

## **CHAPTER 11: CONCLUSION**

### **11.1. Significance**

In this study, new heating methodologies have been developed for the controlled burns of substrates in laboratory to aid in fire debris analysis. Forensic community dealing with fire debris analysis frequently employ paint-cans for the controlled burns in laboratories, however burning the substrates in paint-cans has some limitations. One of the concerns is condensation of the vapors onto the walls and at the brim of paint-cans. Therefore in an attempt to curtail the condensation of vapors, substrates were subjected to controlled heating in steel pans by Top-Heat and Bottom-Heat method in addition to heating them in paint-cans by NDDM and DDNCM. Experiments were also performed to study the influence of hydrocarbons representing ignitable liquids on the formation of pyrolysis products during the controlled heating of substrates. The primary objectives of these experiments and methodologies were to prepare pyrolysis reference samples which would be more reflective of what would be observed in a real fire. All the methods demonstrated in this research has been satisfactory. Some methods produced more pyrolysis products for certain type of substrates and some did not. Therefore in conclusion, all the suggested methods can be adopted for the laboratory controlled burns of substrates in order to reproduce the best match by comparing with the chromatographic results obtained from a real fire.

## 11.2. Future Work

More substrates commonly used in building materials can be subjected to controlled heating in laboratories by itself and in combinations. A separate data base can be created to incorporate the chromatographic results from the controlled heating of substrates for each methods.

## **APPENDIX: COPYRIGHT PERMISSIONS**

4/13/2015

RE: Regarding Copyright permission for my Dissertation - b\_lingam

## RE: Regarding Copyright permission for my Dissertation

Cooks, R. Graham <cooks@purdue.edu>

Wed 6/11/2014 12:52 AM

Inbox

To: b\_lingam <b\_lingam@knights.ucf.edu>;

Hello Bala,  
You have my permission.  
Graham Cooks

---

**From:** b\_lingam [b\_lingam@knights.ucf.edu]  
**Sent:** Tuesday, June 10, 2014 11:56 AM  
**To:** Cooks, R. Graham  
**Subject:** Regarding Copyright permission for my Dissertation

Dr Cooks,

My Name is Balasubramaniam Lingam. I am a graduate student in the department of chemistry at University of Central Florida pursuing Ph.D under the able guidance of Dr Michael E. Sigman. I am writing this email in regards to seek permission to use one of the figures from one of your articles to include in my Dissertation.

The article is: Ion Trap Mass Spectrometry  
Authors : Philip S.H. Wong , R. Graham Cooks

The figure I would like to use is F2, from the above mentioned article. It would of great help if you could assist me in this process of copyright permission

Sincerely  
Bala

4/6/2015

Re: Seeking Permission to use one of the figures for my disserta... - b\_lingam

## Re: Seeking Permission to use one of the figures for my dissertation

Ray March <rmarch@trentu.ca>

Mon 3/30/2015 1:43 PM

Inbox

To: b\_lingam <b\_lingam@knights.ucf.edu>;

Dear Bala,

Thank you for your inquiry.

It is a pleasure to give you permission to reproduce Fig. 2 of *Quadrupole ion trap mass spectrometry: a view at the turn of the century.* *international Journal of Mass Spectrometry, Volume 200, Issues 1–3, 25 December 2000, Pages 285-312, for your dissertation.*

I hope you are being well treated at the University of Central Florida.

With best wishes,

Ray March

---

From: b\_lingam <b\_lingam@knights.ucf.edu>

Sent: March 30, 2015 12:02 PM

To: Ray March

Subject: Seeking Permission to use one of the figures for my dissertation

Dr March,

My name is Balasubramaniam. Lingam (Bala) . I am a graduate student at here at University of Central Florida (Department of chemistry). I am writing this email with regards to seeking permission to use one of the figures from your article to include in my dissertation.

The journal article that i am referring to is titled " **Quadrupole ion trap mass spectrometry: a view at the turn of the century.** *international Journal of Mass Spectrometry, Volume 200, Issues 1–3, 25 December 2000, Pages 285-312.*

The figure that i want to use is (**figure number 2, page 288**). I would really appreciate if you could give me permission to use that figure.

Thank you and please let me know if you need any further details.

<https://outlook.office365.com/owa/projection.aspx>

1/2

4/8/2015

RE: seeking permission to use five figures and one table - b\_lingam

Dr Frisch.

My name is Balasubramaniam Lingam. I am a graduate student here at University of Central Florida (Department of Chemistry). I am writing this email in regards to seeking permission to use some figures and one table from your Ph.D Dissertation (**Tandem mass Spectrometric Analysis of Ammonium and Sodium Oligoperoxides Adducts with the Application of Two-Dimensional Corelation Spectroscopy and Computational Chemistry**) to include in my Dissertation.

The figures that I would like to use are from the simple kinetic model studies.

Figure number 4.2 (page 162, model 2),  
Figure number 4.5 (page 167, model 5),  
Figure number 4.7 (page 171, model 7),  
Figure number 4.8 (page 172, model 8),  
Figure number 4.9 (page 173, model 9) and  
Table number 4.1 (page 160)

I would really appreciate if you could give me permission for the above figures and tables.

Thank you  
Sincerely  
Balasubramaniam.Lingam



4/6/2015

RE: seeking permission to use five figures and one table - b\_lingam

## RE: seeking permission to use five figures and one table

Jessica Frisch-Daiello <jfrisch-daiello@sanfordburnham.org>

Mon 3/30/2015 1:52 PM

Inbox

To: b\_lingam <b\_lingam@knights.ucf.edu>;

Good afternoon Mr. Lingam,

I give you permission to use the mentioned figures and table from my Ph.D. Dissertation to be included in your Dissertation.

Figure number 4.2 (page 162, model 2),  
Figure number 4.5 (page 167, model 5),  
Figure number 4.7 (page 171, model 7),  
Figure number 4.8 (page 172, model 8),  
Figure number 4.9 (page 173, model 9) and  
Table number 4.1 (page 160)

Regards,

Jessica L. Frisch-Daiello

Postdoctoral Research Associate  
Dr. Xianlin Han's Lab  
Diabetes and Obesity Research Center  
Sanford-Burnham Medical Research Institute at Lake Nona  
6400 Sanger Road, Orlando, FL 32827  
407-745-2000 Ext 6019

<http://intranet/administration/communications/Burnham%20Logos/SB%20icon%20and%20wordmark%20with%20tagline%20-%20Lake%20Nona.gif>

<http://www.sanfordburnham.org>

---

**From:** b\_lingam [mailto:b\_lingam@knights.ucf.edu]  
**Sent:** Monday, March 30, 2015 12:22 PM  
**To:** Jessica Frisch-Daiello; jessica.frisch-daiello@valdane.com  
**Subject:** seeking permission to use five figures and one table

<https://outlook.office365.com/owa/projection.aspx>

1/2

**ELSEVIER LICENSE  
TERMS AND CONDITIONS**

Apr 06, 2015

This is a License Agreement between Balasubramaniam Lingam ("You") and Elsevier ("Elsevier") provided by Copyright Clearance Center ("CCC"). The license consists of your order details, the terms and conditions provided by Elsevier, and the payment terms and conditions.

**All payments must be made in full to CCC. For payment instructions, please see information listed at the bottom of this form.**

Supplier	Elsevier Limited The Boulevard, Langford Lane Kidlington, Oxford, OX5 1GB, UK
Registered Company Number	1982084
Customer name	Balasubramaniam Lingam
Customer address	University of Central Florida, ORLANDO, FL 32826
License number	3603150049698
License date	Apr 06, 2015
Licensed content publisher	Elsevier
Licensed content publication	Science & Justice
Licensed content title	Concept of pyrolysis for fire debris analysts
Licensed content author	E. Stauffer
Licensed content date	January 2003
Licensed content volume number	43
Licensed content issue number	1
Number of pages	12
Start Page	29
End Page	40
Type of Use	reuse in a thesis/dissertation
Portion	figures/tables/illustrations
Number of figures/tables/illustrations	1
Format	electronic
Are you the author of this Elsevier article?	No
Will you be translating?	No

Original figure numbers	Figure 1,6 and 10
Title of your thesis/dissertation	Mass spectral Studies to Investigate Fragmentation Pathways of Butylbenzene and Pyrolysis Products
Expected completion date	May 2015
Estimated size (number of pages)	180
Elsevier VAT number	GB 494 6272 12
Permissions price	0.00 USD
VAT/Local Sales Tax	0.00 USD / 0.00 GBP
Total	0.00 USD

Terms and Conditions

### INTRODUCTION

1. The publisher for this copyrighted material is Elsevier. By clicking "accept" in connection with completing this licensing transaction, you agree that the following terms and conditions apply to this transaction (along with the Billing and Payment terms and conditions established by Copyright Clearance Center, Inc. ("CCC"), at the time that you opened your Rightslink account and that are available at any time at <http://myaccount.copyright.com>).

### GENERAL TERMS

2. Elsevier hereby grants you permission to reproduce the aforementioned material subject to the terms and conditions indicated.

3. Acknowledgement: If any part of the material to be used (for example, figures) has appeared in our publication with credit or acknowledgement to another source, permission must also be sought from that source. If such permission is not obtained then that material may not be included in your publication/copies. Suitable acknowledgement to the source must be made, either as a footnote or in a reference list at the end of your publication, as follows:

"Reprinted from Publication title, Vol /edition number, Author(s), Title of article / title of chapter, Pages No., Copyright (Year), with permission from Elsevier [OR APPLICABLE SOCIETY COPYRIGHT OWNER]." Also Lancet special credit - "Reprinted from The Lancet, Vol. number, Author(s), Title of article, Pages No., Copyright (Year), with permission from Elsevier."

4. Reproduction of this material is confined to the purpose and/or media for which permission is hereby given.

5. Altering/Modifying Material: Not Permitted. However figures and illustrations may be altered/adapted minimally to serve your work. Any other abbreviations, additions, deletions and/or any other alterations shall be made only with prior written authorization of Elsevier Ltd. (Please contact Elsevier at [permissions@elsevier.com](mailto:permissions@elsevier.com))

6. If the permission fee for the requested use of our material is waived in this instance, please be advised that your future requests for Elsevier materials may attract a fee.

7. **Reservation of Rights:** Publisher reserves all rights not specifically granted in the combination of (i) the license details provided by you and accepted in the course of this licensing transaction, (ii) these terms and conditions and (iii) CCC's Billing and Payment terms and conditions.

8. **License Contingent Upon Payment:** While you may exercise the rights licensed immediately upon issuance of the license at the end of the licensing process for the transaction, provided that you have disclosed complete and accurate details of your proposed use, no license is finally effective unless and until full payment is received from you (either by publisher or by CCC) as provided in CCC's Billing and Payment terms and conditions. If full payment is not received on a timely basis, then any license preliminarily granted shall be deemed automatically revoked and shall be void as if never granted. Further, in the event that you breach any of these terms and conditions or any of CCC's Billing and Payment terms and conditions, the license is automatically revoked and shall be void as if never granted. Use of materials as described in a revoked license, as well as any use of the materials beyond the scope of an unrevoked license, may constitute copyright infringement and publisher reserves the right to take any and all action to protect its copyright in the materials.

9. **Warranties:** Publisher makes no representations or warranties with respect to the licensed material.

10. **Indemnity:** You hereby indemnify and agree to hold harmless publisher and CCC, and their respective officers, directors, employees and agents, from and against any and all claims arising out of your use of the licensed material other than as specifically authorized pursuant to this license.

11. **No Transfer of License:** This license is personal to you and may not be sublicensed, assigned, or transferred by you to any other person without publisher's written permission.

12. **No Amendment Except in Writing:** This license may not be amended except in a writing signed by both parties (or, in the case of publisher, by CCC on publisher's behalf).

13. **Objection to Contrary Terms:** Publisher hereby objects to any terms contained in any purchase order, acknowledgment, check endorsement or other writing prepared by you, which terms are inconsistent with these terms and conditions or CCC's Billing and Payment terms and conditions. These terms and conditions, together with CCC's Billing and Payment terms and conditions (which are incorporated herein), comprise the entire agreement between you and publisher (and CCC) concerning this licensing transaction. In the event of any conflict between your obligations established by these terms and conditions and those established by CCC's Billing and Payment terms and conditions, these terms and conditions shall control.

14. **Revocation:** Elsevier or Copyright Clearance Center may deny the permissions described in this License at their sole discretion, for any reason or no reason, with a full refund payable to you. Notice of such denial will be made using the contact information provided by you. Failure to receive such notice will not alter or invalidate the denial. In no event will Elsevier or Copyright Clearance Center be responsible or liable for any costs, expenses or damage incurred by you as a result of a denial of your permission request, other than a refund of the amount(s) paid by you to Elsevier and/or Copyright Clearance Center for denied permissions.

**LIMITED LICENSE**

The following terms and conditions apply only to specific license types:

**15. Translation:** This permission is granted for non-exclusive world **English** rights only unless your license was granted for translation rights. If you licensed translation rights you may only translate this content into the languages you requested. A professional translator must perform all translations and reproduce the content word for word preserving the integrity of the article. If this license is to re-use 1 or 2 figures then permission is granted for non-exclusive world rights in all languages.

**16. Posting licensed content on any Website:** The following terms and conditions apply as follows: Licensing material from an Elsevier journal: All content posted to the web site must maintain the copyright information line on the bottom of each image; A hyper-text must be included to the Homepage of the journal from which you are licensing at <http://www.sciencedirect.com/science/journal/xxxxx> or the Elsevier homepage for books at <http://www.elsevier.com>; Central Storage: This license does not include permission for a scanned version of the material to be stored in a central repository such as that provided by Heron/XanEdu.

Licensing material from an Elsevier book: A hyper-text link must be included to the Elsevier homepage at <http://www.elsevier.com> . All content posted to the web site must maintain the copyright information line on the bottom of each image.

**Posting licensed content on Electronic reserve:** In addition to the above the following clauses are applicable: The web site must be password-protected and made available only to bona fide students registered on a relevant course. This permission is granted for 1 year only. You may obtain a new license for future website posting.

**17. For journal authors:** the following clauses are applicable in addition to the above:

**Preprints:**

A preprint is an author's own write-up of research results and analysis, it has not been peer-reviewed, nor has it had any other value added to it by a publisher (such as formatting, copyright, technical enhancement etc.).

Authors can share their preprints anywhere at any time. Preprints should not be added to or enhanced in any way in order to appear more like, or to substitute for, the final versions of articles however authors can update their preprints on arXiv or RePEc with their Accepted Author Manuscript (see below).

If accepted for publication, we encourage authors to link from the preprint to their formal publication via its DOI. Millions of researchers have access to the formal publications on ScienceDirect, and so links will help users to find, access, cite and use the best available version. Please note that Cell Press, The Lancet and some society-owned have different preprint policies. Information on these policies is available on the journal homepage.

**Accepted Author Manuscripts:** An accepted author manuscript is the manuscript of an article that has been accepted for publication and which typically includes author-incorporated changes suggested during submission, peer review and editor-author

communications.

Authors can share their accepted author manuscript:

- immediately
  - o via their non-commercial person homepage or blog
  - o by updating a preprint in arXiv or RePEc with the accepted manuscript
  - o via their research institute or institutional repository for internal institutional uses or as part of an invitation-only research collaboration work-group
  - o directly by providing copies to their students or to research collaborators for their personal use
  - o for private scholarly sharing as part of an invitation-only work group on commercial sites with which Elsevier has an agreement
- after the embargo period
  - o via non-commercial hosting platforms such as their institutional repository
  - o via commercial sites with which Elsevier has an agreement

In all cases accepted manuscripts should:

- link to the formal publication via its DOI
- bear a CC-BY-NC-ND license - this is easy to do
- if aggregated with other manuscripts, for example in a repository or other site, be shared in alignment with our hosting policy not be added to or enhanced in any way to appear more like, or to substitute for, the published journal article.

**Published journal article (JPA):** A published journal article (PJA) is the definitive final record of published research that appears or will appear in the journal and embodies all value-adding publishing activities including peer review co-ordination, copy-editing, formatting, (if relevant) pagination and online enrichment.

Policies for sharing publishing journal articles differ for subscription and gold open access articles:

**Subscription Articles:** If you are an author, please share a link to your article rather than the full-text. Millions of researchers have access to the formal publications on ScienceDirect, and so links will help your users to find, access, cite, and use the best available version.

Theses and dissertations which contain embedded PJAs as part of the formal submission can be posted publicly by the awarding institution with DOI links back to the formal publications on ScienceDirect.

If you are affiliated with a library that subscribes to ScienceDirect you have additional

private sharing rights for others' research accessed under that agreement. This includes use for classroom teaching and internal training at the institution (including use in course packs and courseware programs), and inclusion of the article for grant funding purposes.

**Gold Open Access Articles:** May be shared according to the author-selected end-user license and should contain a [CrossMark logo](#), the end user license, and a DOI link to the formal publication on ScienceDirect.

Please refer to Elsevier's [posting policy](#) for further information.

**18. For book authors** the following clauses are applicable in addition to the above: Authors are permitted to place a brief summary of their work online only. You are not allowed to download and post the published electronic version of your chapter, nor may you scan the printed edition to create an electronic version. **Posting to a repository:** Authors are permitted to post a summary of their chapter only in their institution's repository.

**19. Thesis/Dissertation:** If your license is for use in a thesis/dissertation your thesis may be submitted to your institution in either print or electronic form. Should your thesis be published commercially, please reapply for permission. These requirements include permission for the Library and Archives of Canada to supply single copies, on demand, of the complete thesis and include permission for Proquest/UMI to supply single copies, on demand, of the complete thesis. Should your thesis be published commercially, please reapply for permission. Theses and dissertations which contain embedded PJAs as part of the formal submission can be posted publicly by the awarding institution with DOI links back to the formal publications on ScienceDirect.

### **Elsevier Open Access Terms and Conditions**

You can publish open access with Elsevier in hundreds of open access journals or in nearly 2000 established subscription journals that support open access publishing. Permitted third party re-use of these open access articles is defined by the author's choice of Creative Commons user license. See our [open access license policy](#) for more information.

#### **Terms & Conditions applicable to all Open Access articles published with Elsevier:**

Any reuse of the article must not represent the author as endorsing the adaptation of the article nor should the article be modified in such a way as to damage the author's honour or reputation. If any changes have been made, such changes must be clearly indicated.

The author(s) must be appropriately credited and we ask that you include the end user license and a DOI link to the formal publication on ScienceDirect.

If any part of the material to be used (for example, figures) has appeared in our publication with credit or acknowledgement to another source it is the responsibility of the user to ensure their reuse complies with the terms and conditions determined by the rights holder.

#### **Additional Terms & Conditions applicable to each Creative Commons user license:**

**CC BY:** The CC-BY license allows users to copy, to create extracts, abstracts and new works from the Article, to alter and revise the Article and to make commercial use of the

Article (including reuse and/or resale of the Article by commercial entities), provided the user gives appropriate credit (with a link to the formal publication through the relevant DOI), provides a link to the license, indicates if changes were made and the licensor is not represented as endorsing the use made of the work. The full details of the license are available at <http://creativecommons.org/licenses/by/4.0>.

**CC BY NC SA:** The CC BY-NC-SA license allows users to copy, to create extracts, abstracts and new works from the Article, to alter and revise the Article, provided this is not done for commercial purposes, and that the user gives appropriate credit (with a link to the formal publication through the relevant DOI), provides a link to the license, indicates if changes were made and the licensor is not represented as endorsing the use made of the work. Further, any new works must be made available on the same conditions. The full details of the license are available at <http://creativecommons.org/licenses/by-nc-sa/4.0>.

**CC BY NC ND:** The CC BY-NC-ND license allows users to copy and distribute the Article, provided this is not done for commercial purposes and further does not permit distribution of the Article if it is changed or edited in any way, and provided the user gives appropriate credit (with a link to the formal publication through the relevant DOI), provides a link to the license, and that the licensor is not represented as endorsing the use made of the work. The full details of the license are available at <http://creativecommons.org/licenses/by-nc-nd/4.0>. Any commercial reuse of Open Access articles published with a CC BY NC SA or CC BY NC ND license requires permission from Elsevier and will be subject to a fee.

Commercial reuse includes:

- Associating advertising with the full text of the Article
- Charging fees for document delivery or access
- Article aggregation
- Systematic distribution via e-mail lists or share buttons

Posting or linking by commercial companies for use by customers of those companies.

## 20. Other Conditions:

Questions? [customercare@copyright.com](mailto:customercare@copyright.com) or +1-855-239-3415 (toll free in the US) or +1-978-646-2777.

**Gratis licenses (referencing \$0 in the Total field) are free. Please retain this printable license for your reference. No payment is required.**



## REFERENCES

1. Plomley, J. B.; Londry, F. A.; March, R. E., The Consecutive Fragmentation of n-Butylbenzene in a Quadrupole Ion Trap. *Rapid Communications in Mass Spectrometry* **1996**, *10* (2), 200-203.
2. Croley, T. R.; Zemribo, R.; Lynn Jr, B. C., Waveform activated rearrangement of n-butylbenzene molecular ions during tandem mass spectrometry in the quadrupole ion trap. *International Journal of Mass Spectrometry* **1999**, *190-191* (0), 265-279.
3. Harrison, A. G. L., M. S., *Int. J. Mass Spectrom. Ion Phys.* **1983**, *51*.
4. Chen, J. H.; Hays, J. D.; Dunbar, R. C., Competitive two-channel photodissociation of n-butylbenzene ions in the Fourier-transform ion cyclotron resonance mass spectrometer. *The Journal of Physical Chemistry* **1984**, *88* (20), 4759-4764.
5. Baer, T.; Dutuit, O.; Mestdagh, H.; Rolando, C., Dissociation dynamics of n-butylbenzene ions: the competitive production of m/z 91 and 92 fragment ions. *The Journal of Physical Chemistry* **1988**, *92* (20), 5674-5679.
6. (a) McLuckey, S. A.; Sallans, L.; Cody, R. B.; Burnier, R. C.; Verma, S.; Freiser, B. S.; Cooks, R. G., Energy-resolved tandem and fourier-transform mass spectrometry. *International Journal of Mass Spectrometry and Ion Physics* **1982**, *44* (3-4), 215-229; (b) Knyazev, V. D.; Stein, S. E., Monte Carlo/RRKM/Classical Trajectories Modeling of Collisional Excitation and Dissociation of n-Butylbenzene Ion in Multipole Collision Cells of Tandem Mass Spectrometers. *The Journal of Physical Chemistry A* **2010**, *114* (22), 6384-6393.
7. Oh, S. T.; Choe, J. C.; Kim, M. S., Photodissociation Dynamics of n-Butylbenzene Molecular Ion. *The Journal of Physical Chemistry* **1996**, *100* (32), 13367-13374.
8. Frisch, J. L. Tandem Mass Spectrometric Analysis of Ammonium and Sodium Oligoperoxide Adducts with the Application of Two-Dimensional Correlation Spectroscopy and Computational Chemistry. Doctoral Dissertation, University of Central Florida, Orlando, Florida, 2012.
9. Guan, S.; Marshall, A. G., Stored waveform inverse Fourier transform (SWIFT) ion excitation in trapped-ion mass spectrometry: Theory and applications. *International Journal of Mass Spectrometry and Ion Processes* **1996**, *157-158* (0), 5-37.
10. Dalpathado, D. S.; Chang, Q.; Burkett, C. M.; Bandu, M. L.; Desaire, H., Application of the statistical test of equivalent pathways (STEP) method to the triple quadrupole mass spectrometer. *Rapid Communications in Mass Spectrometry* **2007**, *21* (20), 3365-3372.
11. Chin, T.-L.; Lin, K.-C., Two-Dimensional Correlation Analysis in Application to a Kinetic Model of Parallel Reactions. *Applied Spectroscopy* **2003**, *57* (2), 168-175.
12. Chin, T.-L.; Lin, K.-C., Two-Dimensional Correlation Analysis for a Kinetic Model of Consecutive Reactions. *Applied Spectroscopy* **2003**, *57* (9), 1070-1077.
13. (eds), Y. O. a. I. N., Two-Dimensional Correlation Spectroscopy. In *AIP Conf. Proc.*, pp 3-17.
14. Xiaoming, D.; Bo, Y.; Haiying, Z.; Guangzhong, Y.; Ozaki, Y., Generalized two-dimensional correlation spectroscopy. *Science in China Series B: Chemistry* **2004**, *47* (3), 257-266.

15. I. Noda, Y. O., *Two-dimensional Correlation Spectroscopy Applications in Vibrational and Optical Spectroscopy*. Wiley: Chichester.
16. Sigman, M. E.; Clark, C. D., Two-dimensional correlation spectroscopy techniques applied to ion trap tandem mass spectrometric analysis: nitroaromatics. *Rapid Communications in Mass Spectrometry* **2005**, *19* (24), 3731-3736.
17. Laskay, U. A. Dynamic collision induced dissociation: A novel fragmentation method in the quadrupole ion trap. Dissertation, Ohio University, 2009.
18. Philip S.H. Wong, R. G. C., Ion Trap Mass Spectrometry.
19. Paul, W., Electromagnetic Traps for Charged and Neutral Particles. *Angew. Chem.* **1990**, *29*, 739-748.
20. March, R. E., Quadrupole Ion Trap Mass Spectrometer. *Encyclopedia of Analytical Chemistry*.
21. March, R. E., An Introduction to Quadrupole Ion Trap Mass Spectrometry. *Journal of Mass Spectrometry* **1997**, *32* (4), 351-369.
22. Charles, M. J.; McLuckey, S. A.; Glish, G. L., Competition between resonance ejection and ion dissociation during resonant excitation in a quadrupole ion trap. *Journal of the American Society for Mass Spectrometry* **1994**, *5* (12), 1031-1041.
23. Sleno, L.; Volmer, D. A., Ion activation methods for tandem mass spectrometry. *Journal of Mass Spectrometry* **2004**, *39* (10), 1091-1112.
24. Vachet, R.; Glish, G., Effects of heavy gases on the tandem mass spectra of peptide ions in the quadrupole ion trap. *Journal of the American Society for Mass Spectrometry* **1996**, *7* (12), 1194-1202.
25. Gross, J., Principles of Ionization and Ion Dissociation. In *Mass Spectrometry*, Springer Berlin Heidelberg: 2011; pp 21-66.
26. Schaaff, T. G.; Qu, Y.; Farrell, N.; Wysocki, V. H., Investigation of the trans effect in the fragmentation of dinuclear platinum complexes by electrospray ionization surface-induced dissociation tandem mass spectrometry. *Journal of Mass Spectrometry* **1998**, *33* (5), 436-443.
27. Vékey, K., Internal Energy Effects in Mass Spectrometry. *Journal of Mass Spectrometry* **1996**, *31* (5), 445-463.
28. Halbert, S.; Bouchoux, G., Isomerization and Dissociation of n-Butylbenzene Radical Cation. *The Journal of Physical Chemistry A* **2012**, *116* (4), 1307-1315.
29. Noda, I., Two-Dimensional Infrared (2D IR) Spectroscopy: Theory and Applications. *Applied Spectroscopy* **1990**, *44* (4), 550-561.
30. (a) Harrison, A. G.; Lin, M. S., Energy-Dependence of the Fragmentation of the Normal-Butylbenzene Molecular Ion. *International Journal of Mass Spectrometry and Ion Processes* **1983**, *51* (2-3), 353-356; (b) Mukhtar, E. S.; Griffiths, I. W.; Harris, F. M.; Beynon, J. H., Photo-Dissociation of Mass-Selected Ions Investigated Using a Modified ZAB-2F Spectrometer. *International Journal of Mass Spectrometry and Ion Processes* **1981**, *37* (2), 159-166.
31. Dawson, P. H.; Sun, W. F., Comparison of Low-Energy Collisionally Induced Dissociation of N-Butyl Benzene Ions with Photo-Dissociation. *International Journal of Mass Spectrometry and Ion Processes* **1982**, *44* (1-2), 51-59.
32. Chen, J. H.; Hays, J. D.; Dunbar, R. C., Competitive 2-Channel Photodissociation of Normal-Butylbenzene Ions in the Fourier-Transform Ion-Cyclotron Resonance Mass-Spectrometer. *Journal of Physical Chemistry* **1984**, *88* (20), 4759-4764.

33. Laskay, Ü. A.; Jackson, G. P., Resonance excitation and dynamic collision-induced dissociation in quadrupole ion traps using higher-order excitation frequencies. *Rapid Communications in Mass Spectrometry* **2008**, 22 (15), 2342-2348.
34. Contreras, P. A.; Houck, S. S.; Davis, W. M.; Yu, J. C. C., Pyrolysis Products of Linear Alkylbenzenes— Implications in Fire Debris Analysis\*. *Journal of Forensic Sciences* **2013**, 58 (1), 210-216.
35. (a) Niamh Nic, D. i., An introduction to fires and fire investigation. In *Fire Investigation*, CRC Press: 2004; (b) Eric, S., Sources of interference in fire debris analysis. In *Fire Investigation*, CRC Press: 2004.
36. Stauffer, E., Concept of pyrolysis for fire debris analysts. *Science & Justice* **2003**, 43 (1), 29-40.
37. Stauffer, E.; NicDaéid, N., Interpretation of Fire Debris Analysis. In *Encyclopedia of Forensic Sciences*, Houck, J. A. S. J. S. M., Ed. Academic Press: Waltham, 2013; pp 183-194.
38. (a) Higgins, M., Turpentine, accelerant or natural ??? The Fire and Arson Investigator. **1987**; (b) B. Chanson, E. E., E. Du Pasquier, O. Delemont, and J.C. Martin Turpentine identification in fire debris analysis. .
39. JJ, L., Persistence of floor coating solvents. *J Forensic Sci.* **2001**, 46 (6).
40. Lentini J.J, D. J. A., Cherry C., The petroleum-laced background. *J Forensic Sci.* **2000**, 45 (5).
41. Cavanagh, K.; Pasquier, E. D.; Lennard, C., Background interference from car carpets— the evidential value of petrol residues in cases of suspected vehicle arson. *Forensic Science International* **2002**, 125 (1), 22-36.
42. Lang, T.; Dixon, B. M., The Possible Contamination of Fire Scenes by the use of Positive Pressure Ventilation Fans. *Canadian Society of Forensic Science Journal* **2000**, 33 (2), 55-60.
43. M.T. Pinorini, G. J. L., P. Margot, I. Dustin, and P. Furrer Soot as an indicator in fire investigations: physical and chemical analysis. *Journal of Forensic Sciences* **1994**, 39 (4).
44. Wampler, T. P., Applied Pyrolysis Handbook. In *Applied Pyrolysis Handbook*, Wampler, T. P., Ed. CRC Press Taylor & Francis Group: Boca Raton, FL 33487-2742, 2007.
45. Njuguna, K. P. a. J., *Thermal Degradation of Polymeric Materials*. Rapra Technology Limited: 2005.
46. Materials, A. S. f. T. a., *ASTM E 1412–00 Standard Practice for Separation and Concentration of Ignitable Liquid Residues from Fire Debris Samples by Passive Headspace Concentration With Activated Charcoal*. 2001.
47. Mary Williams, D. F., Candice Bridge, Derek Dorrain, Stefanie Elliot, Michael Sigman, Adsorption Saturation and Chromatographic Distortion Effects on Apssive Headspace Sampling with Activated Charcoal in Fire Debris Analysis. *Journal of Forensic Science* **2005**, 50 (2), 316-325.
48. NicDaéid, N.; Stauffer, E., Analysis of Fire Debris. In *Encyclopedia of Forensic Sciences*, Houck, J. A. S. J. S. M., Ed. Academic Press: Waltham, 2013; pp 177-182.
49. Actlabs, Containers For Fire Debris Samples. **2000**.
50. DeHaan J, B. K., Pyrolysis products of structure fires. *J Forensic Sci Soc.* **1988**, 28 (5-6), 299-309.
51. 13, E., Standard Practice for Separation of Ignitable Liquid Residues from Fire Debris Samples by Dynamic Headspace Concentration. **1995**, 527-529.

52. 12, E., Standard Practice for Separation of Ignitable Liquid Residues from Fire Debris Samples by Passive Headspace Concentration With Activated Charcoal. **1995**, 524-526.
53. Lloyd JA, E. P., Preferential extraction of hydrocarbons from fire debris samples by solid phase microextraction. *J Forensic Sci.* **2003**, 48 (1), 130-134.
54. Almirall, J. R.; Furton, K. G., Characterization of background and pyrolysis products that may interfere with the forensic analysis of fire debris. *Journal of Analytical and Applied Pyrolysis* **2004**, 71 (1), 51-67.
55. (a) Hirz, R.; Rizzi, A. M., Simulation of concentration changes in complex volatile mixtures during evaporation by using gas chromatography. *Chromatographia* **1991**, 31 (5-6), 224-232; (b) Thomas J. Bruno, S. A., Weathering Patterns of Ignitable Liquids with the Advanced Distillation Curve Method. *Journal of Research of the National Institute of Standards and Technology* **2013**, 118.
56. D A Turner, J. P., Y Rodenas, J McKillip, and J V Goodpaster., Microbial Degradation of Gasoline in Soil: Comparison by Soil Type. *J Bioremed Biodeg* **2014**, 5 (2).
57. Materials, A. S. f. T. a., Standard of Ignitable Liquid Residues from Fire Debris Samples by Passive Headspace concentration with Activated Charcoal. **2001 (E1412)**, 1-3.
58. Lewis, J. N. The application of chemometrics to the detection and classification of ignitable liquids in fire debris using total ion spectrum. University of Central Florida, Orlando, 2011.
59. McHugh, K. M. Determining the Presence of an Ignitable Liquid Residue in Fire Debris Samples Utilizing Target Factor Analysis. University of Central Florida, Orlando, 2010.
60. Ettling B, A. M., The study of accelerant residues in fire remains. *J Forensic Sci.* **1968**, 13 (1), 76-89.
61. Howard H, M. A., A Fire Investigation Involving Combustion of Carpet Material. . *J Forensic Sci.* **1984**, 29 (3).
62. W., B., Volatiles from carpet: a source of frequent misinterpretation in arson analysis. *J Chromatogr A.* **1994**, 674 (1-2), 329-333.
63. Castelbuono, J. The Identification of Ignitable Liquids in the Presence of Pyrolysis Products: Generation of a Pyrolysis Product Database University of Central Florida, Orlando, 2008.
64. Sandercock, P. M. L., Preparation of Pyrolysis Reference Samples: Evaluation of a Standard Method Using a Tube Furnace. *Journal of Forensic Sciences* **2012**, 57 (3), 738-743.